TECHNISCHE UNIVERSITÄT MÜNCHEN

Wissenschaftszentrum Weihenstephan für Ernährung, Landnutzung und Umwelt

Lehrstuhl für Molekulare Ernährungsmedizin

Phenotypic characterization of a novel *Ucp1-LUC-iRFP713* reporter mouse model for visualization and quantification of brown and beige fat recruitment

Hui Wang

Vollständiger Abdruck der von der Fakultät Wissenschaftszentrum Weihenstephan für Ernährung, Landnutzung und Umwelt der Technischen Universität München zur Erlangung des akademischen Grades eines

Doktors der Naturwissenschaften

genehmigten Dissertation.

Vorsitzender: Prof. Dr. Michael Schemann

Prüfer der Dissertation: 1. Prof. Dr. Martin Klingenspor

2. Prof. Dr. Thomas Skurk

Die Dissertation wurde am 16.04.2019 bei der Technischen Universität München eingereicht und durch die Fakultät Wissenschaftszentrum Weihenstephan für Ernährung, Landnutzung und Umwelt am 28.05.2019 angenommen.

TABALE OF CONTENTS

TABALE OF CONTENTS

TABALE OF CONTENTS

ABBREVIATIONS

AC	adenylyl cyclase
ACC	acetyl-CoA carboxylase
AdipoQ	adiponectin
ADP	adenosine diphosphate
Adrb3	adrenoceptor beta 3
AMPS	ammoniumperoxodisulfat
AR	adrenoceptor
ATGL	adipose triglyceride lipase
ATP	adenosine triphosphate
BAC	bacterial artificial chromosome
BCA	bicinchoninic acid
BMR	basal metabolic rate
bp	base pairs
BSA	bovine serum albumin
cAMP	cyclic adenosine monophosphate
CD	control diet
CLEC10A (CD301)	C-type lectin domain containing 10A
cDNA	compensatory deoxyribonucleic acid
Cidea	cell death inducing DFFA like effector A
Cox7a1	cytochrome C oxidase subunit 7A1
CO_2	carbon dioxide
CREB	cAMP response element-binding protein
CRTC	CREB regulated transcription coactivator
CTT	cold tolerance test
DNA	deoxyribonucleic acid
Dio2	iodothyronine deiodinase 2
ddPCR	droplet digital polymerase chain reaction
EERa	estrogen related receptor alfa
Elovl3	ELOVL fatty acid elongase 3
eWAT	epididymal white adipose tissue
FA	fatty acid
FABP4	fatty acid binding protein 4
FAM	carboxyfluorescein

ABBREVIATIONS

FASN	fatty acid synthase
fBAT	femoral brown adipose tissue
FBS	fetal bovine serum
FCCP	carbonyl cyanide-p-trifluoromethoxyphenylhydrazone
gDNA	genomic deoxyribonucleic acid
GFP	green fluorescent protein
gWAT	gonadal white adipose tissue
H & E	hematoxylin and eosin
HET	heterozygous
HEX	hexachloro-fluorescein
HFD	high-fat diet
HP	heat production
HP_{max}	maximal heat production
HSL	hormone sensitive lipase
iBAT	interscapular brown adipose tissue
IBMX	3-isobutyl-1-methylxanthin
iWAT	inguinal white adipose tissue
iRFP713	near-infrared fluorescent protein 713
IVIS	*in vivo* imaging system
KI	knock-in
KO	knock-out
LUC	firefly luciferase
mRNA	message ribonucleic acid
MRI	magnetic resonance imaging
NC	nitrocellularose
NE	norepinephrine
NEmax	maximal norepinephrine-stimulated heat production
NET	norepinephrine test
NIR	near-infrared
NMR	nuclear magnetic resonance
Nrg4	neuregulin 4
NST	non-shivering thermogenesis
OCR	oxygen consumption rate
O_2	oxygen

ABBREVIATIONS

PCR	polymerase chain reaction
PET-CT	positron emission tomography and computed tomography
PGC1a	peroxisome proliferator-activated receptor gamma coactivator 1 alpha
poWAT	peri-ovarian white adipose tissue
PPARg	peroxisome proliferator-activated receptor gamma
PRDM16	PR domain containing 16
RA	retinoic acid
RAR	retinoid acid receptor
RER	respiratory exchange ratio
RLU	relative luminescence unit
RNA	ribonucleic acid
ROI	region of interest
RFP	red fluorescent protein
RXR	retinoid X receptor
RT-qPCR	real-time quantitative polymerase chain reaction
SDS	sodium dodecyl sulfate
SIK	salt-inducible kinase
Slc25a1	solute carrier family 25 member 1
SPF	specified pathogen free
SV40 LT	Simian virus 40 large T antigen
SVF	stromal vascular fraction
TBS	tris-buffered saline,
TBST	tris-buffered saline with Tween 20
TEMED	tetramethylethylenediamine
TG	triglyceride
T2A	Thosea asigna virus 2A
T3	triiodo-L-thyronine
T4	thyroxine
TRP	transient receptor potential
UCP1	uncoupling protein 1
UTR	untranslated region
VEGF	vascular endothelial growth factor a
WAT	white adipose tissue
WT	wildtype

ABSTRACT

Brown adipose tissue (BAT) converts chemical energy into heat via the mitochondrial uncoupling protein 1 (UCP1).

To explore novel molecules to recruit and activate UCP1 as a treatment to ameliorate obesity and diabetes, a *Ucp1* reporter gene mouse model (C57BL/6NTac-*Ucp1*[tm3588 *(LUC-T2A-iRFP-T2A-Ucp1) Arte*]) was generated, with simultaneous expression of firefly luciferase (LUC) and near-infrared fluorescent protein (iRFP713) driven by the regulatory elements of the endogenous *Ucp1* gene. The detailed characterization of the reporter mice *in vivo* and *in vitro* confirmed that both LUC activity and iRFP713 protein are reliable markers to reflect variations in endogenous *Ucp1* gene expression in response to external physiological and pharmacological stimulation. After administration of D-Luciferin, LUC activity facilitated the identification of a previously unknown femoral BAT depot (fBAT) by *in situ* imaging. Moreover, the quantitative measurements of *ex vivo* bioluminescence revealed a higher browning propensity in peri-ovarian WAT than in epididymal WAT and revealed the potential *Ucp1* expression in thymus, brain, epididymis and soleus muscle as well. Furthermore, by establishing the *in vitro* cell-based imaging system in primary brown and beige adipocytes, the pan-SIKs inhibitor HG-9-91-01 was identified as a positive modulator to promote *Ucp1* expression. Lastly, LUC and iRFP713 signals were suitable to monitor *Ucp1* expression *in vivo*.

Phenotypic studies revealed that homozygous knock-in (KI) reporter mice exhibited an approximately 80% reduction in UCP1 protein expression, leading to an array of cellular and bioenergetic alterations. Therefore, the reporter mouse, in return, provides a new model to investigate the role of UCP1 in protection against cold and diet-induced obesity. Interestingly, decreased UCP1 protein content in the KI reporter mouse led to dramatic impairment in non-shivering thermogenesis, making KI mice more cold sensitive. High-fat diet (HFD) feeding profoundly increased the UCP1 expression in iBAT of KI mice, but its abundance remained significantly low compared to wildtype (WT) mice. Based on the potential importance of diet-induced thermogenesis, it was expected that WT mice could gain less body mass than KI mice. However, contrary to the expectation, there were no significant differences in body mass across the genotypes, when they were subjected to prolonged HFD feeding at room temperature or at thermoneutrality. Collectively, these data provide evidence that UCP1 does not play a role in protecting mice from diet-induced obesity, possibly due to the insufficient UCP1 activation.

ZUSAMMENFASSUNG

Braunes Fettgewebe (BAT) wandelt chemische Energie über das mitochondriale Entkopplungsprotein 1 (UCP1) in Wärme um. Die Wiederentdeckung von metabolisch aktiven BAT bei gesunden erwachsenen Menschen hat das Interesse an der Biologie des Braunen und Beigen Fettgewebes wiederbelebt.

Um neue Moleküle zur Rekrutierung und Aktivierung von UCP1 zur Behandlung von Fettleibigkeit und Diabetes zu erforschen, wurde ein Ucp1-Reporter-Gen-Mausmodell (C57BL/6NTac-*Ucp1* $^{tm3588\ (LUC\text{-}T2A\text{-}iRFP\text{-}T2A\text{-}Ucp1)\ Arte}$) mit gleichzeitiger Expression von Firefly-Luciferase (LUC) und nahinfrarotem fluoreszierendem Protein (iRFP713) erzeugt, unter Kontrolle die den regulatorischen Elemente des endogenen Ucp1-Gens angetrieben wird. Die detaillierte Charakterisierung unserer Reportermäuse bestätigte, dass sowohl die LUC-Aktivität, als auch das iRFP713-Protein zuverlässig sind um Variationen in der endogenen *Ucp1*-Genexpression zu reflektieren, die auf externe physiologische und pharmakologische Aktivierung Stimulation widerzuspiegeln. Nach der Verabreichung von D-Luciferin erleichterte die LUC-Aktivität die Identifizierung eines bisher unbekannten femoralen BAT (fBAT) durch in situ-Bildgebung. Darüber hinaus zeigten die quantitativen Messungen der *ex vivo* Biolumineszenz eine höhere Bräunungsneigung im periovarianischen WAT als im epididymalen WAT sowie die potenzielle *Ucp1*-Expression in Thymus, Gehirn, Nebenhoden und Soleusmuskel. Darüber hinaus konnte *in vitro* zellbasierten Abbildungssystem einen pan-SIKs-Inhibitor HG-9-9-91-01 als positiver Modulator zur Förderung der Ucp1-Expression identifiziert werden. Zudem waren LUC- und iRFP713-Signale geeignet, die Ucp1-Expression in vivo zu überwachen. Insbesondere der Nachweis von iRFP713 erfordert kein exogenes Substrat.

Phänotypische Studien zeigten, dass homozygote Knock-in (KI) Reportermäuse eine etwa 80%ige Reduktion der UCP1-Proteinexpression aufweisen, was zu einer Reihe von zellulären und bioenergetischen Veränderungen führte. Daher bietet die Reportermaus im Gegenzug ein neues Modell, um die Rolle von UCP1 beim Schutz vor Kälte und diätetischer FAdipositas zu untersuchen. Interessanterweise führte der verminderter UCP1-Proteingehalt in der KI Reportermaus zu einer Beeinträchtigung der nicht zitterfrei Thermogenese, was die Reportermäuse kälterempfindlicher macht. Die fettreiche Ernährung erhöhte die UCP1-Expression in iBAT von KI-Mäusen erheblich, aber blieb auf proteinebene im Vergleich zu Wildtyp-(WT)-Mäusen signifikant niedrig. Basierend auf der physiologischen Bedeutung der

ZUSAMMENFASSUNG

diätinduzierten Thermogenese wurde erwartet, dass WT-Mäuse weniger Körpermasse gewinnen könnten als KI-Mäuse. Entgegen der Erwartung gab es jedoch keine signifikanten Unterschiede in der Körpermasse zwischen den Genotypen, wenn sie einer längeren HFD-Fütterung bei Raumtemperatur oder bei Thermoneutralität ausgesetzt waren. Zusammenfassend liefern diese Daten den Beweis, dass UCP1 keine Rolle beim Schutz von Mäusen vor ernährungsbedingter Adipositas spielt, möglicherweise aufgrund der unzureichenden UCP1-Aktivität.

1 INTRODUCTION

1.1 Adipose tissue

1.1.1 White, brown and beige adipose tissue in rodents

Three types of adipose tissue exist in mammals, with different properties in morphological appearance, molecular architecture, and metabolic roles. White adipose tissue (WAT) is the most abundant fat and is mainly located in subcutaneous and visceral sites. White adipocytes are characterized by a single large lipid droplet (unilocular) and a periphery nucleus (Cinti 2001). The primary purpose of WAT is to store excess energy as triglycerides during energetic surplus and to fuel other tissues and cells during energy deprivation (reviewed in Gesta et al. 2007).

Brown adipose tissue (BAT) is distinctively different from WAT in many aspects (Cannon & Nedergaard 2004). Anatomically, brown fat depots in rodents mainly reside in anterior regions, including interscapular, subscapular, axillary and cervical pads, forming a subcutaneous "heating jacket" beneath the fur (Klingenspor et al. 2017). Among them, interscapular BAT (iBAT) is the most-studied depot for BAT function in rodents. Additional small brown fat depots such as mediastinal BAT and intraperitoneal BAT are found around the aorta within the thoracic cavity and around the kidneys, respectively (Cinti 2001; de Jong et al. 2015). However, the identification of novel brown adipose tissue in laboratory mice such as the supraclavicular BAT (scBAT) (Mo et al. 2017) and the brown-like fat depot underneath the skin of the ears (uBAT) (Mao et al. 2017) highlights the inadequate understanding about the anatomical distribution of brown and beige fat deposits. Functionally, BAT consumes large amounts of chemical energy and generates heat to maintain the core body temperature of newborns, small mammals and animals during arousal from hibernation or torpor (Cannon & Nedergaard 2004; Smith et al. 1963; Townsend & Tseng 2012). This BAT-based heat-producing process is referred to as non-shivering thermogenesis (NST), which is conferred by the action of mitochondrial uncoupling protein 1 (UCP1). UCP1 acts as a proton transporter and thereby collapses the proton motive force from ATP synthesis (Mitchell 1961; Klingenberg & Winkler 1985). Brown adipocytes possess numerous multinodular lipid droplets and large amount of mitochondria (Cinti 2001). Moreover, BAT has a dense vascularization for a sufficient supply of oxygen and energy-rich substrates and a rapid distribution of heat into the circulation (Klingenspor et al. 2017). Furthermore, dense

sympathetic neural outflow into BAT is the essential determinant for its adipocytes development and thermogenic activity (Bamshad et al. 1999; Bartness et al. 2010).

Recently, another subtype of brown-like adipocytes are identified within white adipose and are often known as brite (brown in white), beige, recruitable or inducible adipocytes. The recruitment of these adipocytes is called "browning", which occurs under cold exposure (Young et al. 1984; Cousin et al. 1992; Xue et al. 2007), β_3-adrenergic stimulation (Cousin et al. 1992; Guerra et al. 1998; Himms-Hagen et al. 2000), peroxisome proliferator-activated receptor game (PPARγ) ligands administration (Petrovic et al. 2010) or alternative activation of type 2 macrophage (M2) in WAT (Nguyen et al. 2011; Brestoff et al. 2014). Also, beige adipocytes naturally develop in mice during postnatal development (Xue et al. 2007; Lasar et al. 2013). Although substantial evidence indicate that beige adipocytes are different from classical brown adipocytes in their distinctive embryonic development origins and molecular biomarkers (Petrovic et al. 2010; Wu et al. 2012; Seale et al. 2008), these recruited beige adipocytes have a high propensity for UCP1 expression and thermogenic function (Wu et al. 2012; Shabalina et al. 2013).

1.1.2 Brown adipose tissue in humans

Despite large numbers of studies proposed the essential role of BAT in energy homeostasis in rodents, its corresponding functionality in humans remains largely unclear. This is because BAT was once considered as a unique thermogenic organ only in small mammals and newborns over a long period, until the thermoactive brown fat depots have been identified in healthy adult humans by the means of ^{18}F-fluorodeoxyglucose (^{18}F-FDG) positron emission tomography and computed tomography (PET-CT) scans (Nedergaard et al. 2007; Cypess et al. 2009; van Marken Lichtenbelt et al. 2009; Virtanen et al. 2009; Gerngroß et al. 2017). More exciting, tissue biopsy specimens confirmed that human brown adipose tissue depots have molecular and biochemical properties of classical rodents BAT in terms of UCP1 expression, rich vascularization and sympathetic innervation, suggesting that they could fulfill the functional roles of BAT as in small rodents (Zingaretti et al. 2009). Based on the glucose uptake rates during PET-CT scanning, it was initially estimated that fully activated of supraclavicular BAT (63 g) in one individual could consume an amount of energy equivalent to approximately 4.1 kg of adipose tissue per year(Virtanen et al. 2009). Recently, additional PET-CT scans revealed a total volume of about 300 mL BAT in humans, whose fully

activation could strikingly consume 18 kg fat in one year (Gerngroß et al. 2017). It is, therefore, tempting to speculate that human BAT are the hopeful therapeutic targets to combat obesity.

Indeed, prolonged and repeated cold acclimation significantly increased human BAT activity, and decreased body fat mass (Lans et al. 2013). Likewise, an acute cold exposure was able to promote glucose disposal and energy expenditure, and to improve insulin sensitivity as well (Yoneshiro et al. 2013). A single dose of Mirabegron, a human-selective β_3-adrenergic agonist approved to treat bladder problems, mimics the stimulatory effects of cold on BAT, increasing resting energy expenditure by 13%, but accompanied with the non-selective activation of other β-adrenergic receptors on other tissues (Cypess et al. 2015). Moreover, it has been known that cold-induced thermogenesis is mediated through the activation of the sympathetic nervous system, and is initiated by the stimulation of transient receptor potential (TRP) channels in the sensory neurons (Nakamura 2014). The stimulation of TRP channels by some dietary components (e.g. capsinoids) are effective for enhancement of human BAT activity, thereby boosting energy expenditure and reducing body fat (Yoneshiro et al. 2012; Saito & Yoneshiro 2013; Ohyama et al. 2016; Osuna-prieto et al. 2019). Taken together, these findings inspire the attempt to find more practical and applicable therapeutic avenues to prevent obesity via activation and recruitment of BAT thermogenesis.

1.2 Thermogenic mechanisms

In mammals, a constant core body temperature is maintained by a series of physiological and biochemical adaptations to efficiently modulate rates between heat loss and heat production. Given the thermoneutral zone is around 30°C for mice (Gordon 2012) and naked humans (Kingma 2012), a lower ambient temperature activates adaptive thermogenic processes like shivering and non-shivering thermogenesis (NST) to maintain normothermia.

1.2.1 Muscle-mediated shivering thermogenesis

Cold-stimulated involuntary muscle contraction represents shivering thermogenesis, which is universally important for both birds and mammals (Hohtola 2002; Haman & Blondin 2017). Despite of the pivotal role in heat production, there are several factors restricting the long-term activation of shivering thermogenesis. Firstly, the corresponding efficiency from the chemical energy (ATP) to external output is inherently low: only about 20% of energy is converted (Jubrias et al. 2008). Secondly, the continuous muscle contraction might cause an

uncomfortable state for animals. Last but not least, several studies demonstrated that shivering reduced gradually and disappeared finally under chronic cold acclimation (Hart et al. 1956; van Marken Lichtenbelt et al. 2009; Lans et al. 2013). Therefore, other economical and effective adaptive thermogenesis must be developed in mammals to compensate for the heat loss during cold challenge.

1.2.2 UCP1-mediated non-shivering thermogenesis

In 1961, Peter Mitchell proposed an important chemiosmotic hypothesis to illustrate the relationships between respiration and ATP production (Mitchell 1961). In the respiratory chain, electrons (e⁻) are transferred from electron donors to electron acceptors (respiratory complexes) during a series of redox reactions (Fig. 1). This process couples with protons (H^+) transfer from the mitochondrial matrix to the intermembrane space. As a result, an electrochemical proton gradient is sustained across the mitochondrial inner membrane by the electron transport chain. The energy stored in the proton motive force (Δp) further drives the production of ATP via mitochondrial ATP synthase (complex V), and the return of protons H^+ into the matrix (Mitchell 1961). In brown and beige adipocytes, UCP1 is located in the mitochondrial inner membrane, which was initially named after its specific functions to transport protons back to the matrix, uncouple mitochondrial ATP synthesis from the respiratory chain and to release the energy stored in Δp as heat (Cannon et al. 1982; Nicholls & Locke 1984; Klingenspor et al. 2017).
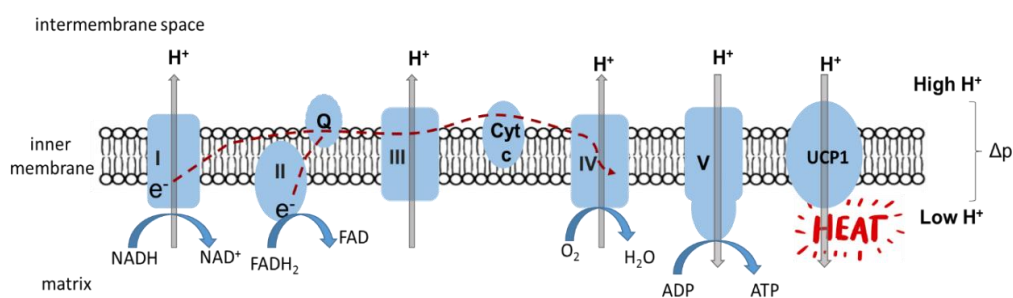
Figure 1: The mechanism of UCP1 mediated uncoupling respiration.
In the respiratory chain, electrons (e⁻) are passed from electron donors to electron acceptors (respiratory complex I and V) during a series of redox reactions. This process couples with protons (H^+) transfer from the mitochondrial matrix to the intermembrane space, which thus generates a proton gradient across the mitochondrial inner membrane. Proton motive force (Δp) is either chemically fixed in the form of ATP via ATP synthase (complex V) or dissipated as heat via UCP1.

INTRODUCTION

BAT is heavily innervated by the sympathetic nervous system (SNS) (Bamshad et al. 1999; Lowell & Spiegelman 2000). In response to nutrient status and ambient temperature, the release of norepinephrine (NE) from SNS stimulates Gs-protein coupled adrenoceptor (AR) that triggers downstream signaling cascades. All three functional β-subtypes (β_1-, β_2- and β_3-AR) co-express in brown adipocytes (Susulic et al. 1995; Atgié et al. 1997), while BAT thermogenesis principally acts through the canonical β_3-AR signaling pathway (Lafontan & Berlan 1993; Atgié et al. 1997).

Upon activation, β_3-AR signal activates adenylyl cyclase (AC), which catalyzes the cyclic adenosine monophosphate (cAMP) formation from ATP (Fig. 2). Sequentially, cAMP-dependent activation of protein kinase A (PKA) complex phosphorylates the downstream lipid droplet-associated proteins, including the lipid droplet coating protein perilipin and the hormone-sensitive lipase (HSL) (Holm 2003). Additionally, adipose triglyceride lipase (ATGL) plays a role in triglyceride catabolism (Gaidhu et al. 2010; Ahmadian et al. 2011; Li et al. 2017). The resulting dissociation of the perilipin and the activation of ATGL and HSL on the lipid droplets triggers the lipid droplet lipolysis. The released free fatty acids (FA) from the triglycerides (TG) either act as allosteric activators of UCP1 or fuel the mitochondrial β-oxidation for NST (Fedorenko et al. 2012). Furthermore, PKA also directly activates cAMP regulatory element binding protein (CREB), increasing adipogenesis (Reusch et al. 2000) and *Ucp1* gene expression (Rim & Kozak 2002; Shore et al. 2010).
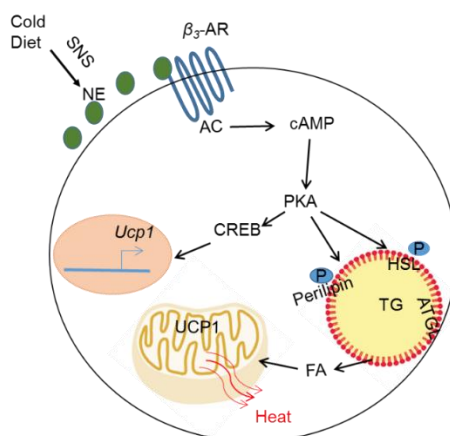
Figure 2: Canonical β_3-AR signaling pathways in brown adipocytes.
Cold or diet induces norepinephrine (NE) release from sympathetic nervous system (SNS). NE binds and stimulates Gs-protein coupled β_3-adrenoceptor (β_3-AR) and triggers the downstream signaling cascade. Upon activation, β_3-AR signal activates adenylyl cyclase (AC), which catalyzes cAMP formation from ATP. Sequentially, cAMP-dependent activation of PKA complex phosphorylates lipid droplet-associated proteins, including perilipin and hormone-sensitive lipase (HSL). Adipose triglyceride lipase (ATGL) also plays a role in lipolysis. Resulting dissociation of the perilipin from lipid droplets and the activation of ATGL and HSL on the lipid droplets trigger lipolysis. Released FA from the TG act as allosteric activators of UCP1 or fuel the mitochondrial β-oxidation. PKA phosphorylates cAMP regulatory element binding protein (CREB) to increase *Ucp1* gene expression.

INTRODUCTION

1.3   Physiological function of BAT

1.3.1   Cold-induced thermogenesis

BAT-based NST was initially identified in cold-acclimated rats (Smith et al. 1963) and hibernators (Smith & Hock 1963) but was underestimated for almost a decade (reviewed in Himms-Hagen 1984). Until 1978-1979, the elegant measurements of blood flow changes across tissues revealed the dominant contribution of BAT to heat-production following the treatments of NE (Foster & Frydman 1978) and cold-exposure (Foster & Frydman 1979). It has been estimated that BAT is adequate for 60% NST as an adaption to cold, which highlights the prominent significance of this thermogenic organ for cold-induced thermogenesis (Foster & Frydman 1979; Heldmaier & Buchberger 1985; Puchalski et al. 1987). As expected, the transgenic *Ucp1* knock-out mice (UCP1-KO) are highly sensitive to acute cold exposure at 4°C, which clearly demonstrate the essential role of BAT in thermoregulation (Enerback et al. 1997; Golozoubova et al. 2001; Liu et al. 2003; Ukropec et al. 2006; Meyer et al. 2010).

1.3.2   Diet- and meal-induced thermogenesis

It is generally accepted that BAT hold great promises to defend against obesity via the implement of diet induced-thermogenesis. This observation was initially described in overfeeding rats, whose metabolically active BAT contributed significantly to enhanced energy expenditure and thus limited the profound increases in body weight gain (Rothwell & Stock 1979). Consistently, several transgenic mice with defective brown fat were susceptible to gain more body weight at room temperature. For example, UCP1-DTA mice, which were generated by introduction of toxin under the control of *Ucp1* promoter, developed obesity under a regular chow diet (Lowell et al. 1993). The *β*-less mice that lack all three subtypes of *β*-ARs gained more body weight than control mice under a chow diet, and became markedly obese when they were fed with a high-fat diet (HFD) (Bachman et al. 2002). In similar, the germline UCP1-KO mice developed a late-onset obesity consuming HFD (Kontani et al. 2005). Despite of the strong correlations between BAT function and reduced body weight gain, conflicting results were demonstrated by others that UCP1-KO mice consuming a HFD were not prone but rather resistant to diet-induced obesity at room temperature (Enerback et al. 1997). To explain the discrepancy, one study proposed that the importance of housing mice at thermoneutral condition (Feldmann et al. 2009). Since the UCP1-KO are sensitive to cold exposure, the normal laboratory housing environment at an ambient temperature of 23°C

represents a chronic mild cold acclimation to mice (Feldmann et al. 2009). In this scenario, alternative UCP1-independet thermogenic mechanisms are largely recruited in UCP1-KO mice. Therefore, to eliminate thermal stress, it is of importance to investigate BAT-mediated thermogenesis at thermoneutrality (Feldmann et al. 2009). Indeed, UCP1-KO mice only developed more diet-induced obesity than their WT controls at thermoneutral condition (Feldmann et al. 2009). However, again, their observations were not reproducible by the other studies, when the HFD feeding experiments were conducted at an ambient temperature of 20°C or under a sub-thermoneutral conditions of 27-28°C (Liu et al. 2003; Anunciado-Koza et al. 2008). In conclusion, the paradoxical response of UCP1-KO to prolonged HFD feeding raises the crucial question whether UCP1 plays a role in the controlling of whole-body energy expenditure and body fat.

In addition to diet-induced thermogenesis during the long-term overfeeding on palatable cafeteria-diets, a thermogenic effect was also seen after a single meal in both rodents and humans, which is normally known as the postprandial thermogenesis, meal-induced thermogenesis or meal-associated thermogenesis (Glick et al. 1981; Vosselman et al. 2013; Din et al. 2018; Li and Schnabl et al. 2018). It has been recently revealed that a single meal triggers the secretin release from gut to activate BAT thermogenesis, which consequentially promotes satiation (Li and Schnabl et al. 2018). The identification of the unknown BAT function in the regulation of satiation may provide novel treatment alternatives for obesity or diabetes.

1.4 Molecular control of *Ucp1* gene expression

Given BAT's metabolic benefits, it is highly important to identify potential factors or modulators that could active brown adipocyte differentiation and enhance *Ucp1* expression. The *β*-ARs signaling cascades are the principal activator pathways for brown/beige fat thermogenesis and adipocyte development in response to various physiological or pharmacological inducements. Since UCP1 protein abundance is largely dependent on the levels of *Ucp1* gene transcription, a detailed understanding of *Ucp1* gene pre-transcriptional control is the crucial prerequisite for understanding the effects of various stimuli on BAT-mediated thermogenesis. Previous studies have proposed two cis-regulatory DNA sequences in *Ucp1* gene, including a proximal promoter region and a distal enhancer box. In rodents, the former region represents the basal *Ucp1* gene promoter and contains biding sites for cAMP response element binding protein (CREB) and CCAAT/enhancer binding protein (C/EBP).

16

INTRODUCTION

While the cis-regulatory elements are required for specific *Ucp1* expression in brown fat cell and for stimulatory responsiveness to norepinephrine and cold exposure (Cassard-Doulcier et al. 1993; Cassard-Doulcier et al. 1998; Kozak et al. 1994). This complex enhancer region is composed of peroxisome proliferator-activated receptor (PPAR) response elements, retinoic acid (RA) response elements, cAMP response elements and elements responsiveness to thyroid hormone and estrogen-related receptor α (Rial et al. 1999; Rim & Kozak 2002). Their corresponding transcriptional regulators powerfully regulate *Ucp1* gene expression and adipocytes adipogenensis.

In vitro, activation of PPARg response element significantly increased *Ucp1* expression in brown preadipocytes (Sears et al. 1996). *In vivo*, prolonged PPARg agonist administration substantially increased mitochondrial biogenesis, UCP1 expression and beige adipocytes recruitment in typical white adipose tissue (Koh et al. 2009; Petrovic et al. 2010). Afterwards, PPARg coactivator α (PGC-1α) is identified as a cold-induced PPARγ-binding partner in brown adipocytes (Puigserver et al. 1998). Loss of the PGC-1α in BAT significantly decreases *Ucp1* abundance but without any changes in brown adipocytes differentiation, suggesting that PGC1 is essential for *Ucp1* expression, but is dispensable for the determination of brown fat cells (Uldry et al. 2006; Kajimura & Saito 2014)

The molecular basis for the specific development and identity of brown adipocytes remains unknown until the identification a 140 kDa PR (PRD1-BF1-RIZ1 homologous)-domain-containing protein (PRDM16) (Seale et al. 2007). PRDM16 is preferentially expressed in brown adipocytes than the typical white adipocytes and PRDM16 functions directly through protein-protein interactions with PPARg, PGC1α and C/EBP-β (Seale et al. 2008; Kajimura et al. 2009). Interestingly, exogenous expression of PRMD16 in either white progenitors or myoblast results in robust brown-fat phenotypes, evidenced by increased expression of browning maker genes and enhanced uncoupling respiration (Seale et al. 2007; Seale et al. 2008). Prdm16 powerfully regulates thermogenic programs of the subcutaneous WAT *in vivo* (Seale et al. 2011; Cohen et al. 2014). Furthermore, Prdm16 is sufficient to turn off the expression of key white-fat selective gene expression in BAT, maintaining brown adipocyte molecular and functional features (Harms et al. 2014).

The vitamin-A derivative RA has also been identified as a strong trans-activator of *Ucp1* gene expression and cell differentiation in brown adipocytes (Larose et al. 1996). Retinoid acid receptor (RAR) and retinoid-X receptor (RXR) are the major ligand-dependent transcriptional

factors that bind to elements in the *Ucp1* enhancer in response to different isomers of RA (Alvarez et al. 2000; Teruel et al. 2003; Schlüter et al. 2002).

1.5   Modalities to visualize thermogenic fat

A series of general techniques have been developed to assess BAT and its thermogenic function, by testing the changes in BAT fat mass, lipid droplet content, thermogenic marker genes expression (mainly UCP1) and the core body temperature (Virtue & Vidal-Puig 2013). It would be compelling when interpreting these data in combination with the whole-organism metabolism.

1.5.1   PET-CT scanning

Until now, ^{18}F-FDG PET-CT scanning is the major imaging approach for functional detection and characterization of BAT activity for humans and is widely used in model animals, although it has several limitations. Firstly, the radioactive traces used for imaging are problematic for human subjects, and the glucose derivatives might elevate blood sugar as well, particularly for diabetic patients. Secondly, radiological imaging only provides a snapshot of BAT prevalence based on substrate uptake and thereby might underestimate BAT thermogenesis. Lastly, the β_3-adrenorecptor agonist (CL-316,243) induced ^{18}F-FDG uptake into the BAT of UCP1-KO mice, implying the existence of UCP1-independent glucose metabolisms (Olsen et al. 2017). Additional PET-CT scans using ^{18}F-fluoro-thia-heptadecanoic acid (^{18}FTHA) has also been used to study BAT thermogenesis in humans, which requires radioactivity as well (Din et al. 2016). Therefore, more reliable and safe imaging strategies are urgently needed.

1.5.2   Emerging imaging technology

It is widely known that BAT-based thermogenesis requires large amounts of nutrients and oxygen delivered by blood flow. Multiple imaging methodologies thus use the principle of blood flow or oxygen consumption as an analogue to BAT activity. For example, functional magnetic resonance imaging (MRI) has been developed to define BAT deposits and to track the changes in BAT sizes and chemical depositions in intact animals, whereas MRI has the inherently low resolution and could not distinct small deposits of brown fat from its surrounding white adipose tissue (Sbarbati et al. 1991; Zancanaro et al. 1994; Sbarbati et al. 1997; Branca et al. 2014).

INTRODUCTION

Recent studies have introduced contrast ultrasound (CU) (Baron et al. 2012) and high-resolution laser-Doppler as novel noninvasive approaches to monitor and characterize the activation of BAT in rodents by measuring blood flow (Abreu-vieira et al. 2015). Near-infrared (NIR) fluorescence imaging permits to measure blood flow to BAT in a noninvasive manner, but its non-specific and insensitive variable NIR signals were detected in lung, liver, and spleen (Nakayama et al. 2003). However, blood flow based technologies have been questioned recently as the adrenergic stimulation of blood flow was preserved in *Ucp1*-KO animals, indicating that BAT blood flow is not a convincing parameter for the estimation of BAT activation and heat generation in rodents (Abreu-Vieira et al. 2015). A straightforward measurement of BAT temperature using infrared imaging allows for the sensitive visualization of BAT activation, but provides only dorsal surface temperature changes without directly quantifying BAT-thermogenesis capacity (Crane et al. 2014). Very recently, a label-free non-invasive imaging of BAT activation and the BAT metabolic activity was established based on hemoglobin signals (Reber and Willershäuser et al. 2018).

Therefore, in the future it would be critical vital to combine different imaging and quantifying methods to determine BAT activity following various metabolic prompts.

1.5.3 Reporter genes system

To monitor endogenous *Ucp1* expression, multiple reporter gene mouse models have been generated by using luciferase or fluorescent proteins (Galmozzi et al. 2014; Mao et al. 2017; Rosenwald et al. 2013). Firefly luciferase-based bioluminescent imaging is increasingly becoming widely utilized as an effective biomarker for optical imaging in terms of robust bioluminescence emission over a wide dynamic range of detection. For example, ThermoMouse (*luciferase2-T2A-tdTomato*) conveys a mutagenesis encoding luciferase, T2A peptides and tdTomato proteins driven by UCP1 promoter, was capable of monitoring changes in *Ucp1* expression. However, the *luciferase2-T2A-tdTomato* cassette was randomly inserted into the Y chromosome, restricting the usage of the imaging in male mice only (Galmozzi et al. 2014).

Additionally, green fluorescent protein (GFP) or GFP-like fluorescent proteins that are normally operated in the visible spectrum have been adapted for extensive biological applications and are invaluable transgenic tools for optical imaging (Richie et al. 2018). For example, ThermoMouse (tdTomato), UCP1-GFP and UCP1-CreER: ROSA-tdRFP mice were generated to transiently or permanently label *Ucp1*-positive adipocytes, respectively.

Moreover, another *Ucp1*-2A-GFP reporter mouse was constructed with a CRISPR-Cas9 approach, in which GFP intensity serves as a surrogate of UCP1 protein expression *in vitro* (Qiu et al. 2018). However, all the fluorescent proteins utilized above have notable limitations due to restraints on light penetration through the surrounding biological tissue, and still requires sacrifice of the animal and tissue dissection. Therefore, none of the above reporters models generated so far is suitable for monitoring *Ucp1 in vivo* imaging. The application of the next-generation fluorescent protein like NIR can therefore be preferable reporters for *in vivo* and *ex vivo* optical imaging applications.

1.6   Aims of the present work

Obesity develops when energy intake constantly exceeds energy expenditure. This global pandemic disease is often associated with type 2, cardiovascular problems and many intercurrent diseases (Tseng et al. 2010). Current therapeutic strategies for obesity treatment are normally accomplished by decreasing energy uptake through bariatric surgery or administration of appetite suppressants. However, these procedures have many various side effects (Encinos et al. 2006). The rediscovery of active BAT in adult humans offers efficacious and safe possibilities to remedy obesity by promoting energy expenditure (Cypess & Kahn 2013). The subsequent testing and validation of novel agents that increase BAT activity necessitates accurate pre-clinical measurements in rodents regarding the *Ucp1* expression and the capacity for BAT-mediated NST. In this regard, a new reporter gene mouse model C57BL/6NTac-*Ucp1*[tm3588 (LUC-T2A-iRFP-T2A-Ucp1) Arte] was established.

The first aim of this dissertation was to verify whether reporter genes coding for firefly luciferase (LUC) and near-infrared fluorescent protein (iRFP713) in the *Ucp1-LUC-iRFP713* reporter mice could fulfil the requirements to track the changes in endogenous *Ucp1* expression. Afterwards, the reporter mice were used to profile the putative presence of *Ucp1*-expressing cells in adipose and non-adipose tissues. In addition, the primary brown and beige adipocytes isolated from reporter mice was utilized as the *in vitro* imaging system to search for new chemicals in the control of *Ucp1* gene expression.

To simultaneously express three separate proteins of LUC, iRFP713 and UCP1, Thosea asigna virus 2A (T2A) peptides were added to the N-terminus of LUC and iRFP713, respectively. The second aim of the study was to investigate whether the insertion of the reporter gene cassette affects endogenous *Ucp1* gene expression or the BAT functionality. Molecular analysis revealed the drastically reduced UCP1 expression in interscapular BAT

(iBAT) and in inguinal WAT (iWAT). Therefore, this reporter mouse model was further used as a new model to test the role of UCP1 in cold induced thermogenesis and in the protection against diet-induced obesity.

2 MATERIAL AND METHODS

2.1 Animal experiments

2.1.1 Generation of reporter mouse model by Taconic Biosciences GmbH

The *Ucp1* reporter gene mouse model (C57BL/6NTac-*Ucp1*[tm3588 *(LUC-T2A-iRFP-T2A-Ucp1) Arte*]) was generated on a C57BL/6N background by Taconic Biosciences GmbH. The *LUC-T2A-iRFP713-T2A* cassette contains a 2706 base pairs (bp) exogenous DNA encoding a firefly luciferase (LUC) and the near-infrared fluorescent protein 713 (iRFP713) and Thosea asigna virus 2A (TA2) peptides, which was inserted into the 5'-untranslated region (UTR) of the endogenous *Ucp1* gene using homologous recombination (Fig. 3). The piRFP vector was kindly donated by Prof. Dr. Vladislav Verkhusha of Department of Anatomy & Structural Biology at Albert Einstein College of Medicine (USA) and the firefly luciferase vector was provided by Promega. The T2A sequence allows for the individual translation of multiple proteins during translation (Donnelly et al. 2001; Doronina et al. 2008; Kim et al. 2011). In addition, FRT-flanked puromycin resistance cassette is utilized to enable the embryonic stem cell selection.
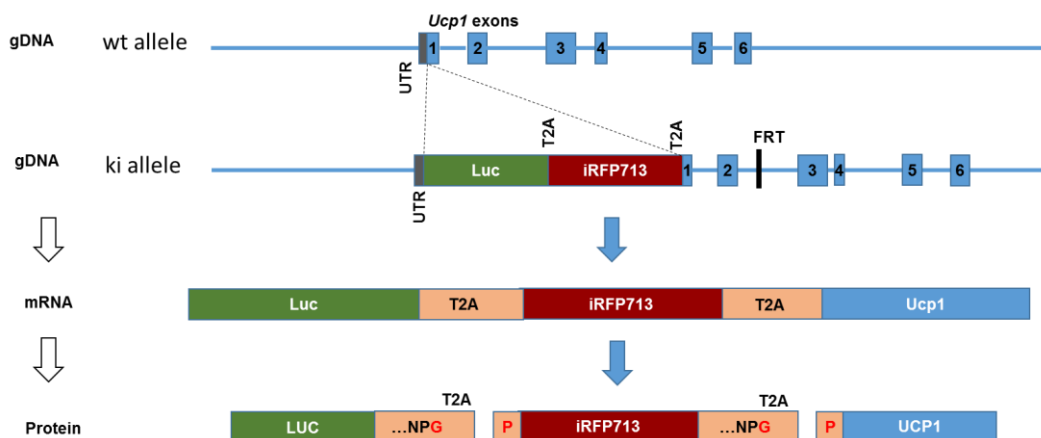
Figure 3: Schematic diagram of *Ucp1*-LUC-iRFP713 knock-in cassette in genome.
The foreign DNA sequences expressing LUC, iRFP713 and T2A under the control of cis-regulatory elements of the *Ucp1* gene, was inserted into the mouse genome by homozygous recombination. Specific forward and reverse primers were indicated with the black arrows (Figures modified from.Wang et al.2019).

The genomic DNA (gDNA) comparison between WT and KI alleles is shown in Appendix 1. Matched littermates were obtained by mating heterozygous male (HET) with homozygous female (HET) reporter mice. All litters were weaned at 21 day after birth, and ear punches were collected and digested for genotyping. Primer pair for genotyping was offered by

Taconic Biosciences GmbH. Primers were produced by Eurofins Genomics (Ebersberg/Germany):

Forward AGACTTTCCCAAACAGCACG

Reverse CTTTCATTGGCCAACCGAG

The polymerase chain reaction (PCR) was conducted using the following program (Table 1).

Table 1: PCR reaction program for genotyping

Program	Temp	Time	
Initialization	95°C	5 sec	
Denaturation	95°C	30 sec	
Annealing	60°C	30 sec	35 cycles
Elongation	72°C	60 sec	
Final elongation	72°C	10 sec	
Cooling	4°C	-	

2.1.2 Animals housing

Unless otherwise stated, all experimental procedures were performed in specified-pathogen-free (SPF) animal facility at the Kleintierforschungszentrum Weihenstephan, at room temperature of 23 ± 1°C, with 12h-light/12h-dark. Mice had the free access to water and a chow diet (SSniff Spezialdiäten GmbH, Germany), except when stated otherwise. All experiments and animal husbandry were conducted in accordance with German animal welfare law and were approved by the regional government of Upper Bavaria, Germany (approval number: ROB-55.2-2532.Vet_02-16-159). Body weight was determined using a precision balance. Non-invasive body composition (including absolute body fat mass and lean mass) was quantified by nuclear magnetic resonance spectrometer (NMR, Minispec, Bruker). The rectal body temperature was measured with a rectal probe (temperature measuring device ALMEMO, Ahlborn, Germany), and Vaseline was used as a lubricant.

2.1.3 Visualization and quantification of luciferase activity *in vivo* and *ex vivo*

IVIS® Lumina (Xenogen) instrument was utilized to image *in vivo* firefly luciferase bioluminescence. All mice were anesthetized (intraperitoneal injection, i.p.) by a mix of Medetomidinehydrochlorid (0.5 mg/kg, Dorbene vet, Zoetis), Midazolam (5 mg/kg, Dormicum, Roche) and Fentanyl (0.05 mg/kg, Fentadon, Albrecht). The fur of C57BL/6N mice quenched the bioluminescence, thus the fur above region of interest (ROI) was removed

with an electrical razor (Veet Sensitive Prescision) and a depilatory cream (Veet). To avoid the thermal stress during the above procedure, anesthetized mice were placed on an electric heating pad. After injection of firefly luciferase substrate, D-luciferin (150 mg/kg, i.p., VivoGlo™ Luciferin, Promega GmbH), firefly luciferase catalyzes a chemical reaction where D-luciferin is converted to oxyluciferin. During the process, the energy is released in the form of light. Based on this, mice were imaged every 2 min using the IVIS® Lumina Imaging System, the settings of 60 sec exposure, small binning, F/Stop of 1 open emission filter, and 12.5 cm field of view. To quantify *in vivo* bioluminescence, light intensity from ROI was assessed with the imaging software Version 2.6 (Xenogen).

For *ex vivo* bioluminescence imaging, another commercial membrane-permeable D-luciferin (PJK GmbH) was used. Freshly excised tissues were directly sprayed with the D-luciferin just prior to imaging under a charge-coupled-device (CCD) camera (Hamamatsu 1394 ORCA II-ERG) with 60 sec exposure time.

To quantify *ex vivo* bioluminescence in frozen tissues, another luciferase assay system (E4030 Freezer Pack, Promega GmbH) was utilized, which contains 5 x lysis buffer and a D-luciferin as substrate. For every 100 mg tissue, 313 µl 1 x diluted lysis buffer was added and the mixture was immediately homogenized for 30 sec on ice, using a Miccra D-1 homogenizer (Miccra GmbH) (Manthorpe et al., 1993). Afterwards, the mixture was centrifuged with 10,000 g at 5°C for 3 min using the Eppendorf 5417R refrigerated centrifuge. The resulting supernatant was collected afterwards. For quantification of luciferase activity, 96-well white-bottom microplates (Greiner Bio-one) containing 10 µl sample supernatant were immediately placed into the microplate luminometer (Infinite M200 reader, Tecan). Inside the luminometer, 50 µl D-luciferin solutions were automatically injected into each sample and shaken for 2 sec prior to measurements. Another 30 µl supernatant was used for quantification of protein concentration. Bioluminescent readout was normalized to the protein concentrations of each sample.

2.1.4 Repeated CL316, 243 injection

Mice were administrated (intraperitoneal injection, i.p.) with the β_3-adrenergic receptor agonist CL316, 243 (Tocris Bioscience, 1.0 mg/kg) for 5 consecutive days at an age of 13 weeks. While the control mice were injected with a vehicle of phosphate-buffered saline (i.p., 0.9% NaCl, B. Braun Melsungen AG). After *in vivo* imaging, mice were killed to compare the *ex vivo* luciferase activity and the expression of *Ucp1* on both RNA and protein levels.

2.1.5 Chronic cold acclimation

By study design, male WT, HET and KI mice were born at room temperature (23 ± 1°C, RT). At an age of 10 weeks, animals were divided into two groups: one was continuously kept at RT, while the other was exposed to a weekly decreasing ambient temperature from 18°C, 15°C, 10°C to 5°C, which was performed inside a controlled climate cabinet (HPP750life, Memmert GmbH + Co. KG). Within the cabinet, animals were housed in groups of 2-3 individuals in type II cages (370 cm^2, Tecniplast GmbH) with free access to food and water. Body weight of the mice was determined weekly starting from an age of 4 weeks. Rectal body temperature and body composition were measured every two weeks starting from an age of 10 to 14 weeks. After 7 days at 5°C, mice acclimated to 23°C or 5°C were assessed by measuring *in vivo* luciferase bioluminescence or iRFP713 fluorescence. Afterwards, mice were killed to compare the *ex vivo* luciferase activity and the expression of *Ucp1* on both RNA and protein levels.

2.1.6 Detection of iRFP713

To detect the *ex vivo* iRFP713 fluorescence, tissues were dissected from 5-weeks old WT, HET and KI male mice and immediately scanned using an Odyssey infrared imager (LI-COR Biosciences GmbH) with a 700 nm excitation wavelength (Wang et al. 2018).

For *in vivo* iRFP713 detection, male animals were kept either at room temperature or under prolonged cold acclimation (from 18°C, 15°C, 10°C to 5°C) as described above (section 2.1.4). Three days before imaging, all mice received an alfalfa-free diet (Experimental diet 2222, Provimi Kliba) to reduce the food auto-fluorescence. During the measurement day, WT, HET and KI mice kept at the same ambient temperature were anesthetized with 2-3% isofluran (Isothesia, Henry Schein Vet Pharma). The fur of the mice above the interscapular region was removed and all mice were placed on an electronic heating pad during imaging. A 670 nm wavelength laser (300 mW, BWF1-670-300E, B&W Tek, Inc.) initiated the excitation of iRFP713, while a 740/40 nm filter (Chroma Technology) was used to detect the fluorescence emission in a iXon electron multiplying charge-coupled device (EMCCD, DV897DCS-BV, Andor Technology) (Wang et al. 2018).

For cryoslicing, one WT and one KI mouse were immediately killed and frozen at -80°C after *in vivo* iRFP713 imaging. Then the mice were sectioned with a Leica CM 3500 cryostat (CM3500, Leica, Wetzlar, Germany) to a slice of 20 μm at -17°C. The cylindrical block was

imaged after every two slices, which yielded a 40 μm resolution at the sectioning axis (z-axis). The imaging system consisted of a highly sensitive fluorescence camera, mounted onto the cryostat (Sarantopoulos et al. 2011). Three reflectance images at 630/60 nm (red channel), 535/38 nm (green channel) and 460/50 nm (blue channel) for color imaging and one fluorescence image at 730/50 nm, which is close to the maximum emission of the iRFP713 (i.e. 713 nm), were acquired at each sectioning loop. A halogen light sthece (KL2500, Schott AG, Mainz, Germany) coupled to a fiber bundle projected the white-light required for the color imaging, while fluorescence was induced by a 670 nm continuous wave diode laser (BWF1-670-300E, Polytec, Waldbronn, Germany). The imaging system and acquisition protocol was fully automated. The custom software was implemented in LabView (National Instruments, Austin, USA) to analyze iRFP713 brightness (Symvoulidis et al. 2014).

2.1.7 Indirect calorimetry, basal metabolic rate and NST capacity

Indirect calorimetry was performed using the LabMaster (TSE Systems, Germany). During experiment, oxygen consumption (VO_2, ml/h), carbon dioxide production (VCO_2, ml/h) and respiratory exchange rate (RER, VCO_2/VO_2 ratio) of each cage were recorded. The resulting heat production (HP) was calculated according to the following metabolic equation (Heldmaier 1975): HP (mW) = (4.44 + 1.43 * RER) * VO_2 (ml/h)

To determine the basal metabolic rate (BMR), mice were single housed in metabolic cages (3L volume) with no access to water and food. During the measurement, metabolic cages were positioned inside a controlled climatic cabinet (TPK 600, Feutron, Germany), preconditioned to 30°C. Every cage was connected to a temperature sensor and was recorded in 4 min intervals over a period of 4 h. BMR was calculated from the lowest mean of three consecutive VO_2 (ml/h). After BMR measurements, mice were briefly removed from the climate cabinet. Every single mouse was injected subcutaneously with 1 mg/kg norepinephrine (NE, Arterenol, Sanofi, Paris/France), and was placed back into the climate cabinet at an ambient temperature of 26°C. As above, changes of VO_2 (ml/h), VCO_2 (ml/h) and RER were continuously recorded in 2 min interval for 60-70 min. Non-shivering thermogenesis (NST) capacity was calculated from the differences between the BMR and the highest NE-induced heat production (NEmax) reached within 20-30 min post NE injection.

To compare the maximal cold-induced heat production (HPmax) among genotypes, WT, HET and KI mice were measured in 4 min intervals with decreasing ambient temperature. On the

measurement day, the ambient temperature of each mouse was lowered stepwise from 30°C, 25°C, 15°C, 10°C, 5°C, to 0°C, with each temperature maintained for 45-90 min until a stable reading could be observed. The whole measurement lasted up to 8 h, while no food or water was supplied. The resting metabolic rate (RMR) at each temperature was defined as the lowest O_2 readings, while the maximal heat production (HPmax) was calculated from the highest MR observed in a non-exercising mouse.

2.1.8   High-fat diet feeding experiment

Animals were born and maintained at either room temperature (23°C) or at thermoneutrality (30°C), in a controlled climate cabinet (HPP749 and HPP750life, Memmert, Castrop-Rauxel, Germany).

Male (8 weeks-old) and female (9 weeks-old) mice first received a semi-purified control diet (CD, ~12 kJ% fat, Sniff Spezialdiäten GmbH, Germany) for 4 weeks. Afterwards, half of the mice were fed a high-fat diet (HFD, ~48 kJ% fat, Sniff Spezialdiäten GmbH, Germany) *ad libitum* for a period of 8 weeks, while the other mice maintained on CD. The comparison of the diets is included in Appendix 2. Body weight was determined weekly. After the start of HFD feeding, fat mass and lean mass were determined by NMR (Minispec, Bruker) in a two-week interval. The rectal body temperature was measured with a rectal probe (temperature measuring device ALMEMO, Ahlborn, Germany) and Vaseline was used as a lubricant.

At the end of the experiment, two mice of the same genotype fed either a CD or HFD were imaged using IVIS® Lumina (Xenogen) as mentioned above (section 2.1.2). Afterwards, organs were removed for analysis of *Ucp1* mRNA and UCP1 protein expression as well as *ex vivo* bioluminescence.

2.2   Cell cultivation

2.2.1   Primary cell culture

For primary cell culture, stromal vascular fraction (SVF) cells were isolated from iBAT and iWAT of 5-6 weeks old male KI mice using 1mg/ml collagenase (Biochrom) for digestion. Preadipocytes was proliferate in standard culture medium with 20% fetal bovine serum (FBS, Sigma) (Table 2).

MATERIAL AND METHODS

Table 2: Recipe for basal culture medium

Culture medium	Used for 50 ml
DMEM high glucose (Sigma)	40 ml
FBS (Biochrom)	10 ml
Gentamycin (10mg/ml) (Biochrom)	200 µl
Penicillin/streptomycin (10 mg/ml) (Biochrom)	200 µl
Amphotericin B (Fungizone) (Biochrom)	100 µl

Reaching 90% confluence, cell cultures were initially administrated with 2-days induction medium (Table 3) followed by 7-days differentiation medium (Table 4).

Table 3: Recipe for induction medium

Induction medium	Used for 50 ml
DMEM high glucose (Sigma)	40 ml
FBS (Biochrom)	10 ml
Gentamycin (10mg/ml) (Biochrom)	200 µl
Penicillin/streptomycin (10 mg/ml) (Biochrom)	200 µl
Insulin (Sigma)	850 nM
Triiodo-L-thyronine (T3, Sigma)	1 nM
3-isobutyl-1-methylxanthin (IBMX, Sigma)	500 µM
Dexamethason (Sigma)	1 µM
Indometacin (Sigma)	125 µM
Rosiglitazone (Biomol)	1 µM

Table 4: Differentiation medium recipe

Differentiation medium	Used for 50 ml
DMEM High glucose (Sigma)	40 ml
FBS (Biochrom)	10 ml
Gentamycin (10mg/ml) (Biochrom)	200 µl
Penicillin/streptomycin (10 mg/ml) (Biochrom)	200 µl
Insulin (Sigma)	850 nM
T3 (Sigma)	1 nM

2.2.2 Imaging and quantification of bioluminescence in living cells

The modest cell permeability of D-luciferin allows for the imaging of luciferase activity in living cells. To do so, the fully differentiated adipocytes were directly treated with pre-warmed

D-luciferin working solution (150 µg/ml) just prior to imaging bioluminescence using the IVIS® Lumina instrument (Xenogen).

To quantify luciferase activity *in vitro*, Luciferase Assay System E4030 Kit (Promega GmbH) was used. Cells were washed gently with PBS for twice, and 1 x reporter lysis buffer (E4030 Kit, Promega) was added onto cells, shake 20 min, at RT. Fifty µl D-luciferin solution and 10 µl cell culture lysed sample were mixed in a tube for 6 sec, which were inserted into the Single Tube Luminometer (Titertek-Berthold GmbH). The relative bioluminescence unit (RLU) was normalized to the corresponding protein concentration of single samples.

2.2.3 Establishment of immortalized brown fat cell line

Although primary cell cultures supply controlled complement to animal experiment *in vitro*, primary preadipocytes retain low proliferative capacity over passaging. To circumvent this problem, immortalized brown fat cell line was established via retrovirus mediated Simian virus 40 large T antigen (SV40 LT) expression (Klein et al., 2002). The protocol for immortalization was describes as following. Firstly, 5 µg pBABE-puro SV40 LT plasmid DNA (donated from Professor C. Ronald Kahn) was transduced into Bos23 virus packing cell line through calcium-phosphate-precipitation method. After 48 h incubation, retrovirus-containing medium was collected using a 0.45 µm filter. Meanwhile, cells of SVF were isolated from 5 weeks 129S6sv/evTac mice. At 70-80% confluence, preadipocytes was transfected with 1 ml virus mixture, including SV40LT retrovirus-containing medium (200 µl), fresh culture medium (800 µl), and polybrene (2 mg/ml, Sigma). At 90-100% confluence, preadipocytes were splitted into a 15cm plate (P1), and a culture medium containing 2 ug/ml puromycin (Sigma) were added to select the positively transfected cells.

2.2.4 Cellular oxygen consumption rate

Cellular respirometry was conducted by XF96 extracellular flux analyzer (Seahorse Bioscience). Initially, the oxygen consumption rate (OCR, pMol/min) of mature adipocytes was firstly recorded at the baseline. Sequentially, the following chemicals were injected: oligomycin (5 µM Biomol), isoproterenol (1 µM, Sigma), carbonyl cyanide-p-trifluoromethox-yphenyl-hydrazon (FCCP, 1 µM, Sigma) and Antimycin A (5 µM, Sigma) into each well, according the protocol previously published (Li, et al., 2014). Oligomycin is an inhibitor for complex V in the respiration chain, inhibiting ATP-synthase and leaving basal leak respiration. Next, isoproterenol drives the *Ucp1*-mediated respiration via the canonical

β-adrenergic signaling pathway. Then, an unspecific uncoupling reagent, (FCCP), allows for maximal leak respiration. Lastly, Antimycin A allows to quantify the non-mitochondrial respiration by inhibition of complex III and I. The detailed Seahorse program is shown in Appendix 3. UCP1-dependent respiration was calculated by subtracting basal leak respiration from isoproterenol-induced leaking capacity.

2.3   Molecular analyses

2.3.1 RNA isolation and RT-qPCR

Frozen tissues were homogenized for 20 sec in 500 µl TRIsure (Bioline) using MiccraD Homogenizer (Miccra GmbH). Homogenates were incubated at RT for 5 min, then centrifuged with 2500 g at 4°C for 5 min. After centrifugation, clear liquid products between pellets and fats were transferred into a new Eppendorf tube containing 100 µl chloroform (Carl Roth). The mixture was vigorously shaken for 15 sec, incubated at RT for 3 min, and centrifuged with 12.000 g at 4°C for 15 min. Afterwards, chloroform functions to separate the mixed solution into three immiscible layers: a green phenol-chloroform phase in the bottom, a white interphase, and a colorless watery phase on the top. Containing total RNA, the top liquids were transfer into a fresh Eppendorf tube and mixed with 500 µl 75% ethanol in edetic acid (EDTA) water. All mixed solution were transferred into column from the SV Total RNA Isolation kit (Promega GmbH), then centrifuged with 8000 g at RT for 15 sec and the flow was discarded. Next, the RNA washing and DNase digestion was processed according to the quick protocol of SV Total RNA Isolation kit (Promega). Total RNA was eluted into 30 µl DNase/RNase free-water. RNA concentration was quantified with Infinite M200 Microplate reader (Tecan). To synthesize cDNA, total RNA was reverse transcribed with SensiFast cDNA Synthesis Kit (Bioline) (Table 5), using the program in Table 6.

Table 5: SensiFAST cDNA Synthesis systems

Solutions	Used for 10 µl
Total RNA	500 ng
5x Buffer	2 µl
Reverse Transcriptase	0.5 µl
DNase/RNase free-water	Up to 10 µl

Table 6: SensiFAST cDNA Synthesis program

Program	Temp	Time
Primer annealing	25°C	10 min
Reverse transcription	42°C	15 min
Inactivation	85°C	5 min
Cooling	4°C	-

For real-time quantitative PCR (RT-qPCR), acquired cDNA products were diluted in a factor of 1:10. SensiMix SYBR® No-ROX Kit (Bioline) and specific RT-qPCR primers were utilized (Appendix 4). All reactions were performed in 384-well plates using LightCycler 480 instrument II (Roche) according to the protocol and program in Table 7 and 8.

Table 7: RT-qPCR reaction system compositions

Solutions	Used for 12.5 µl /well
SensiMix SYBR®	6.25 µl
primer forward (100 nM)	0.03125 µl
primer reverese (100 nM)	0.03125 µl
DNase/RNase free-water	5.19 µl
cDNA	1µl (1:10 diluted)

Table 8: RT-qPCR reaction program

Program	Temp	Time	
Initialization	95°C	7 min	
Denaturation	97°C	10 sec	
Annealing	53°C	15 sec	45 cycles
Elongation	72°C	20 sec	
Melting curve	60-95°C	31 sec	

2.3.2 Droplet digital PCR (ddPCR)

To determine the absolute transcripts from the WT allele and KI allele in heterozygous UCP1 knock-in mice (*Ucp1^{wt/ki}* (HET)), droplet digital PCR (ddPCR) was performed on cDNA of iBAT (1:60 dilution) of HET knock-in mice. The primer pairs amplifying *Ucp1* exon1 in WT allele and LUC in KI allele were identical to those applied in RT-qPCR (Appedix 4). Allele-specific probes labeled with carboxyfluorescein (FAX) and hexachloro-fluorescein (HEX) fluorescent dyes were designed as follows:

FAM-WT allele probe: 5'-FAM-TGCCAGGCAAGCTGAAACTCC-Quencher-3';

HEX-KI allele probe: 5'-HEX-CTCTCCAGCGGTTCCATCTTCCAG-Quencher-3'.

Both hydrolyzed probes were synthesized by Eurofins genomics (Eurofins MWG Operon, Ebersberg/Germany) and were diluted with Eurofins aqueous probe buffer to a stock solution of 100 nM. To ensure the probe homogeneity, the above mixed solution was vigorously vortexed for 10 min. Then the mixtures of probes and primers were prepared according to the Bio Rad manufacturer's instructions (BIO-Rad 2014) as shown in Table 9.

Table 9: ddPCR maxiMIX for probe and prime

MaxiMIX for FAM probe	Used for 20 µl	MaxiMIX for HEX probe	Used for 20 µl
Ucp1 exon1 Primer forward (100 nM)	3.6 µl	LUC primer forward (100 nM)	3.6 µl
Ucp1 exon1 primer reverse (100 nM)	3.6 µl	LUC primer reverse (100 nM)	3.6 µl
FAM probe (100 nM)	1.0 µl	HEX probe (100 nM)	1.0 µl
DNase/RNase free-water	11.8 µl	DNase/RNase free-water	11.8 µl

Next, ddPCR reaction system was arranged according to Table 10, 21 µl out of the reaction buffer and 70 µl ddPCR droplet generation oil (Bio-Rad) were separately loaded on the disposable DG8™ cartridges (Bio-Rad), which was inserted QX200™ droplet generator (Bio-Rad) to generate 20000 nanoliter-sized droplets for each sample.

Table 10: ddPCR reaction system

Solutions	Used for 23 µl
2x ddPCR buffer	11.5 µl
MaxiMIX for FAM probe	1.15 µl
MaxiMIX for HEX probe	1.15 µl
cDNA	2.0 µl
DNase/RNase free-water	11.8 µl

Afterwards, 40 µl droplets were picked up and transferred into ddPCR 96-well plate (Bio-Rad). The follow-up PCR reaction was performed in T100TM Thermal Cycler with the program in Table 11.

Table 11: ddPCR reaction program

Program	Temp	Time	
Initialization	95°C	10 min	
Denaturation	94°C	30 sec	
Annealing	60°C	60 sec	40 cycles
Elongation	98°C	20 sec	
Cooling	12°C		

During PCR, the DNA polymerase extends the primer situated on the same strand as the probes until it reaches the probe position. The inherent exonuclease activity hydrolyzes the probe from 5' to 3', which releases the reporter dye into solution and thereby causes an increase in fluorescence. The fluorescence signal in single droplet was measured by QX Droplet Reader (Bio-Rad), which is proportional to the amount of target DNA. Finally, brightness of FAM and HEX fluorescence in each sample was analyzed with QuantaSoft analysis software (Bio-Rad).

2.3.3 Protein isolation and Western blot

Proteins from cells or isolated tissues were lysed with 1 x Radio Immunoprecipitation Assay (RIPA) buffer with 0.1% protease-inhibitor (Sigma) and 0.1% phosphatase-inhibitor (Sigma), at RT. For lysis of cultured adipocytes, 100 µl of RIPA was added to each well of 12-well cell culture plate and incubated for 15 min on ice. Afterwards, cells were scraped form plate and centrifuged with 14,000 g at 4°C for 10 min. The resulting clear supernatant was removed for use. The tissue samples was extracted with a ratio of 30 mg of tissue to 200 µl of RIPA buffer. A homogenization step on ice was required to lyze samples completely. Lysates were then centrifuged with 16,000 g at 4°C for 15 min. Likewise, aqueous supernatant (without the fat layer) was harvested for protein concentration quantification and for western blot.

Protein concentrations were measured by BCA (bicinchoninic acid) protein Assay Reagent Kit (Thermo Scientific™ Pierce™). Protein samples were mixed with 2 x sample buffer (with 5% 2-mercaptoethanol), boiled at 95°C for 5 min, and cooled down at room temperature

before loading onto the SDS-gel, which were casted according to the following SDS-gel recipes (Table 12). Meanwhile, 4 µl protein ladder marker (Thermo Fisher Scientific, Waltham MA/USA) followed was added onto the gel.

Table 12: SDS- gel recipes for two mini-gel

Solutions	Separating gel (12.5%)	Stacking gel (5%)
Acrylamid	4.17 ml	0.8 ml
Buffer	8 x Separating buffer, 1.25 ml	4 x Stacking buffer, 1.25 ml
H_2O	4.43 ml	2.86 ml
SDS (10%)	100 µl	50 µl
AMPS (10 mg/100 ul)	50 µl	30 µl
TEMED	5 µl	10 µl

Once the electrophoresis finished, the SDS-gels were cutted and placed in the blotting buffer immediately. Afterwards, blotting procedure was conducted with the sequential order: three layers of filter paper at bottom, Nitrocellularose (NC) membrane, SDS-gel and another three layers of filter paper on the very top. For a mini gel (48 cm^2), the blotting was performed at 48 mA for 1 h. After transfer, NC membrane was incubated in 3% bovine serum albumin (BSA, Carl Roth) blocking buffer for at least 1 h. All primary and secondary antibodies were diluted in tris-buffered saline (TBS) buffer. To detect the relative abundance of UCP1 and luciferase protein in the same sample, the primary antibodies for UCP1, luciferase and Actin (housekeeper) were incubated at 4°C overnight (Table 13). On the second morning, NC membrane was washed with 1 x tris-buffered saline containing 0.1% Tween20 (Carl Roth) for 15 min.

Table 13: Primary antibodies used for western blotting

Primary antibody	Dilution
mouse anti-chicken actin antibody (EMD Millipore, MAB1501), monoclonal	1: 5000
rabbit anti-human UCP1 peptide (Abcam, ab10983), polyclonal	1: 10000
rabbit anti-LUC peptide (Abcam, EPR17790), monoclonal	1: 10000

Then, the secondary antibodies including donkey-anti- mouse (1: 20000) and goat-anti-rabbit (1: 20000) were used for at least 1 h incubation. The signal detection was performed on Odyssey infrared imager (LI-COR Biosciences GmbH).

2.3.4 Hematoxylin and eosin staining

For hematoxylin and eosin (H&E) staining, tissue samples were collected and were fixed in 3.7% para-formaldehyde at RT for at least two days. Afterwards, tissues went thought the dehydration process overnight according to the protocol in the Appendix 5. In the next morning, specimens were embedded in paraffin and were hereafter sectioned using a microtome (Leica). The acquired sections were mounted on microscope slides (Carl Roth), dried at 37°C overnight. Afterwards, staining was automatically performed using a Leica multistainer (Leica) according to Appendix 5.

2.4 Statistics

All data graph were generated with Graphpad Prism 6 software (Graphpad Software Inc, USA). Data were expressed as mean ± SD. The statistical significance were analyzed by unpaired two-tailed t-tests and One-way ANOVA (Dunnet's Test), or two-way ANOVA (Tukey'stest) as indicated in the figure legends. The data was considered as significance when $p < 0.05$.

3 RESULTS

3.1 Verification of reporter genes in the *Ucp1-LUC-iRFP713* reporter mice

To detect the exogenous genes expression in mouse genome, ear punches from wildtype (WT), heterozygous (HET) and homozygous (KI) engineered mice were collected for genotyping. As expected, gDNA PCR amplified 330 base-pairs (bp) and 403 bp fragments from WT and KI allele, respectively (Fig. 4).
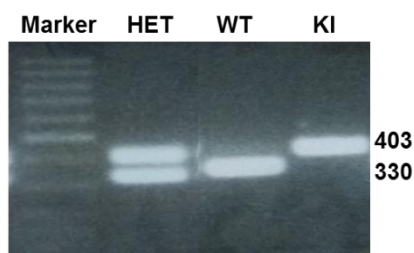
Figure 4: The gDNA PCR yields specific products from WT and KI allele. M = molecular weight marker. (From Wang et al. 2019).

3.1.1 Luciferase activity faithfully reflects *Ucp1* expression upon stimulation

3.1.1.1 Detection of firefly luciferase expression in *Ucp1-LUC-iRFP713* reporter mice

In KI mice, immunoblotting analysis revealed UCP1 protein expression is higher in interscapular BAT (iBAT), lower in inguinal WAT (iWAT), and was nearly undetectable in gonadal WAT (gWAT). Firefly luciferase (LUC) protein in KI mice was parallel to UCP1 protein levels, displaying the tissue-specific expression pattern of UCP1 in individual fat depots (Fig. 5).

Due to the lack of available primary antibody, the near infrared fluorescent protein (iRFP713) was not detectable by western blot.
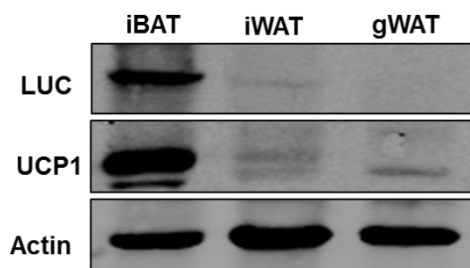
Figure 5: Representative immunoblotting of LUC, UCP1 and Actin protein abundance in iBAT, iWAT and gWAT of homozygous KI mice. (Figures from.Wang et al.2019).

RESULTS

3.1.1.2 Visualization and quantification of luciferase activity *ex vivo*

To assess the LUC activity in excised tissues, membrane-permeable D-luciferin was directly sprayed onto the freshly isolated iBAT, iWAT, gWAT, skeletal muscle and liver from all three genotypes. The iBAT and iWAT depots from KI and HET mice showed the strongest bioluminescence, while no signals were observed in livers (Fig. 6A). These results were further confirmed with *ex vivo* relative luminescence unit (RLU) quantification in tissue lysates, where the highest bioluminescent intensity was found in iBAT of KI and HET mice (Fig. 6B).
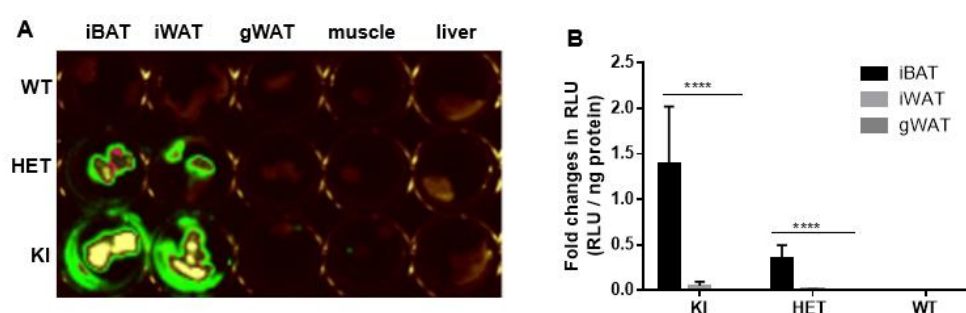
Figure 6: Assessment of *ex vivo* luciferase activity from freshly isolated tissues.
A. Membrane-permeable D-luciferin. Images were captured using a charge-coupled-device (CCD) camera with 60s exposure time. **B.** Luciferase assay system was used to quantify relative light unit (RLU) in isolated tissues. Afterwards, RLU was normalized to protein concentrations (n=6). Error bars show mean ± SD, data were analyzed with Two-way-ANOVA, *** $p < 0.001$. (From Wang et al. 2019)

3.1.1.3 Visualization and quantification of luciferase activity *in vitro*

To determine whether firefly luciferase can be used to track the intracellular *Ucp1* dynamics in *in vitro* settings, brown preadipocytes were isolated from iBAT of WT, HET and KI mice. After fully differentiation, D-luciferin (150 ug/ml) were directly added to the pre-warmed cell culture medium just prior to the CCD imaging, and the strong light intensity was selectively detected in living brown adipocytes of KI and HET genotypes, but not in WT cells (Fig.7).
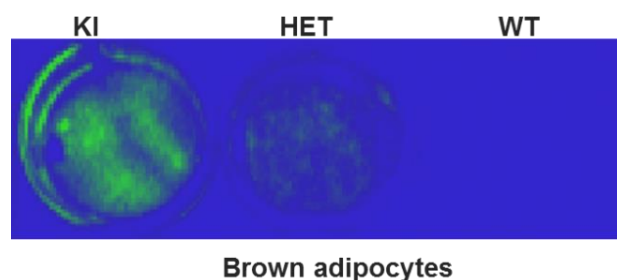
Figure 7: *In vitro* imaging of living brown adipocytes by CCD camera.

RESULTS

Next, the degradation rates of the LUC and UCP1 protein in brown adipocytes were determined by the administration of cycloheximide (25 mg/ml) to stop protein biosynthesis. Immunoblotting analysis showed the parallel decreases in UCP1 and LUC protein abundance in brown adipocytes (Fig. 8A). The calculated protein half-life revealed that UCP1 and LUC protein have the very similar half-lives of approximately10 h in brown adipocytes, which suggest that LUC protein works as a reliable surrogate for UCP1 protein abundance in cell cultures (Fig. 8B).
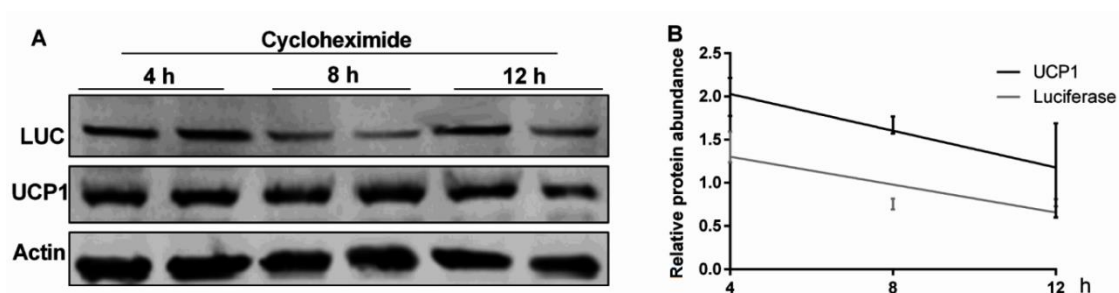
Figure 8: Half-life of UCP1 and LUC in brown adipocytes.
A. Protein abundance of UCP1, LUC and Actin in fully differentiated brown adipocytes isolated from KI mice. To measure the individual protein half-life, mature adipocytes were treated with 25 µg/ml cycloheximide for 4 h, 8 h or 12 h. **B.** Quantitative analysis of the relative UCP1 and LUC protein abundance in **A**. (From Wang et al. 2019)

To determine whether *in vitro* luciferase activity could reflect changes in *UCP1* expression, multiple *Ucp1* transcriptional activators was employed in brown and brite adipocytes. Among them, Rosiglitazone (Rosi), a PPARγ agonist, which is the most robust *Ucp1* inducer, has been widely used in cell cultures and in mouse models to recruit *Ucp1* expression. Additionally, Isoproterenol (Iso) and Retinoic acid (RA) also function to boost *Ucp1* transcription as well, by activating the *β*-ARs signaling pathway or binding to the RA element in *Ucp1* enhancer region.

Compared to controls, chronic Rosi treatments powerfully drove the bioluminescence in a dose dependent manner, with the strongest induction by 1000 nM Rosi in brown and beige adipocytes (Fig. 9A). The acute administration with Iso or RA also strongly promoted bioluminescent signals, whose effects were quantitatively similar to 100 nM Rosi (Fig. 9A-B). Moreover, both LUC activity and LUC protein levels were in tight correlation with the UCP1 protein abundance in brown adipocytes under the pharmacological stimuli (Fig. 9B)
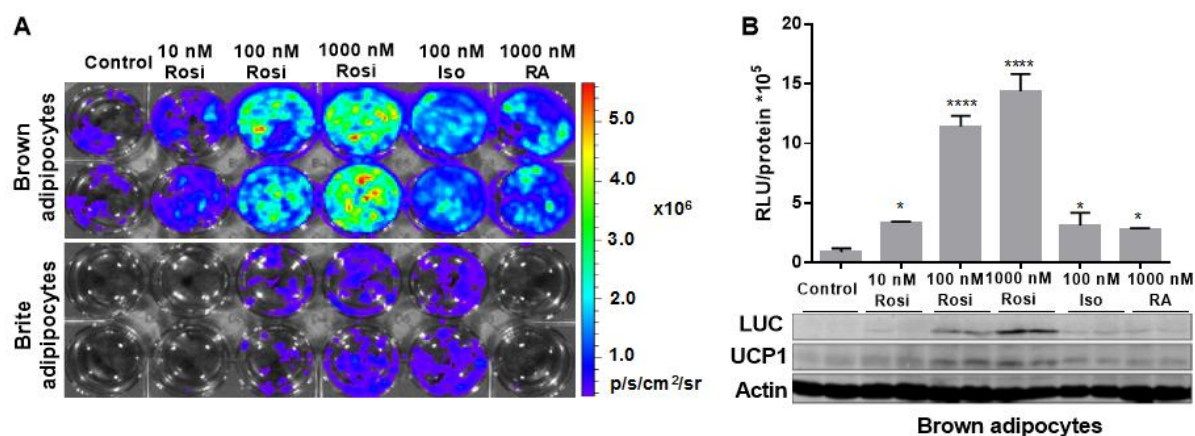
Figure 9: **LUC activity reliably reports UCP1 alterations upon stimulation *in vitro*.**
A. Representative *in vitro* bioluminescence imaging of brown and beige adipocytes under the chronic stimulation of increasing dosages of Rosi, and the acute treatments with Iso and RA (n=3). **B.** Assessment of the relative bioluminescence units and the corresponding UCP1 protein levels in brown adipocytes upon various activators (n=3). Error bars show mean ± SD, data were analyzed with One-way ANOVA, *$p < 0.05$, *** $p < 0.001$. (From Wang et al. 2019)

3.1.1.4 Visualization and quantification of luciferase activity *in vivo*

To detect the *in vivo* luciferase activity in mice, an *in vivo* imaging system (IVIS) was utilized. To obtain an optimal imaging time point for iBAT, it was necessary to determine the standard kinetics of luciferase activity above the region of interest (ROI). To do so, a pilot study with mice of all three genotypes was conducted after i.p. injection of D-Luciferin (150 mg/kg) and all images were captured in a 2-min interval. Following the D-luciferin injection, the light intensity emitted from KI and HET increased progressively from the dorsal view, reaching the plateau after approximately 20 min (Fig. 10A). Accordingly, all the sequential bioluminescence images were imaged at 20-30 min post D-luciferin addition in the following studies.

The strongest bioluminescence was visualized in the ROI above iBAT of KI mice, followed by HET mice but not in WT mice (Fig. 10B). It is important to point out that luciferase catalyzed bioluminescence was also detectable from the lateral and ventral view in both HET and KI mice, the area corresponding to inguinal WAT (Fig. 10C), suggesting that the novel *Ucp1-LUC-iRFP713* reporter mouse model is also capable of monitoring the browning state of subcutaneous WAT.

RESULTS
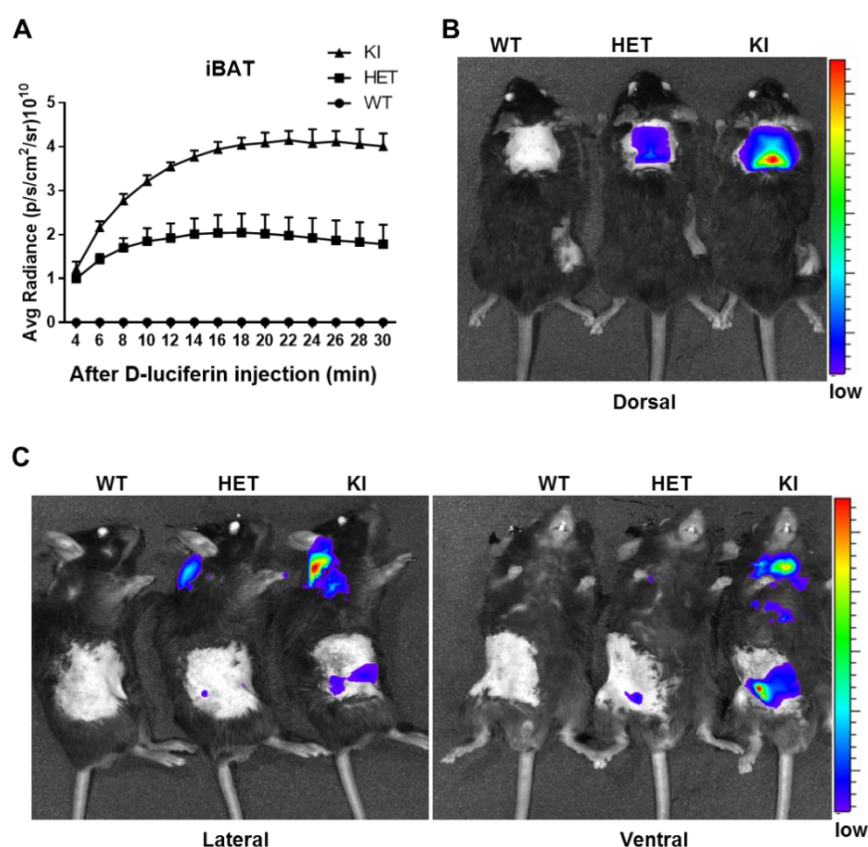
Figure 10: Visualization and quantification of bioluminescence *in vivo*.
A. Kinetic curves for the luciferase activity above iBAT (n=3). Error bars show mean ± SD. **B.** Representative imaging of bioluminescence in anesthetized mice of three genotypes (n=6). **C.** Imaging of anesthetized animal from the lateral and ventral views (n=6). (From Wang et al. 2019)

The selective β_3-AR agonist (CL316,243) is widely used to active brown and beige fat, mimicking physiological stimulation of cold-induced NST (Strosberg & Pietri-Reuxel 1996; Collins et al. 1997). To assess whether *in vivo* bioluminescence imaging in the *Ucp1-LUC-iRFP713* reporter mice could report the adaptive variations in *Ucp1* expression, reporter mice were exposed to a weekly decreasing ambient temperature from 23°C, 18°C, 15°C, 10°C to 5°C or were repeatedly injected with CL316,243 for 5 consecutive days at room temperature (23°C), while the control mice were repeated injected with saline at room temperature.

Firstly, homozygous KI mice were used for *in vivo* bioluminescence imaging. Compared to control mice, both CL316,243 and cold acclimation profoundly increased the bioluminescent intensity above the regions corresponding to iBAT and iWAT, with much more stronger effects in cold acclimated mice. However, the saturated bioluminescence signals were observed in KI mice, which interfered with the accurate quantification of bioluminescence (Fig.11A). To avoid of the saturated signals, HET mice were thus utilized for the *in vivo*

imaging under the same stimulation. Likewise, bioluminescence above the iBAT and iWAT region of HET mice were robustly enhanced by CL316,243 injection and chronic cold acclimation (Fig. 11B)
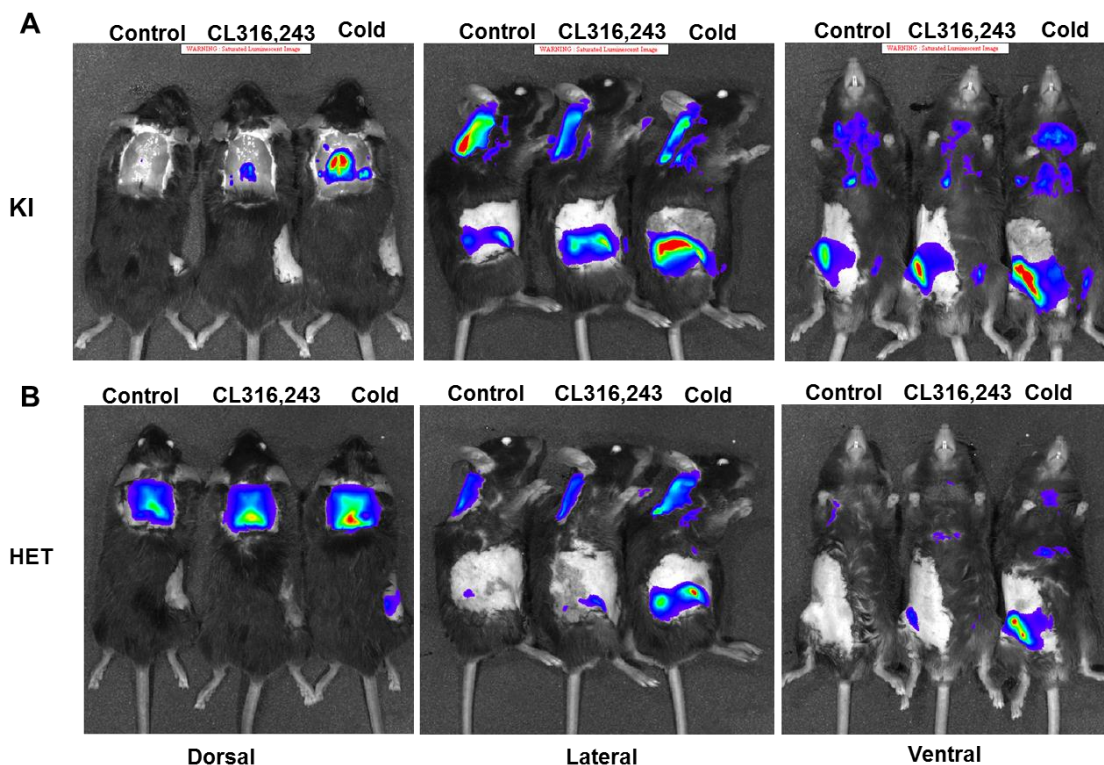
Figure 11: *In vivo* imaging of reporter mice under various stimuli.
A. Representative *in vivo* imaging of KI mice in response to repeated administration of CL316,243 or the prolonged cold acclimation from 18°C, 15°C, 10°C to 5°C, with the control mice received saline injection at room temperature. **B**. Representative *in vivo* imaging of HET mice under stimulation (n=3). (From Wang et al. 2019)

To quantify the *in vivo* bioluminescent intensity, images of HET mice were analyzed using IVIS imaging software Version 2.6. However, the random pigmentation above the ROI (mainly above iBAT) quenched the accurate quantification of bioluminescence (Fig. 12A). Even though, the acquired bioluminescent signals (Fig. 12B-C) were consistent with the changes in UCP1 protein levels in both iBAT and iWAT (Fig. 12D-E).
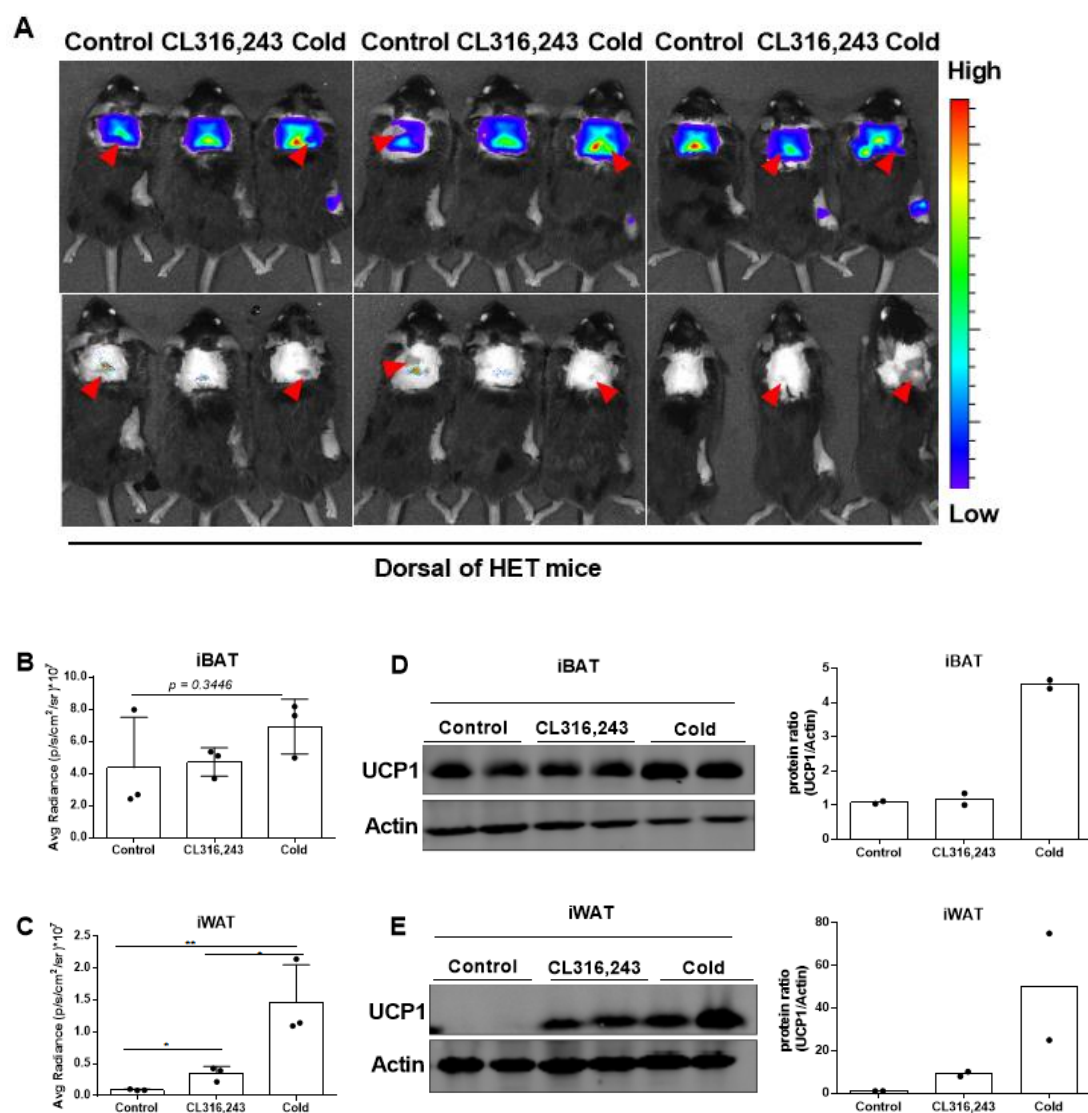
Figure 12: *In vivo* **bioluminescent intensities are closely correlated with changes in UCP1 expression.**
A. Pigmentation randomly appears on the skin of HET reporter mice. Pigmentation was pointed by red arrows. **B.** Quantification of bioluminescence in areas referring to iBAT (n=3). Error bars show Mean ± SD, data were analyzed with One-way-ANOVA. **C.** Quantification of bioluminescence in areas referring to iWAT (n=3). Error bars show mean ± SD, data were analyzed with One-way-ANOVA, * $p < 0.01$, ** $p < 0.05$. **D-E.** Immunoblotting detection and analysis of relative UCP1 protein abundance in iBAT. (From Wang et al. 2019)

It has been known that mice maintained at standard laboratory condition at an ambient temperature of 23°C (RT) are under a constant mild cold exposure, leading to profound activation of adaptive thermogenesis. While decreasing thermal stress by housing mice under thermoneutral conditions at 30°C significantly suppresses *Ucp1* mRNA and protein levels in both brown fat and white fat depots (Feldmann et al. 2009; Cui et al. 2016). To study this temperature-dependent effect, KI mice were kept either at room temperature (RT) or at thermoneutrality (TN) for 8 consecutive weeks. Compared to mice kept at RT, *in vivo*

imaging revealed that the intensity of bioluminescence emitted from iBAT (dorsal view) or iWAT (lateral and ventral view) regions were dramatically decreased under thermoneutral condition, indicating the attenuated UCP1 expression at TN (Fig. 13A). Moreover, *ex vivo* measurements in tissue lysates of KI mice confirmed the significant decreases in bioluminescent signals under thermoneutrality (Fig. 13 B-C).
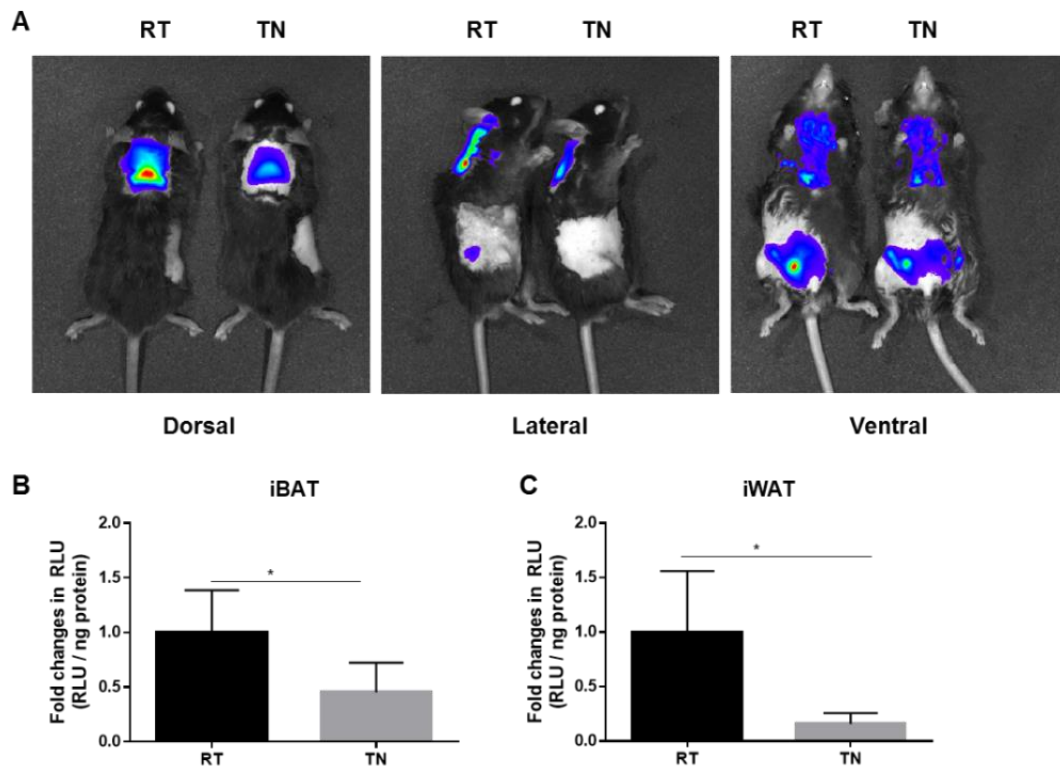
Figure 13: Thermoneutral housing strongly decreases bioluminescence in KI mice.
A. Representative *in vivo* bioluminescence imaging of KI mice kept at either RT or at TN conditions (n=6). **B.** Quantitative analysis of *ex vivo* bioluminescence in tissue lysates of KI mice kept at either RT or TN conditions (n=6). Error bars show mean ± SD, data were analyzed with Student's unpaired two-tailed *t* test, * *p < 0.01*.

In summary, these results powerfully demonstrate that firefly luciferase protein and its enzymatic activity can faithfully report *Ucp1* expression in dissected tissues, isolated cell cultures and in anesthetized animals as well, which offers an easy-to-use qualitative and quantitative platform to monitor *Ucp1* expression.

RESULTS

3.1.2 iRFP713 protein reliably reports *Ucp1* expression upon stimulation

Engineered iRFP713 has higher brightness, deeper tissue penetration, intracellular stability and lower cytotoxicity than conventional fluorescent proteins and requires no exogenous supply of the chromophore biliverdin, thereby making it feasible to extend the capabilities for imaging genetically-tagged tissues and mice (Filonov et al. 2011; Richie et al. 2018). Given that iRFP713 protein has an excitation and emission maxima at 673 nm and 702 nm, respectively, freshly dissected tissues of fat depots, skeletal muscle and livers were directly imaged using the 700 nm excitation channel of a Li-COR Odyssey near-infrared scanner, without any substrate.

Although liver samples exhibited an unspecific signal due to the auto-florescence, the selective iRFP713 signals were only detected in excised brown and beige fat in transgenic mice (Fig. 14A). The *ex vivo* imaging revealed the specific expression of iRFP713 protein in brown and beige adipose tissue.

To examine the iRFP713 *in vivo*, mice of the three genotypes were either maintained at room temperature (RT, 23°C) or at an ambient temperature stepwise decreased from 23°C to 5°C in 4 weeks. Although the iRFP713 fluorescence was not detectable in mice maintained at RT, cold acclimation profoundly activated bright fluorescence in both HET and KI mice in an allele-dependent fashion (Fig. 14B). In particular, its most exciting feature is the ability to image *Ucp1* expression without the supply of any exogenous substrate, enabling the non-invasive *in vivo* imaging.
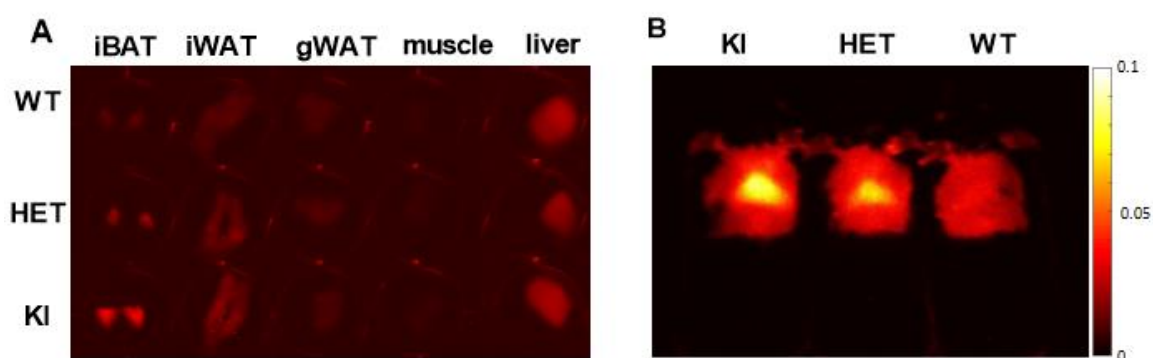
Figure 14: Detection of iRFP713 fluorescence in tissues and in anesthetized mice.
A. Representative imaging of isolated tissues from 5-weeks old male WT, HET and KI mice. **B.** *In vivo* imaging of iRFP713 in KI, HET and WT mice, which were kept at either RT or after chronic cold exposure. (Figures modified from Wang et al.2019).

RESULTS

To gain better insight into the fluorescence distribution and thereby the *Ucp1* expression in an entire mouse, a cryo-imaging system was utilized. After *in vivo* imaging, two cold-exposed mice, one KI and one WT mice were sectioned with the cryostat and each slice was imaged with a highly sensitive fluorescence camera. Transverse slices revealed a striking brightness in an area corresponding to iBAT of KI mouse (Fig. 15A). Finally, all cry-slices were compiled based on the acquired iRFP713 signals in entire mouse for a three-dimensional (3D) reconstruction. Although unspecific fluorescence appeared in the digestive tracts of both transgenic and non-transgenic mice, specific signals representing iBAT and iWAT were only present in KI mouse, not WT mouse (Fig. 15B).
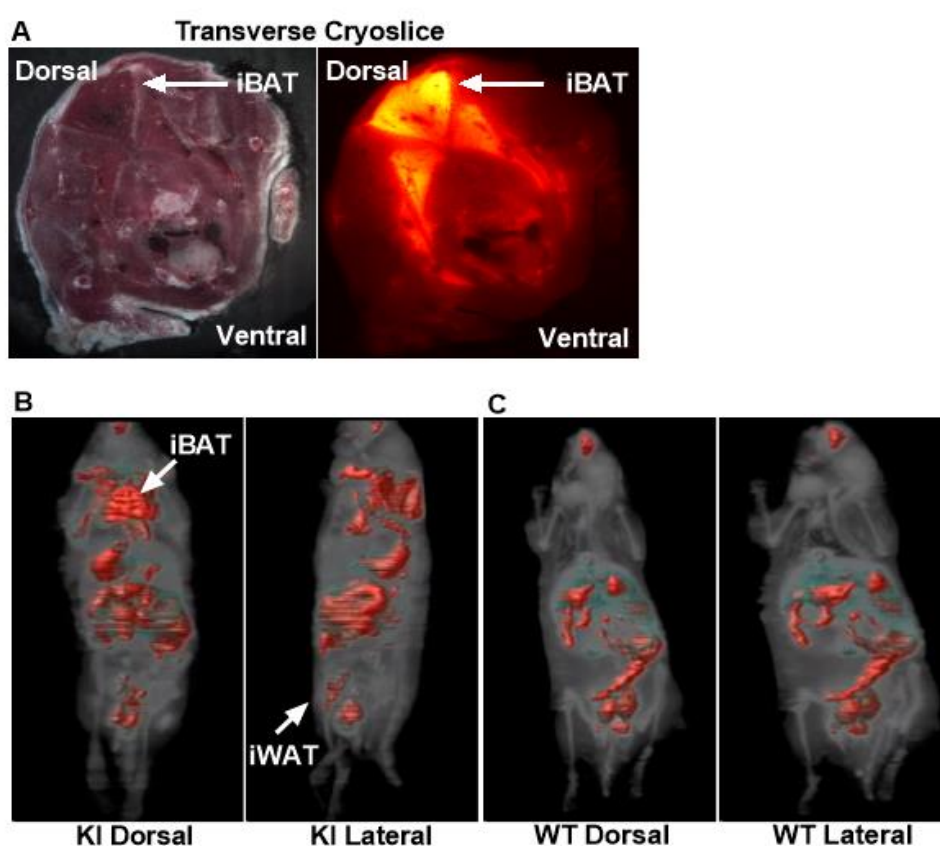
Figure 15: Cryoslicing and imaging of *Ucp1*-LUC-iRFP713 reporter mice.
A. Representative images of a transverse cryoslice of a KI mouse after cold exposure. During every cryoslice, iRFP713 fluorescence intensity was measured. As shown, robust signal was identified in areas representing iBAT, as pointed with a white arrow. **B.** Reconstructed 3D fluorescent images of a KI mouse based on the acquired iRFP713 signals during cryoslice. **C**. Reconstructed fluorescent 3D image of a WT mouse based on the acquired iRFP713 signals during cryoslicing. (Figures modified from Wang et al.2019).

In summary, these data demonstrate the successful detection of iRFP713-labeld brown and beige adipose tissues in the *Ucp1-LUC-iRFP713* reporter mice, suggesting that iRFP713 is a applicable marker gene for *Ucp1* expression.

RESULTS

3.2   Versatile applications of the *Ucp1-LUC-iRFP713* reporter mice

The firefly luciferase activity in the *Ucp1-LUC-iRFP713* reporter mice works as a simple, sensitive and reliable surrogate for *Ucp1* expression. The qualitative and quantitative bioluminescence analysis can be used to profile broadly of *Ucp1*-positive tissues/cells and to search for new modulators targeting *Ucp1* expression.

3.2.1   Identification of a new brown adipose tissue in mice

To determine the anatomical origins of the emitted bioluminescence, homozygous KI mice were dissected to expose tissues *in situ*. Of note, bright luciferase-catalyzed bioluminescence was visualized in multiple sites, which highlighted the iBAT in the dorsal region, cervical (cBAT) and axillary regions (aBAT) as well beige fat in iWAT from the ventral view (Fig. 16).
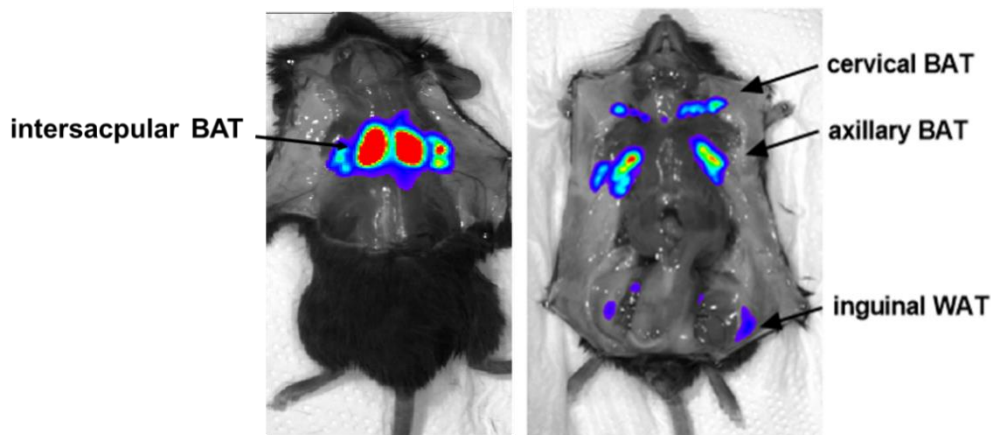
Figure 16: Detection of UCP1-expressing tissues in reporter mice
KI mice were dissected after *in vivo* imaging. Black arrows point to the adipose depots representing the main sites of bioluminescence from dorsal and ventral view. (Figures modified from Wang et al.2019).

Additionally, a bright bioluminescence site was identified in a small triangular reddish tissue embedded in the cleft of femoris muscle, adjunct to the apex of the iWAT (Fig. 17A-B). Immunoblotting analysis revealed that UCP1 protein in this tissue was expressed at the intermediate levels between iWAT and iBAT (Fig. 17C). Relative mRNA quantification showed that *Adiponectin (AdipoQ)*, a gene highly specific to adipose tissue, was comparable across the three tissues, indicating that this tissue would be an adipose depot. Consistent with UCP1 protein levels, the expression of brown marker genes such as *Ucp1*, *cell death-inducing DFFA-like effector A (Cidea), peroxisome proliferator-activated receptor gamma coactivator 1 alpha (Pgc1a), PR domain zinc finger protein 16 (Prdm16), deiodinase-2 (Dio2) and*

RESULTS

ELOVL fatty acid elongase 3 (Elovl3) were all intermediate to iWAT and iBAT (Fig. 17D). Histological analysis revealed the abundant fat accumulation in this depot, showing the similar morphological characteristics to both iBAT and iWAT (Fig. 17E). Taken together, these data shows the newly identified adipose tissue shares the typical molecular and morphological properties of both brown and beige fat. Thereby, it was named to be femoral brown adipose tissue (fBAT) here.
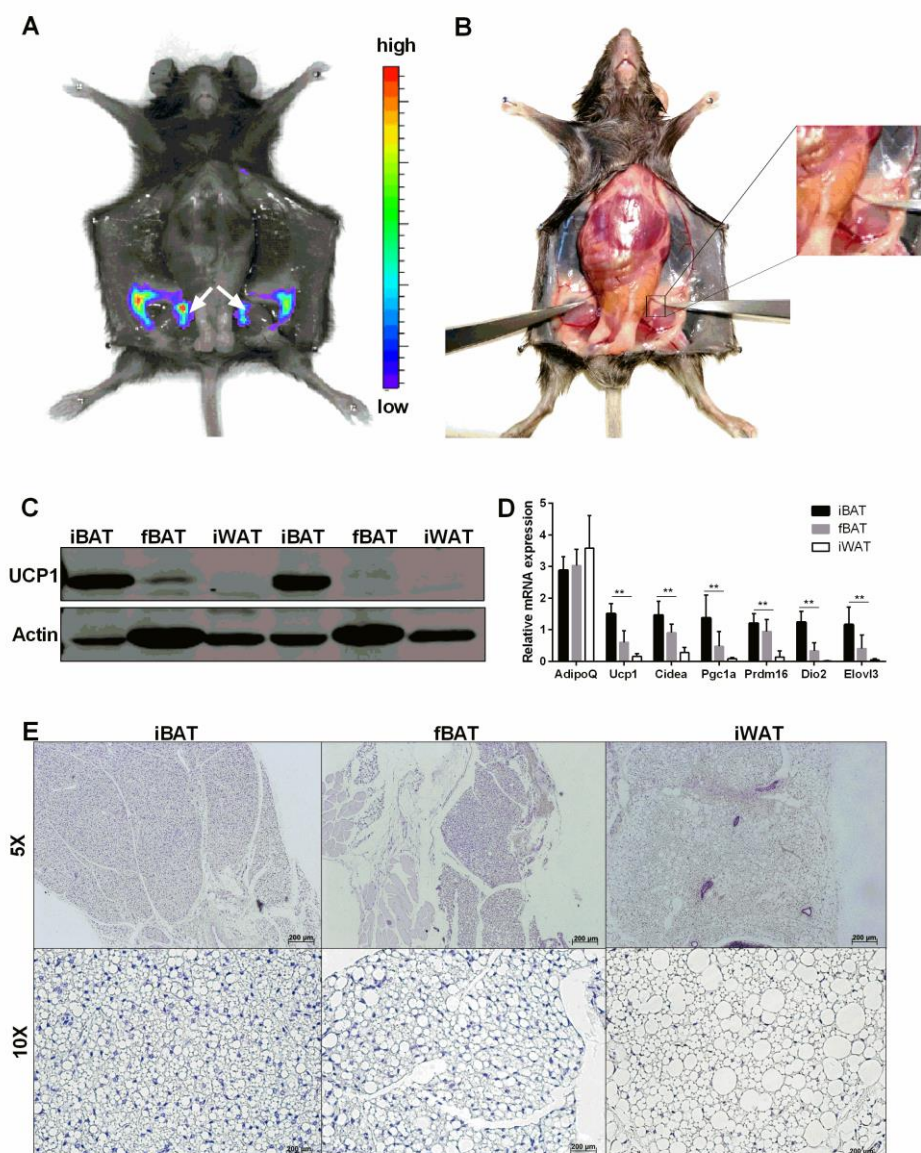
Figure 17: A new *Ucp1*-poisitive adipose tissue was identified in the femoral cleft of KI mice.
A. Post dosing of D-luciferin, KI mice were sacrificed. Robust signals were visualized in iWAT and fBAT (pointe with white arrows). **B.** Anatomical location of the fBAT in mouse *in situ*. **C.** Comparisons of fBAT UCP1 expression to that in iBAT and iWAT by western blotting. **D.** Relative genes expression in iBAT and iWAT and fBAT (n=6). Error bars show mean ± SD, data were analyzed with Two-way ANOVA, * $p < 0.05$, ** *p < 0.001*. **E.** Representative hematoxylin and eosin staining for iBAT, iWAT and newly identified fBAT. (Figures modified from Wang et al.2019).

RESULTS

3.2.2 Higher browning capacity in peri-ovarian WAT than in epidydimal WAT

To evaluate the sex-associated differences in *Ucp1* expression, adipose tissues of the anatomically analogous fat pads from male and female littermates were analyzed. Luciferase activity in iBAT, iWAT and muscle was equivalent between sexes, and UCP1 protein in iBAT was expressed in a similar level between two genders (Fig. 18A-B). However, significant sex-related differences were detected in peri-gonadal WAT, with higher signals in peri-ovarian (poWAT) WAT than in epididymal WAT (eWAT) (Fig. 18A). Moreover, the expression of browning marker genes such as *Ucp1*, *Pgc1a, Cidea*, s*olute carrier family 25A1 (Slc25a1)*, *cytochrome c oxidase subunit 7A1 (Cox7a1)* and the gene coding for a brown-fat-derived adipokine, *neuroregulin 4 (Nrg4)* was substantially higher in poWAT as well (Fig. 18B). While the expression of *fatty acid binding protein 4 (Fabp4)*, *adiponectin (Adipoq)*, *β3-adrenoceptor (Adrb3)*, *hormone-sensitive lipase (Hsl)*, *estrogen-related receptor α (ERRα)* and *vascular endothelial growth factor (VEGF)* was comparable between genders (Fig. 18C). The higher browning propensity was further confirmed by the abundant multilocular adipocytes in poWAT (Fig. 18D).
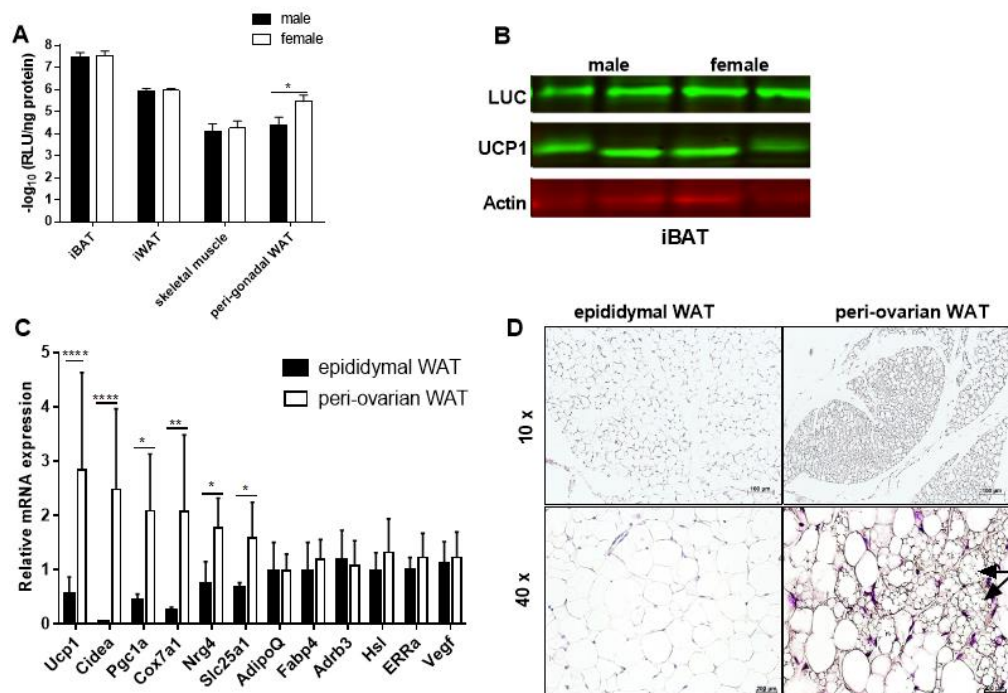
Figure 18: Sex-specific differences in poWAT and eWAT.
A. *Ex vivo* quantification of bioluminescence in iBAT, iWAT, gWAT and skeletal muscle from both male and female KI mice (n=6).Error bars show mean ± SD, data were analyzed with Two-way ANOVA, * $p < 0.05$, **B.** Immunoblotting of LUC, UCP1 and Actin protein levels in iBAT of male and female mice. **C.** Comparison of relative gene expression between poWAT and eWAT (n=6). Error bars show mean ± SD, data were analyzed with Two-way ANOVA, * $p < 0.05$, ** $p < 0.001$ *** $p < 0.0001$. **C.** Representative hematoxylin and eosin staining for eWAT and poWAT in KI mice. (Figures modified from Wang et al.2019).

3.2.3 Profiling of *Ucp1* expression in multiple tissues by luciferase activity

The newly identified of fBAT in the reporter mice indicates the limited understanding of brown/beige adipose tissues distribution in rodents. To systematically profile *Ucp1* gene expression in rodents by sensitive luciferase activity. To do so, tissues and organs were collected from 5-weeks-old male and female mice. Collectively, bioluminescent signals were especially high in iBAT, aBAT, fBAT and cBAT, followed by iWAT, poWAT and eWAT. Of note, signals were also detected in thymus, brain, epididymis and soleus muscle. Whereas no detectable signal was found in gastrocnemius muscle, uterus, bladder, heart, stomach, small intestine or liver (Fig. 19). Since the firefly luciferase activity is selectively active in *Ucp1*-positive tissues, these results highly suggest the potential *Ucp1* expression beyond the traditional brown and beige adipose tissues, which requires further investigation for their specific physiological roles.
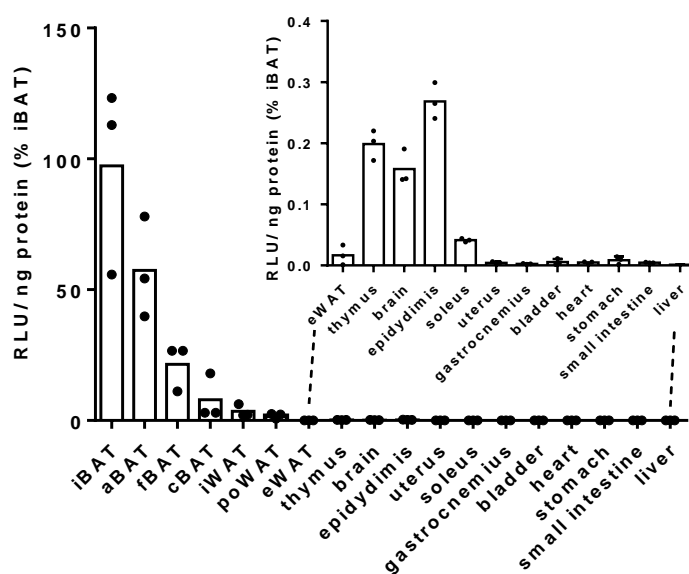
Figure 19: Bioluminescence quantification in multiple tissues of KI mice.
All samples were isolated from 5-weeks old male and female mice (n=3). (Figures modified from Wang et al.2019).

RESULTS

3.2.4   The application of cell-based imaging platform

The significance of BAT in energy homeostasis inspires the search for new chemicals and molecules to recruit and activate *Ucp1* expression. The firefly luciferase activity in the reporter acts as a *bona fide* surrogate for *Ucp1* gene in cultured brown and beige adipocytes, which can be used as an effective cell-based platform to perform high-throughput screening of new drugs and molecules.

Upon β_3-AR stimulation, adenylate cyclase converts ATP into cAMP. The activated PKA by increased levels of cAMP sequentially phosphorylates cAMP response element-binding protein (CREB), which is generally considered as a primary regulator of adipogenesis and as a key factor in controlling *Ucp1* gene expression (Reusch et al. 2000; Thonberg et al., 2002). Recently studies revealed that CREB actions on target genes expression requires the stimulation of its regulated transcription coactivators (CRTCs) (Katoh et al. 2006; Patel et al. 2014). Meanwhile, its has been described that salt inducible kinases (SIKs) exert inhibitory effects on cAMP signaling pathway, mostly by promoting phosphorylation CRTCs and stopping the CRTCs translocation into nucleus (Kim et al. 2015; Paulo et al. 2018).

As a proof of concept, a pan SIKs inhibitor HG-9-91-01 was added on the primary preadipocytes that were isolated from brown and beige fat depots of KI mice. The increasing concentration of HG-9-91-01 enhanced the *in vitro* bioluminescence in both brown and beige adipocytes, in a dose-dependent manner (Fig 20A-D).

In addition, to study whether the increased *Ucp1* expression is thermogenic functional, cellular respirometry was performed in immortalized brown adipocyte cell lines (129S6 sv/ev Tac background) to quantify intracellular oxygen consumption rate (OCR) in real time. Interesting, brown adipocytes treated with 100 nM and 400 nM HG-9-91-01 exhibited significant higher OCR than control cells during the entire measurement, including the higher basal OCR, which suggests that HG-9-91-01 plays a role to increase mitochondrial biogenesis (Fig. 20E). Of note, after the administration of isoproterenol, there was a slight increase in OCR in control groups, while HG-9-91-01 treatments significantly promoted cellular OCR, in a dose-dependent manner (Fig. 20E-F). The UCP1-dependent respiration calculated form the isoproterenol-induced respiration and the basal proton leak suggests that HG-9-91-01 is a powerful stimulant for both *Ucp1* gene expression and UCP1-mediated oxygen consumption (Fig. 20F).
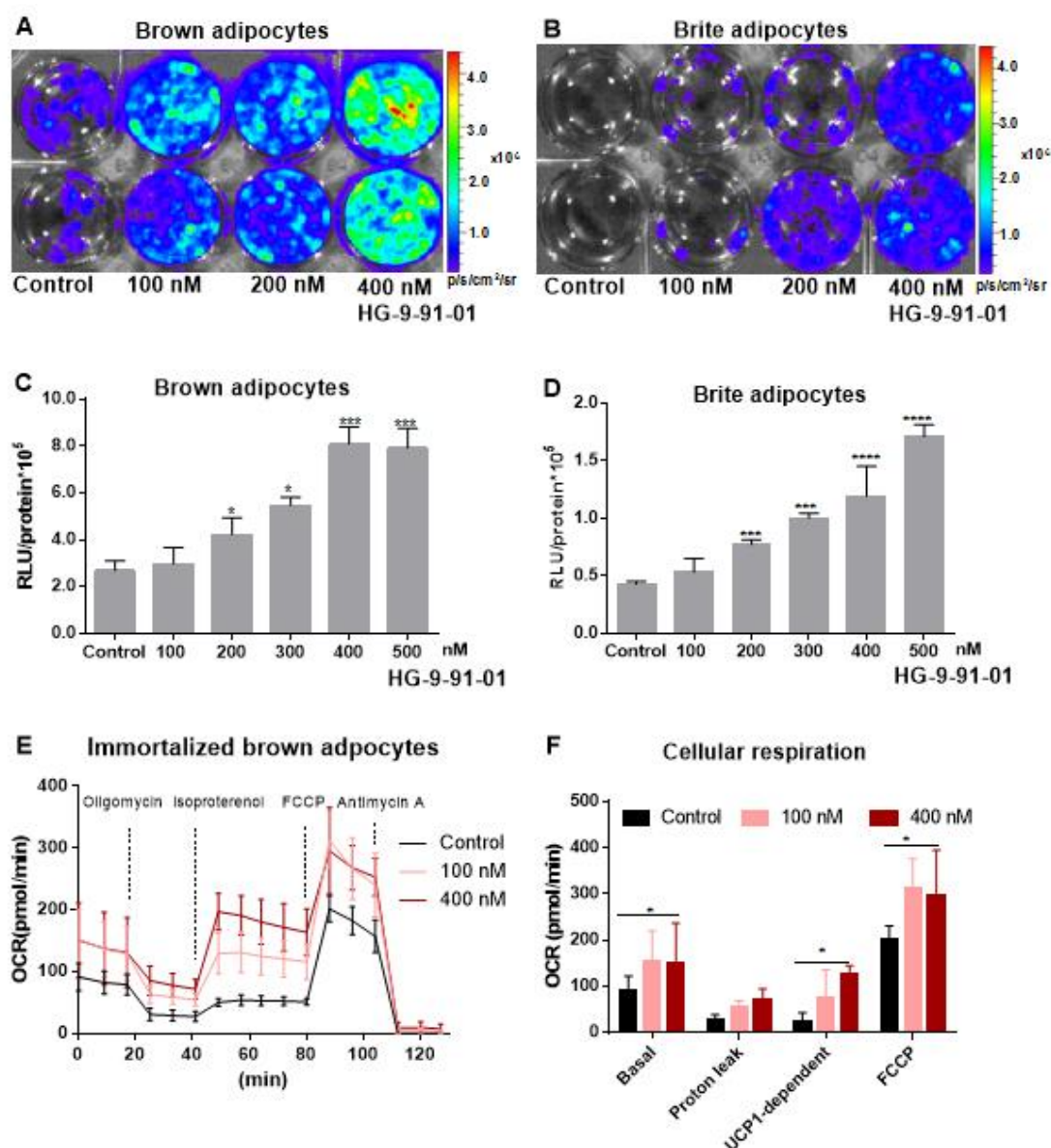
Figure 20: Cell-based imaging platform facilitates identification of a new *Ucp1* modulator.
A. Representative *in vitro* bioluminescence imaging of cultured brown adipocytes treated with the increasing concentration of a pan SIKs inhibitor HG-9-91-01 treatment (n=3). **B.** Representative *in vitro* bioluminescence imaging of cultured beige adipocytes treated with the increasing concentration of a pan SIKs inhibitor HG-9-91-01 treatment (n=3). **C.** *In vitro* bioluminescence quantification of cultured brown adipocytes treated with the increasing concentration of a pan SIKs inhibitor HG-9-91-01 treatment (n=3). Error bars show Mean ± SD, data were analyzed with One-way ANOVA, $* p < 0.05$, $*** p < 0.0001$. **D.** *In vitro* bioluminescence quantification of cultured beige adipocytes treated with the increasing concentration of a pan SIKs inhibitor HG-9-91-01 treatment (n=3). Error bars show mean ± SD, data were analyzed with One-way ANOVA, $*** p < 0.0001$. **E-F.** Measurements of cellular OCR in immortalized brown fat cells established from a 129S6 sv/ev Tac gene background mouse (N=3, n=32). Immortalized brown fat cells were treated with 100 nM or 400 nM HG-9-91-01. During the measurement, Oligomycin, isoproterenol, FCCP and Antimycin A were injected in sequence. Oligomaycin is an inhibitor of ATP synthase. Isoproterenol is a pan β-ARs agonist. FCCP induces the maximum respiratory capacity, while Antimycin A inhibits all cellular reparation. Basal respiration and proton leak were recorded before and after the Oligomycin injection. UCP1-dependent OCR was obtained by subtracting proton leak from isoproterenol-induced OCR. Error bars show mean ± SD, data were analyzed with One-way ANOVA, $* p < 0.05$. (Figures modified from Wang et al.2019).

RESULTS

3.3 Phenotypic characteristics of the *Ucp1-LUC-iRFP713* reporter mice

All mice derived from heterozygous mice breeding pairs were born at an expected Mendelian ratio of 0.79: 2.05: 1.0 (*Ucp1^{wt/wt}* (WT): *Ucp1^{wt/ki}* (HET): *Ucp1^{ki/ki}* (KI)), indicating the stable genetic inheritance in their offspring. HET and KI mice were morphologically indistinguishable from WT controls. However, it is crucial to determine whether the expression of *Ucp1* in the modified allele is affected by upstream proteins (LUC, iRFP713 and T2A) and whether the modified allele functions like the WT allele. In this regard, mice of all there genotypes were further analyzed on molecular and whole-animal level.

3.3.1 Diminished UCP1 protein abundance in brown and beige fat of KI mice

3.3.1.1 Reduced UCP1 expression in iBAT of KI mice

At an age of 5 weeks, a slightly lower body weight was observed in homozygous KI mice compared to WT littermates (Fig. 21A), although the individual fat explants analysis revealed a significantly oversized iBAT in KI mice (Fig. 21B-C). Whereas the iWAT of KI mice exhibited a tendency towards a decrease in size (Fig. 21D).
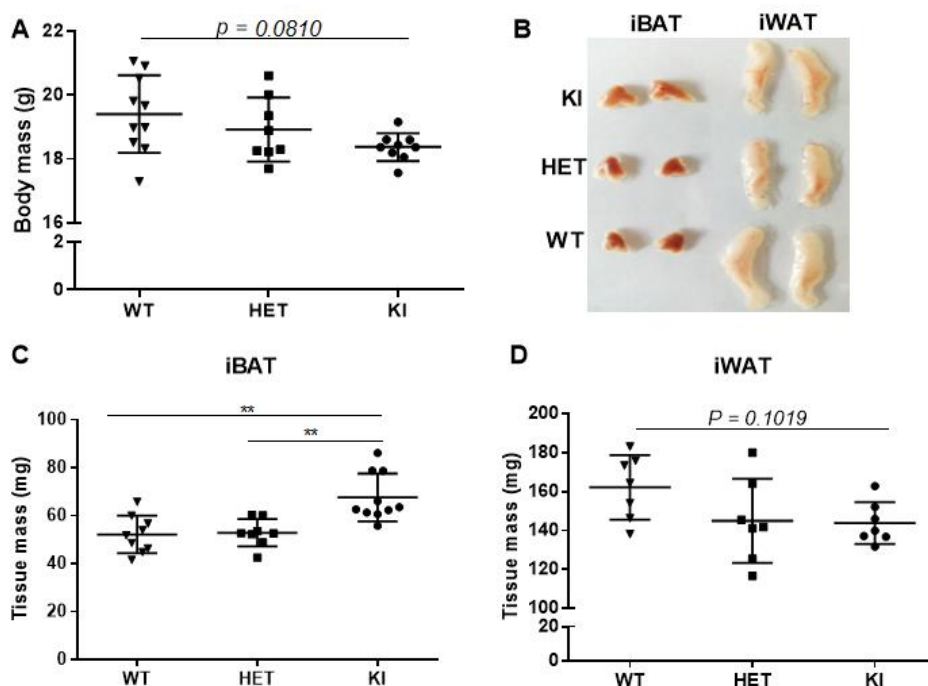
Figure 21: The construction of the reporter gene cassette leads to BAT hypertrophy at an age of 5-6 weeks. **A.** Body mass of WT, HET and KI male mice at an age of 5 weeks (n=8-10). Error bars show mean ± SD, data were analyzed with One-way ANOVA. **B.** Gross morphology of interscapular BAT and inguinal WAT from KI, HET and WT mice at an age of 5 weeks. **C-D.** iBAT (**C**) and iWAT (**D**) tissue mass in WT, HET and KI male mice at an age of 5-6 weeks (n=8-10). Error bars show mean ± SD, data were analyzed with One-way ANOVA, ** $p < 0.01$.

Moreover, theses phenotypic features persisted in reporter mice at an age of 16 weeks. KI mice maintained an enlarged iBAT depot, with mild reductions in body weight as well as in their iWAT mass (Fig. 22A-C). Taken together, these results suggest that the knock-in cassette integrated into mouse genome leads to a specific hypertrophy of iBAT but not iWAT.
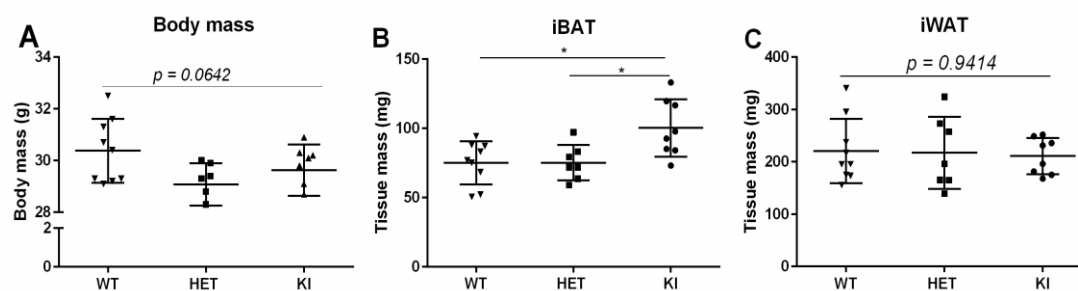
Figure 22: The body mass and tissue mass of mice at an age of 16 weeks.
A. Body mass of WT, HET and KI male mice at an age of 16 weeks (n = 6-10). **B.** iBAT tissue mass of WT, HET and KI male mice at an age of 16 weeks (n = 6-10). **C.** iWAT tissue mass of WT, HET and KI male mice at an age of 16 weeks (n = 6-10). From **A** to **C**, error bars show mean ± SD, data were analyzed with One-way ANOVA, ** $p < 0.01$.

To assess whether the morphological changes are originating from molecular dissimilarities, the relative gene expression in iBAT of the three genotypes was first quantified with real-time quantitative PCR (RT-qPCR).

Several pairs of primers were designed for the selective detection of WT and KI alleles (Fig. 23A). Compare to WT controls, the transcriptional levels of *Ucp1* exon 5 were dramatically reduced in iBAT of KI mice (Fig. 23B). While the expression of other classical brown-maker genes such as *Zic family member 1* (*Zic1*), *Cidea, Cox7A1, Pgc1a* and *Prdm16* were unchanged across the three genotypes (Fig. 23B). Western blot revealed the drastically decreased UCP1 protein content in iBAT of KI mice relative to the higher UCP1 abundance in HET and WT counterparts (Fig. 23C).

To evaluate the absolute transcripts from WT and KI allele, digital droplet PCR (ddPCR) was employed to quantify their variation copy numbers (VCN) from HET cDNA. FAM and HEX fluorescent probes were used to label WT and KI allele, respectively. During the measurement, every cDNA sample was partitioned into 20000 lipid droplets, whose fluorescence signals were afterwards counted in a droplet reader by passing them in a single stream through a fluorescence detector. Intriguingly, the dual-probe system revealed that among the 20000 lipid droplets of single cDNA sample from the iBAT of HET mice, approximately 9000 droplets

RESULTS

were FAM-WT positive, while only 2500 contained HEX-KI signals (Fig. 23D). The compiled analysis from six independent cDNA samples indicated that the absolute KI transcripts was only one tenth of the quantity from WT allele, indicting the impaired transcription in KI allele (Fig. 23E).
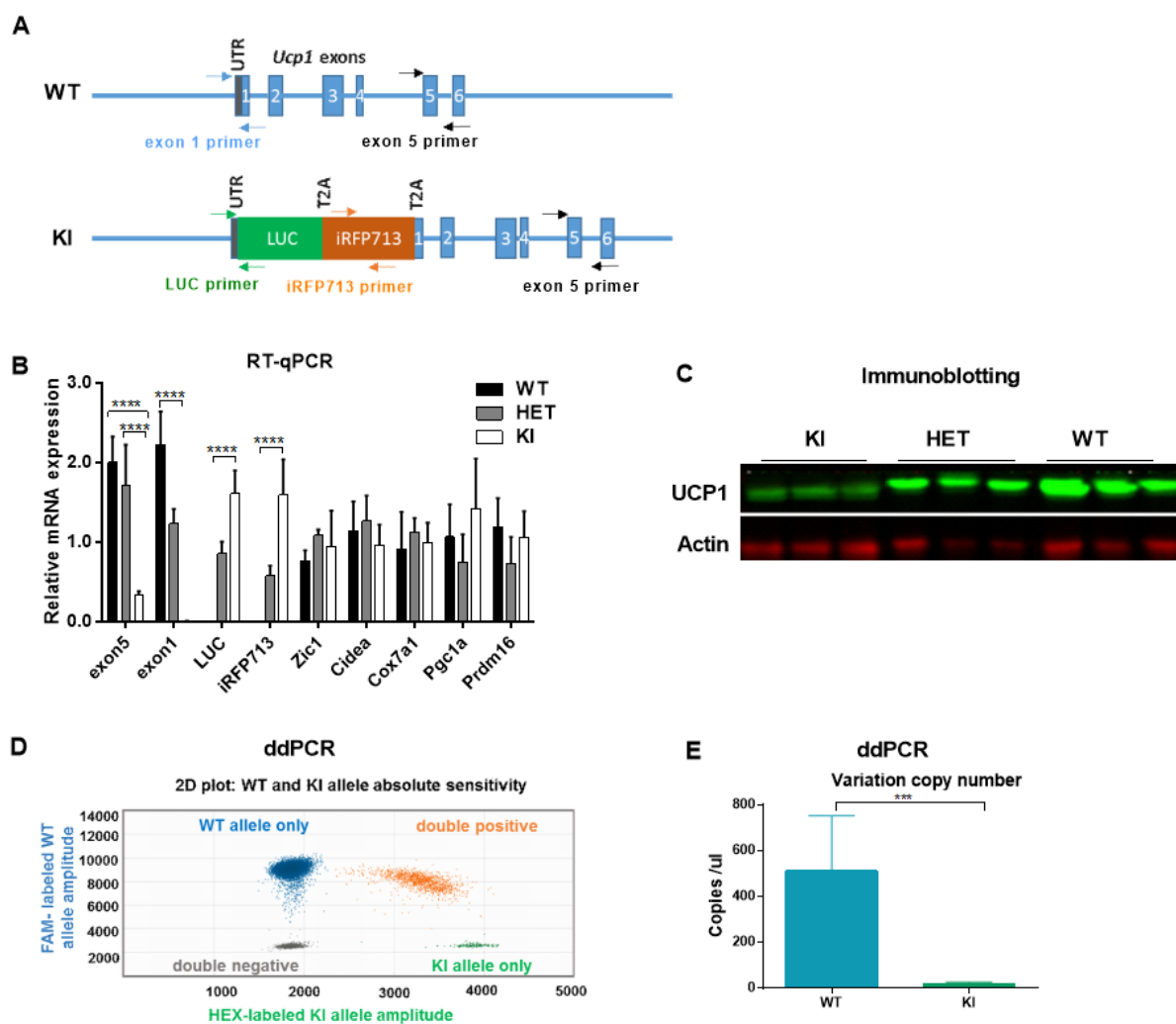
Figure 23: The insertion of the reporter genes impairs *Ucp1* expression in KI allele.
A. Schematic representation of WT allele and KI allele as well as the designed primers for RT-qPCR and ddPCR. **B.** Relative mRNA levels of reporter genes and brown fat-enriched genes expressed in iBAT of WT, HET and KI mice at an age of 5-6 weeks (n = 6). Error bars show mean ± SD, data were analyzed with Two-way ANOVA, **** $p < 0.0001$. **C.** Representative immunoblotting analysis of UCP1, LUC and Actin in iBAT (30 µg protein) of all three genotypes at an age of 5-6 weeks. **D.** The ddPCR 2-dimensional (2-D) plotting of droplet populations by FAM labeled and HEX-labeled fluorescence amplitude. FAM-positive signal indicates WT transcripts; HEX-positive represents KI transcripts. **E.** ddPCR quantification of absolute transcripts of WT and KI allele from the same heterozygous iBAT cDNA samples (n=6). Error bars show mean ± SD, data were analyzed with Student's unpaired two-tailed *t* test, *** $p < 0.001$.

3.3.1.2 Reduced UCP1 expression in brown adipocytes of KI mice

In an attempt to investigate whether the decreased UCP1 protein expression affects its metabolic functions in cultured brown adipocyte; stromal vascular fraction (SVF) progenitors were isolated from iBAT depots of three genotypes. Primary brown adipocytes derived from iBAT of KI mice had the cell-autonomous ability to fully differentiate *in vitro*, but severe decreases in their *Ucp1* mRNA (Fig. 24A) and protein levels (Fig. 24B) were noticed, accompanied with minor reductions in *Cidea* and *Pgc1a* mRNA expression (Fig. 24A). Consequently, UCP1-dependent oxygen consumption rate (OCR) induced by isoproterenol was dramatically reduced in cultured brown adipocytes of KI mice, indicating that cell-autonomous impairment of UCP1-meaidted thermogenic capacity in KI brown adipocytes (Fig. 24C-D). Meanwhile, primary brown fat cells from HET mice showed similar capacity to WT adipocytes in terms of intracellular molecular and functional characteristics (Fig. 24A-D).
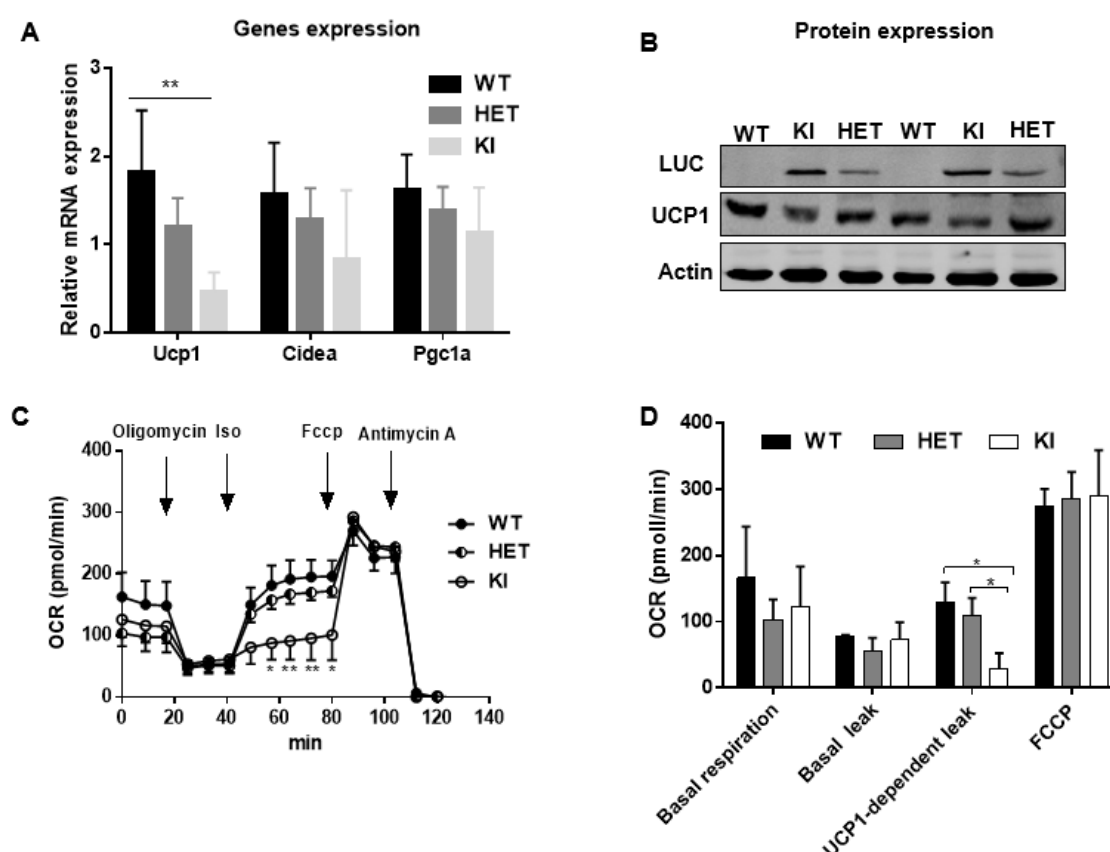
Figure 24: Reduced UCP1 expression and UCP1-mediated respiration in brown adipocytes of KI mice.
A. The mRNA expression of brown-maker genes in primary brown adipocytes of all three genotypes (n=3). Error bars show mean ± SD, data were analyzed with One-way ANOVA, * $p < 0.05$ **B.** Immunoblotting analysis of UCP1, LUC and Actin in primary brown adipocytes isolated from all three genotypes. **C-D.** Oxygen consumption rate (OCR) of primary brown adipocytes from WT, HET and KI mice (N=3, n=32). Error bars show mean ± SD, data were analyzed with Two-way ANOVA, * $p < 0.05$, ** $p < 0.01$.

RESULTS

3.3.1.3 Reduced UCP1 expression induces browning of subcutaneous WAT

It has been suggested that iWAT is the subcutaneous fat depot with a high browning propensity, which promoted the investigation of the molecular and physiological alterations in iWAT of KI mice. Unlike the gene expression pattern in iBAT, the relative expression of exon 5 in iWAT of KI mice was similar to that in HET and WT, while the expression of other browning-selective genes such as *Cidea*, *Pgc1a*, *Prdm16* and *Cox7a1* was highly expressed in iWAT of KI mice (Fig. 25A). Even though UCP1 protein in iBAT of KI mice was lower than HET and WT counterparts (Fig. 25B), hematoxylin and eosin (H&E) staining revealed a great number of small adipocytes recruited in iWAT of KI mice (Fig. 25C). The combination of the molecular and histological evidence showed the browning effects in iWAT of KI mice. Based on the comparable levels of *Ucp1* mRNA expressed in iWAT of all three genotypes, it seems that the KI reporter gene cassette caused impairment in protein translation (Fig. 25B), likely due to the Proline attachment to UCP1 during the post-transcriptional process.

In summary, these results demonstrate the reduced UCP1 protein expression in the U*cp1-LUC-iRFP713* reporter mice leads to the browning of iWAT.
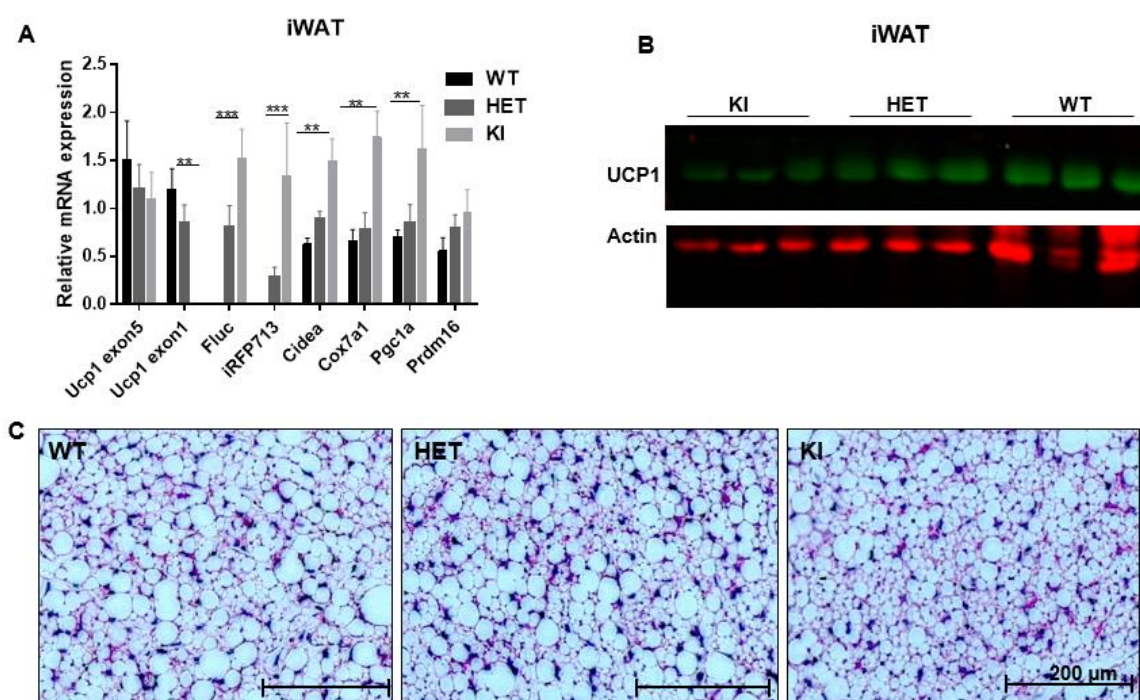
Figure 25: Reduced UCP1 protein in iBAT leads to remodeling of iWAT.
A. Relative gene expression analysis in iWAT of WT, HET and KI mice at an age of 5-6 weeks (n=6). Error bars show mean ± SD, data were analyzed with Two-way ANOVA, ** $p < 0.01$, *** $p < 0.001$. **B.** Immunoblotting detection of UCP1, LUC and Actin protein in iWAT (30 µg protein) of all three genotypes at an age of 5-6 weeks. **C.** Representative hematoxylin and eosin staining of iWAT from WT, HET and KI mice at an age of 5-6 weeks.

RESULTS

3.3.2   Reduced BAT thermogenic capacity in KI mice

3.3.2.1 The blunted NET capacity in KI mice

The major function of BAT is UCP1-mediated non-shivering thermogenesis (NST). In mice, the norepinephrine (NE) stimulated NST quantitatively equals to BAT thermogenic capacity (Cannon & Nedergaard 2004). To gain better insight into the BAT thermogenesis in reporter mice, oxygen consumption of WT, HET and KI mice was recorded before and after administration of NE by using indirect calorimetry. Afterwards, oxygen consumption was converted to heat production (mW).

The basal metabolic rate (BMR) was determined as the lowest mean of three consecutive heat production in mice that were kept at thermoneutrality for 4 h. The resulting BMR was comparable among the three genotypes in both sexes (Fig. 26A-B). Afterwards, NE-stimulated heat production was measured at an ambient temperature of 26°C. In males, NE-administration resulted a rapid rise of heat production in WT, HET and KI mice, peaking the maximal NE-stimulation (NEmax) after 20-30 min and following with the subsequent declines. However, the maximal capacity for heat production in KI mice was stimulated to a lesser extant than the WT and HET mice (Fig. 26A). In similar, robust elevations in heat production were observed in female WT mice, while female HET and KI mice exhibited blunted responsiveness to NE-stimulation, in an allele-dose dependent manner (Fig. 26B).

Generally, the differences between BMR and NEmax was considered as NST capacity. When compared to WT mice of both sexes, the NST capacity was slightly reduced in HET mice but was severely impaired in KI mice (Fig. 26C). Meanwhile, body mass was measured before and after the NE administration on the same measuring day. Before NE-stimulation, there was no differences in body weight among WT, HET and KI mice within the same gender. In both male and female animals, NE-stimulation drove concurrent decreases in body mass of each genotype, leaving the body mass comparable across the there genotypes (Fig. 26D).

Taken together, these results indicate that the impairment in UCP1 protein levels causes the diminished NST capacity in KI mice.
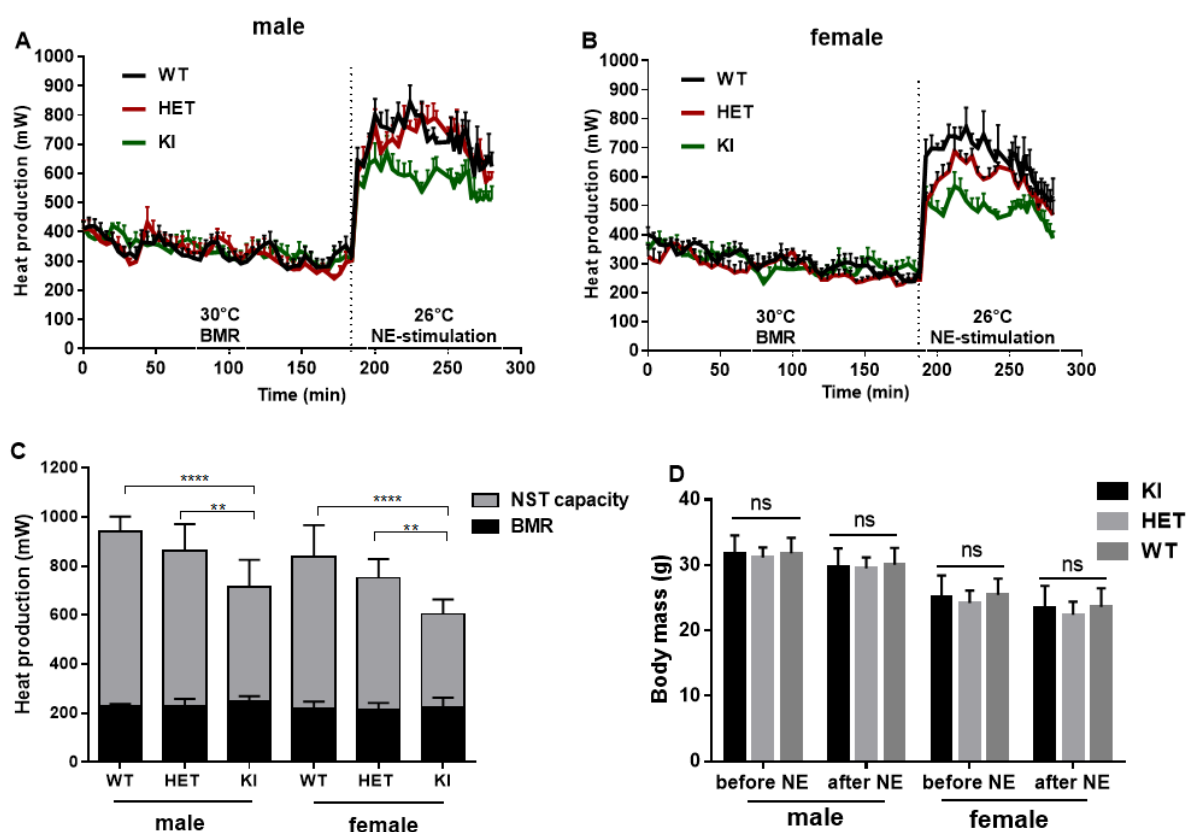
Figure 26: The impaired NST capacity in KI mice.
A-B. Metabolic rates were measured in male and female mice that were kept at thermoneutrality for 4 h. After the determination of BMR, mice were injected with over-dosed NE (1 mg/kg), and NEmax was determined as the maximal heat production within 20-30 min following NE injection. Error bars show mean $\pm$ SD. **C.** Compilation of basal metabolic rate (BMR) and NST capacity in WT, HET and KI mice. Error bars show mean $\pm$ SD, data were analyzed with Two-way ANOVA, ** $p < 0.01$, *** $p < 0.001$. **D.** Measurements of body mass before and after NE stimulation. Error bars show mean $\pm$ SD, data were analyzed with Two-way ANOVA.

3.3.2.2   KI mice are more cold-sensitive than WT mice

Next, to compare the thermogenic behavior across the three genotypes, the maximal capacity for heat production (HPmax) and the resting metabolic rate (RMR) were measured in a decreasing ambient temperature. During the measurement day, the ambient temperature was stepwise decreased from 30°C, 25°C, 15°C, 10°C, 5°C to 0°C, with each temperature maintained for 45-90 min until a stable reading could be observed.

As the ambient temperature decreases, heat production was gradually but markedly increased in all three genotypes of both sexes. In males, HET mice produced similar heat production as WT controls throughout the stepwise cold-exposure settings. However, the KI mice generated remarkable lower heat than HET and WT mice at an ambient temperature of 5°C, and the difference became more pronounced when the ambient temperature gradually dropped to 0°C

RESULTS

(Fig. 27A and C). In females, HET mice failed to further increase heat production at 0°C. The female KI mice started to show impairment in heat production when the ambient temperature was 10°C, and they mice rapidly succumb to cold when the ambient temperature was lower to 0°C (Fig. 27B and D). Additionally, there was no difference in body mass among WT, HET and KI mice of the same sex after cold challenge (Fig. 27E), KI had the significantly low body temperature than HET and KI mice (Fig. 27F).
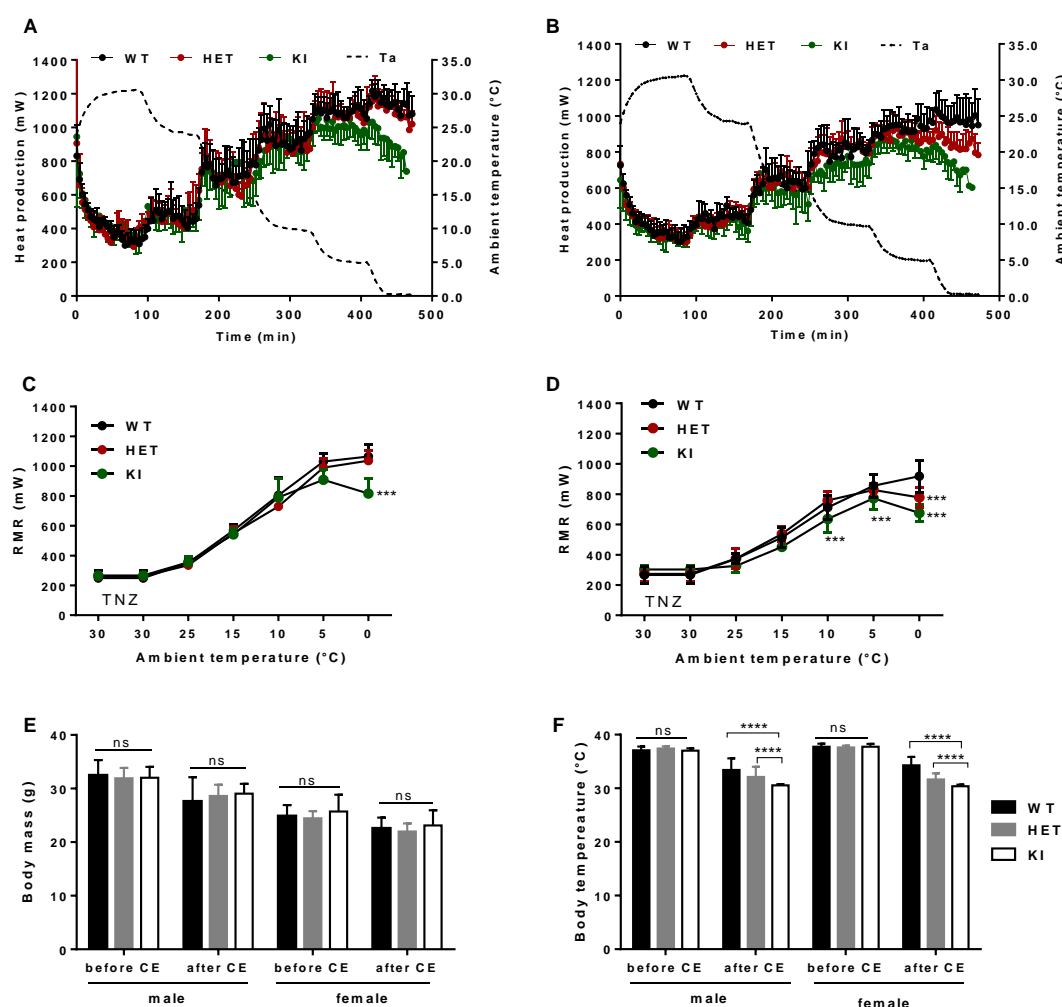
Figure 27: Determination of the thermogenic capacity in mice at a decreasing ambient temperature.
A-B. During the measurement day, the ambient temperature of each mouse was lowered stepwise from 30°C, 25°C, 15°C, 10°C, 5°C, to 0°C, with each temperature maintained for 45-90 min. A whole measurement lasted up to 8 h, while no food or water was supplied. Maximal resting metabolic rate (HPmax, mW) was defined as the highest metabolic rate observed in a non-exercising mouse. **C-D.** Analysis of the heat production in both male and female mice. Error bars show mean ± SD, data were analyzed with Two-way ANOVA. * $p < 0.05$, *** $p < 0.001$. **E.** Measurements of body mass before and after cold exposure. Error bars show mean ± SD, data were analyzed with Two-way ANOVA. **F.** Measurement of rectal temperature before and after cold exposure. Error bars show mean ± SD, data were analyzed with Two-way ANOVA, *** $p < 0.001$.

Finally, the three major components of thermogenesis were compiled, including basal metabolic rate (BMR), NST capacity and maximal cold-induced heat production (HPmax). Male HET mice behaved like WT mice under both basal and stimulated conditions, while male KI mice exhibited strong reduction in NST capacity and HPmax. For the female animals, HET and KI mice showed lower NST and HPmax than the WT mice, with even less thermogenic capacity in KI genotype. Of note, the blunted NE-stimulated thermogenic capacity for NST capacity accounted for the reduced HPmax in transgenic mice and made the KI mice more sensitive to cold challenge (Fig. 28).
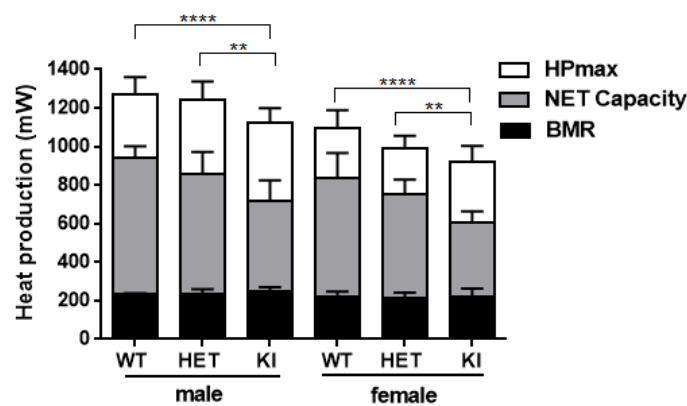
Figure 28：Compilation of the three major components of thermogenesis
The overall thermogenesis including basal metabolic rate (BMR), NST capacity and maximal cold-induced heat production (HPmax). Error bars show mean ± SD, data were analyzed with Two-way ANOVA, ** $p < 0.01$, *** $p < 0.001$.

In conclusion, KI mice displayed a remarkable reduction in UCP1 protein expression due to the knock-in strategy. Consequentially, the reduced UCP1 expression in KI allele causes sever phenotypic consequences in thermogenic capacity in an allele-dosage dependent manner. These data strength the physiology significance of UCP1-mediated non-shivering thermogenesis in protecting of body temperature.

RESULTS

3.4 UCP1 does not protect mice from diet-induced obesity

3.4.1 HFD induces UCP1 expression in a tissue-specific manner

To investigate the effects of dietary fat on *Ucp1* expression, WT, HET and KI mice of both sexes were subjected to a feeding experiment with either a low-fat control diet (CD, ~12 kJ% fat) or a high-fat diet (HFD, ~48 kJ% fat) *ad libitum* for 8 consecutive weeks. At the end of feeding, *in vivo* bioluminescence imaging was performed to reflect the changes in *Ucp1* expression between the two diets. To do so, two mice of the same genotype were simultaneously imaged using an *in vivo* imaging system (IVIS) after dosing of D-luciferin. Remarkably, HFD feeding profoundly increased the bioluminescent brightness in the ROI above iBAT of both male and female KI and HET reporter mice, when compared to the mice fed with a CD. However, the light intensity in the areas representing iWAT was drastically reduced in reporter mice on a HFD (Fig. 29A-B).
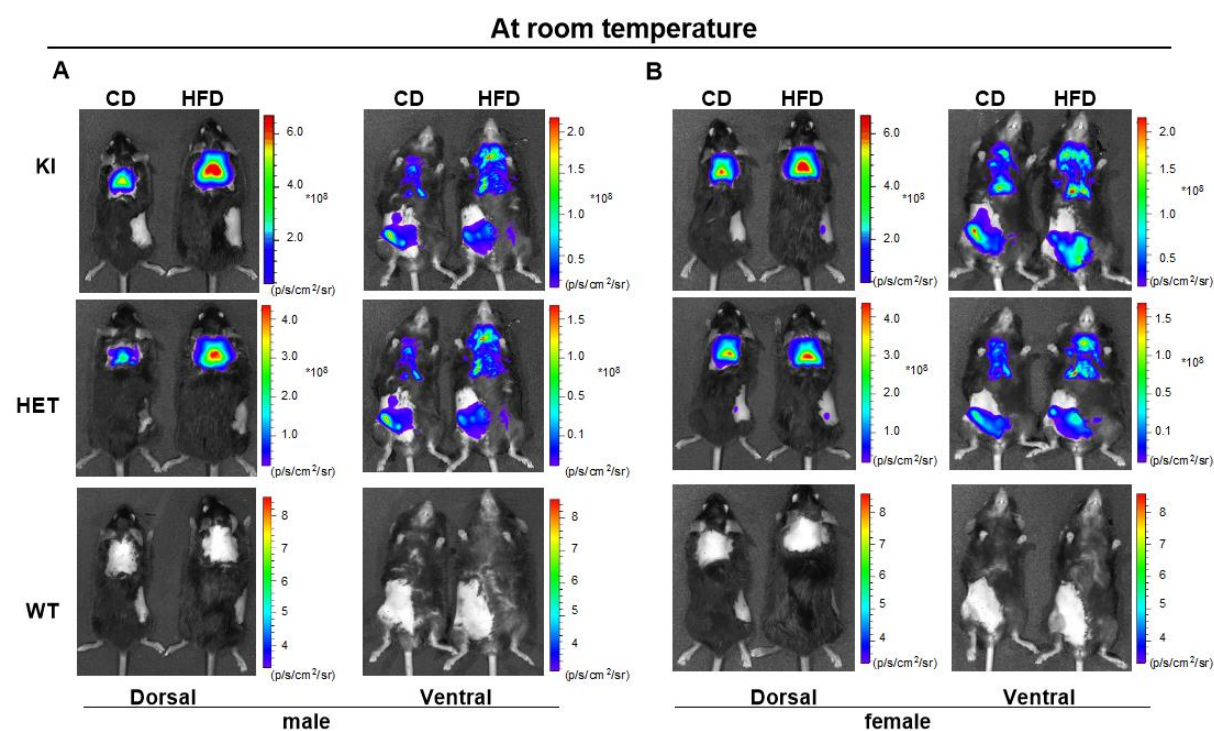
Figure 29: Effects of HFD feeding on *in vivo* bioluminescence in reporter mice.
A. KI, HET and KI male mice were fed with a CD or HFD for 8 weeks. After the feeding experiment, mice were imaged using an in vivo imaging instrument (n=6). **B.** KI, HET and KI female mice were fed with a CD or HFD for 8 weeks before *in vivo* imaging (n=6).

After the *in vivo* imaging, fat pads of KI mice were excised for further analyses. In male mice, HFD feeding caused significant increases in tissue mass of iBAT (Fig. 30A), iWAT (Fig. 30B) and gWAT (Fig. 30C). Histological analysis revealed a corresponding rise in the adipocyte

size of adipose tissue depots (Fig. 30D). In female, the long-term HFD feeding also increased iBAT and iWAT tissue mass, but the differences were not significant between the two diets (Fig. 30A-B). Meanwhile, gWAT mass was substantially enhanced by HFD feeding, when compared to the mice on a CD (Fig. 30C).
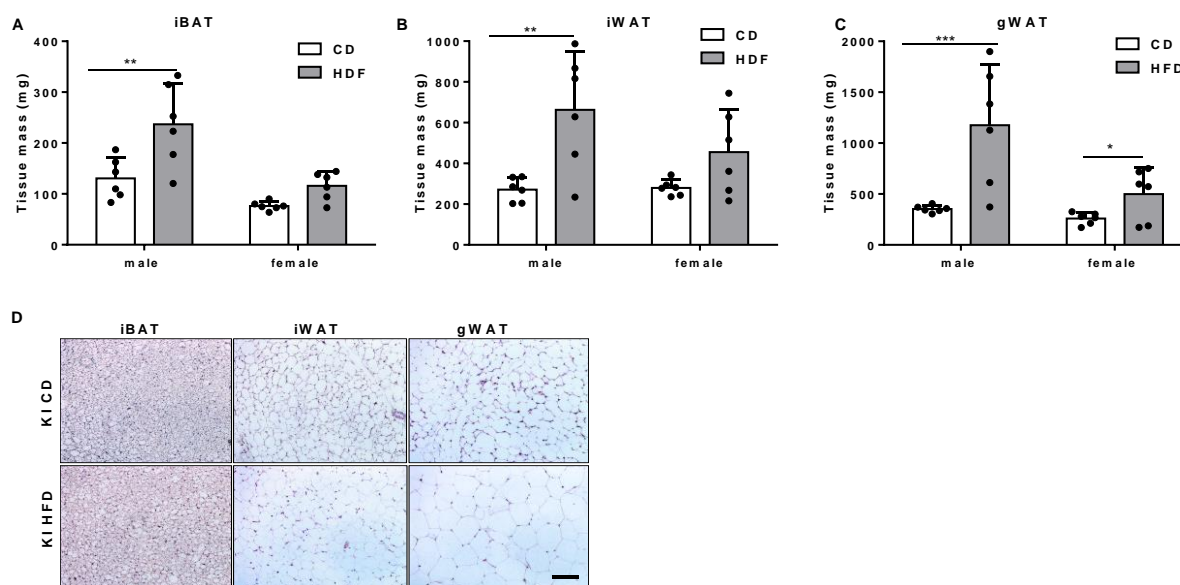
Figure 30: Analysis of adipose tissue explants from KI mice.
A. Tissue mass of iBAT in male and female KI mice upon the terminus point of 8 weeks CD or HFD feeding (n=6). **B.** Tissue mass of iWAT in male and female KI mice upon the terminus point of 8 weeks CD or HFD feeding (n=6). **C.** Tissue weights of gWAT in male and female KI mice upon the terminus point of 8 weeks CD or HFD feeding (n=6). From **A** to **C**, error bars show mean ± SD, data were analyzed with Two-way ANOVA, * $p < 0.05$, ** $p < 0.01$, *** $p < 0.001$. **D.** Representative hematoxylin and eosin staining of iBAT, iWAT and gWAT from KI mice fed with either CD or HFD. Scale bars indicates 50 µm

To verify the *in vivo* bioluminescence imaging, adipose tissue depots isolated from KI mice were analyzed using *ex vivo* bioluminescence assay. In strong correlation with the *in vivo* data, the quantification of *ex vivo* relative luminescent unit (RLU), normalized by protein content revealed the higher bioluminescence in iBAT of KI mice feeding a HFD but a drastically lower signals in iWAT of KI mice (Fig. 31A-C). Interestingly, the total bioluminescence amount calculated from an entire iBAT tissue depot was profoundly higher in mice fed with HFD, whereas HFD feeding dramatically declined the overall bioluminescence emitted from an iWAT depot (Fig. 31D-F).
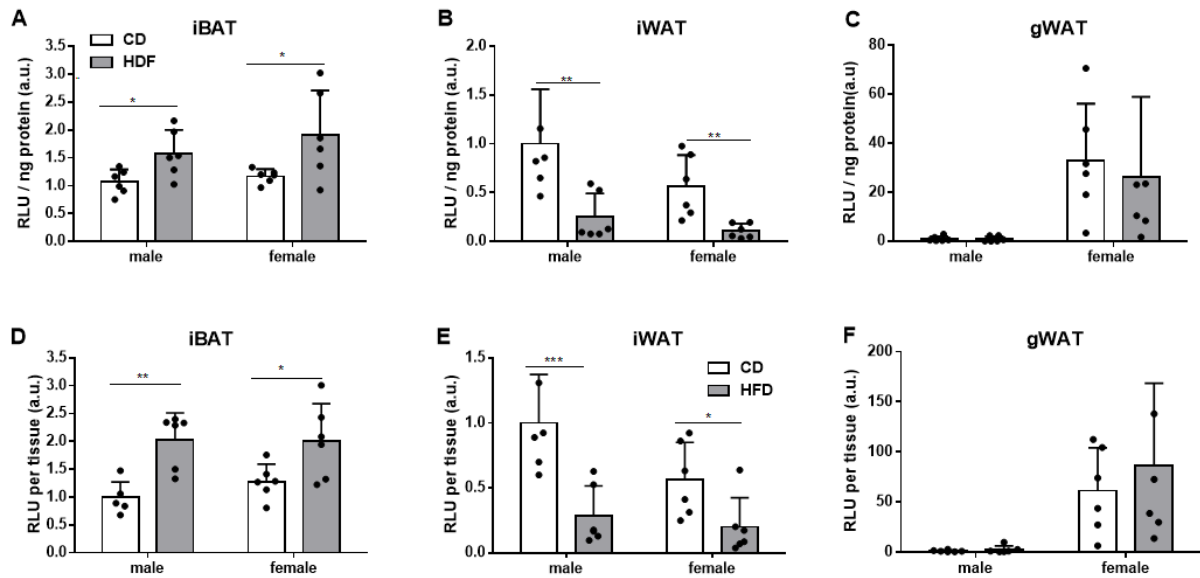
Figure 31: Analyses of adipose tissue explants from KI mice.
A-C. *Ex vivo* RLU normalized to protein content (n=6). **D-F.** The total RLU calculated from the entire tissue (n=6), From **A** to **F**, error bars show mean ± SD, data were analyzed with Two-way ANOVA, $* p < 0.05$, $** p < 0.01$, $*** p < 0.001$.

Next, the relative genes expression under the two diet feeding were assessed by RT-qPCR. Compared to CD feeding, *Ucp1* gene was largely detected in iBAT of KI mice on a HFD, but the other browning marker genes such as *Cidea* and *Cox7al* persisted unaltered (Fig. 32A). In contrast, the expression of all above thermogenic genes, including *Ucp1, Cidea* and *Cox7al* in iWAT, were dramatically downregulated by HFD feeding (Fig. 32B). In both iBAT and iWAT depots, HFD feeding resulted in similar effects on fatty acid metabolism. The 8-weeks HFD feeding attenuated fatty acid *de novo* lipogenesis by reducing the expression of its rate-limiting enzyme expression of *acetyl-CoA carboxylase* (*ACC*) and *fatty acid synthase* (*Fasn*), but promoted triglyceride lipolysis by enhancing the expression of a*dipose triglyceride lipase* (*Atgl*) and h*ormone-sensitive lipase* (*Hsl*) (Fig.32A-B). It has been demonstrated previously that alternative activation of macrophage (M2), also known as an anti-inflammatory macrophage, plays an important role in regulating *Ucp1* expression by secreting catecholamine in white adipose tissue depots in mice (Nguyen et al. 2011; Brestoff et al. 2016; Kumari et al. 2016). Thus, we measured the expression of *CD310,* a marker gene for M2 polarization state, which was highly increased in iBAT but was decreased in iWAT by HFD feeding (Fig. 32A-B).

RESULTS

Moreover, immunoblotting analysis confirmed the enhanced UCP1 protein expression in iBAT of KI mice fed a HFD (Fig. 32C). Even though, the UCP1 expression in iBAT of KI mice remained substantially lower than HET and WT mice under HFD. In conclusion, these data demonstrate the profound effects of dietary fat on the induction of *Ucp1* mRNA and UCP1 protein levels in classical brown fat but not in beige fat.
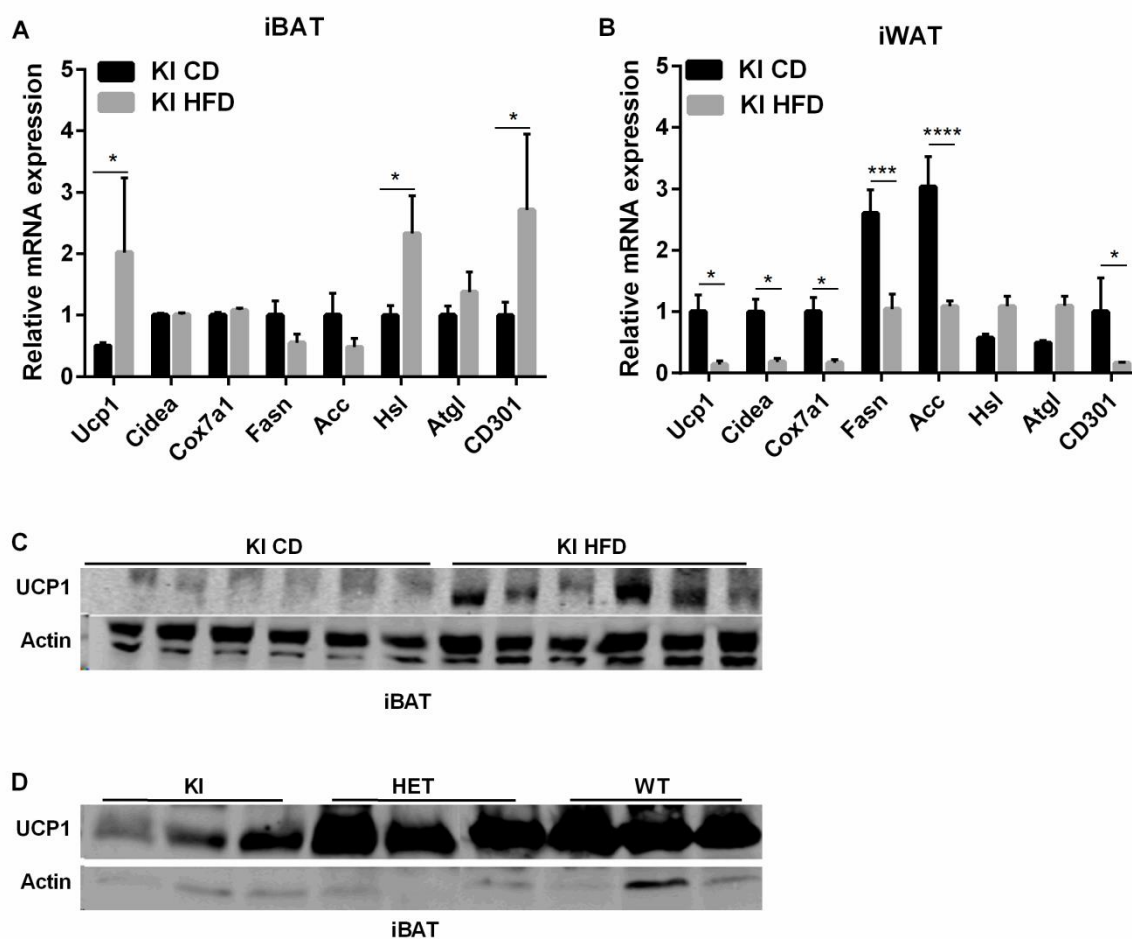
Figure 32: Effects of HFD feeding on iBAT and iWAT of KI mice
A. Relative gene expression analysis in iBAT of male KI mice fed with a CD or HFD (n=6). Error bars show mean ± SD, data were analyzed with One-way ANOVA, * $p < 0.05$. **B.** Relative gene expression analysis in iBAT of male KI mice fed with a CD or HFD (n=6). Error bars show mean ± SD, data were analyzed with One-way ANOVA, * $p < 0.05$, *** $p < 0.001$. **C.** Western blotting of UCP1 protein in iBAT of KI mice fed with either a CD or HFD (n=6). **D.** Western blot detection of UCP1 protein expression in iBAT of KI, HET and WT mice after 8 weeks of HFD feeding at room temperature (n=3).

RESULTS

3.4.2   UCP1 does not protect mice from diet-induced obesity at room temperature

Previous studies using genetic mouse models implied BAT plays a major physiological role in regulating body weight. However, UCP1-KO mice exhibited contradictory phenotypes in body mass accumulation, conditioned by various ambient temperature, age-related responsiveness and different genetic background (Lowell et al. 1993; Liu et al. 2003; Kontani et al. 2005; Feldmann et al. 2009). In the present study, the reduced UCP1 expression in KI mice, instead of the complete loss of BAT function in UCP1-KO mice, in return, provides an opportunity to explore whether BAT thermogenesis burns off excess calories in a state of positive energy balance to maintain energy homeostasis.

In males, switching to HFD led to a rapid and progressive increase in body weight, while genotype-matched mice maintained on a control diet gained the body weight gradually and slightly (Fig. 33A). At the end of 8-weeks HFD feeding, body mass of male WT, HET and KI on a HFD was substantially higher than the same-genotype mice on a CD (Fig. 33B). Measurement of body composition revealed the massively accumulated fat mass (Fig. 33C) and slightly increased lean mass in male mice consuming the HFD (Fig. 33D). However, there were no differences in body weight and body composition across the three genotypes (Fig. 33A-D).

Additionally, a remarkable sex-related difference was observed that HFD feeding only induced minor enhancement in body mass and fat mass in WT and KI mice, with the exception that HET mice on a HFD accumulated significantly higher body weight than WT and KI mice (Fig. 33E-H). However, in females, there were no differences between WT and KI mice with each types of diet (Fig. 33E-H). These results indicate that UCP1 expression in WT mice dose not protect mice from diet-induced obesity at room temperature.
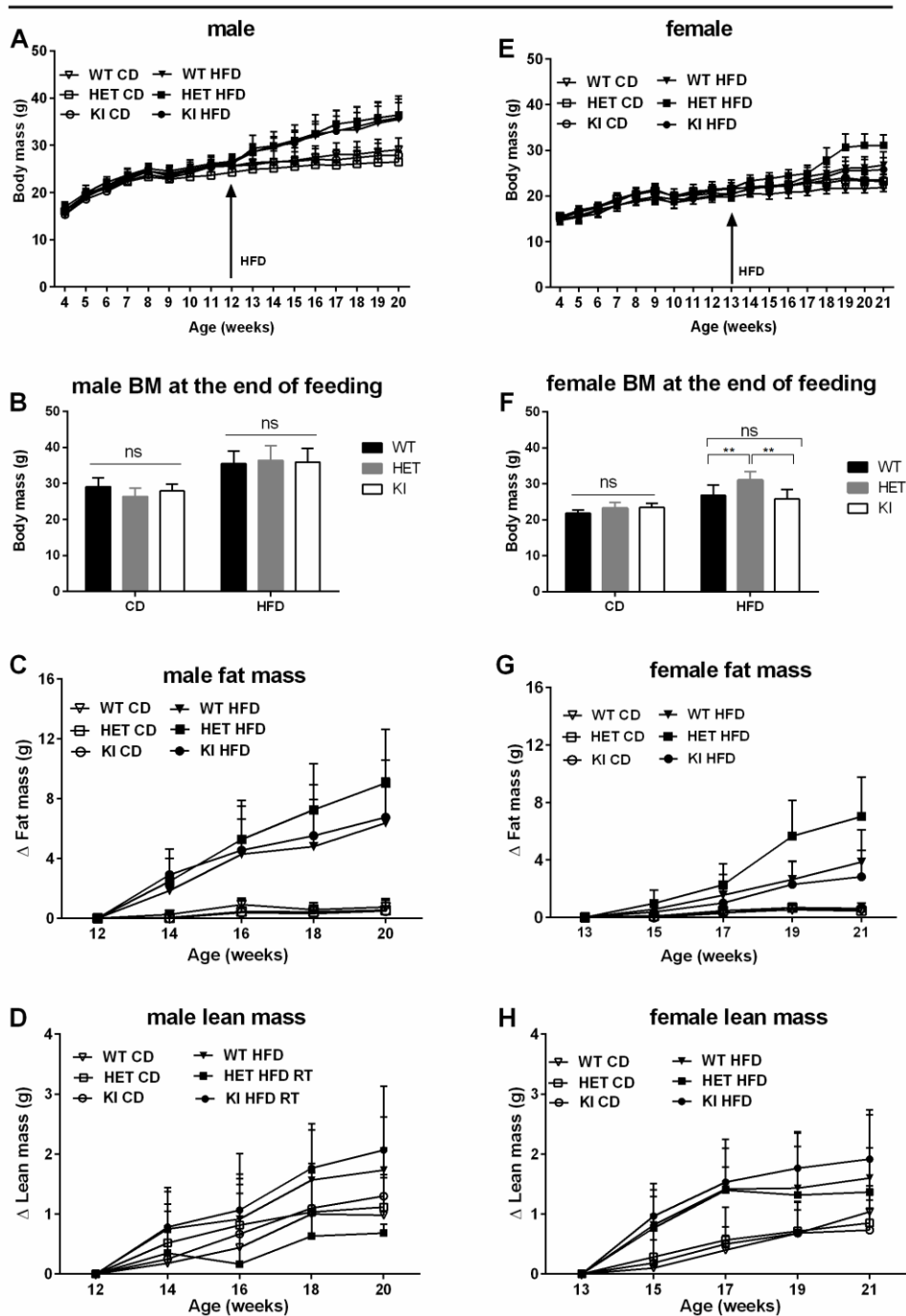
Figure 33: Effects of HFD feeding on body mass and body composition development at room temperature.
A. Body mass development of male WT, HET and KI mice fed with 8 weeks CD or HFD (n=6). **B.** Body mass of male WT, HET and KI mice at the end of the feeding experiment. **C.** Fat mass increases in male WT, HET and KI mice fed with 8 weeks CD or HFD (n=6). **D.** Lean mass increases in male WT, HET and KI mice fed with 8 weeks CD or HFD (n=6). **E.** Body mass development of female WT, HET and KI mice fed with 8 weeks CD or HFD (n=6). **F.** Body mass of female WT, HET and KI mice at the end of the feeding experiment (n=6). **G.** Fat mass increases in WT, HET and KI mice fed with 8 weeks CD or HFD (n=6). **H.** Lean mass increases in female male WT, HET and KI mice fed with 8 weeks CD or HFD (n=6). From **A** to **H**, error bars show mean ± SD, data were analyzed with Two-way ANOVA, ** $p < 0.01$.

RESULTS

3.4.3 UCP1 dose not protect mice from diet-induced obesity at thermoneutrality

To eliminate the thermal stress, HFD feeding experiment was conducted on mice that were born and maintained at thermoneutral condition (30°C). HFD feeding significantly increased light intensity above iBAT of reporter mice (dorsal view). Notably, iWAT bioluminescence was dramatically decreased by HFD, while the signals in aBAT and fBAT were profoundly increased (ventral view) (Fig. 34A-B). At thermoneutrality, UCP1 protein was hardly detected in iBAT of KI mice consuming a HFD, being the lowest among the three genotypes (Fig. 34C).
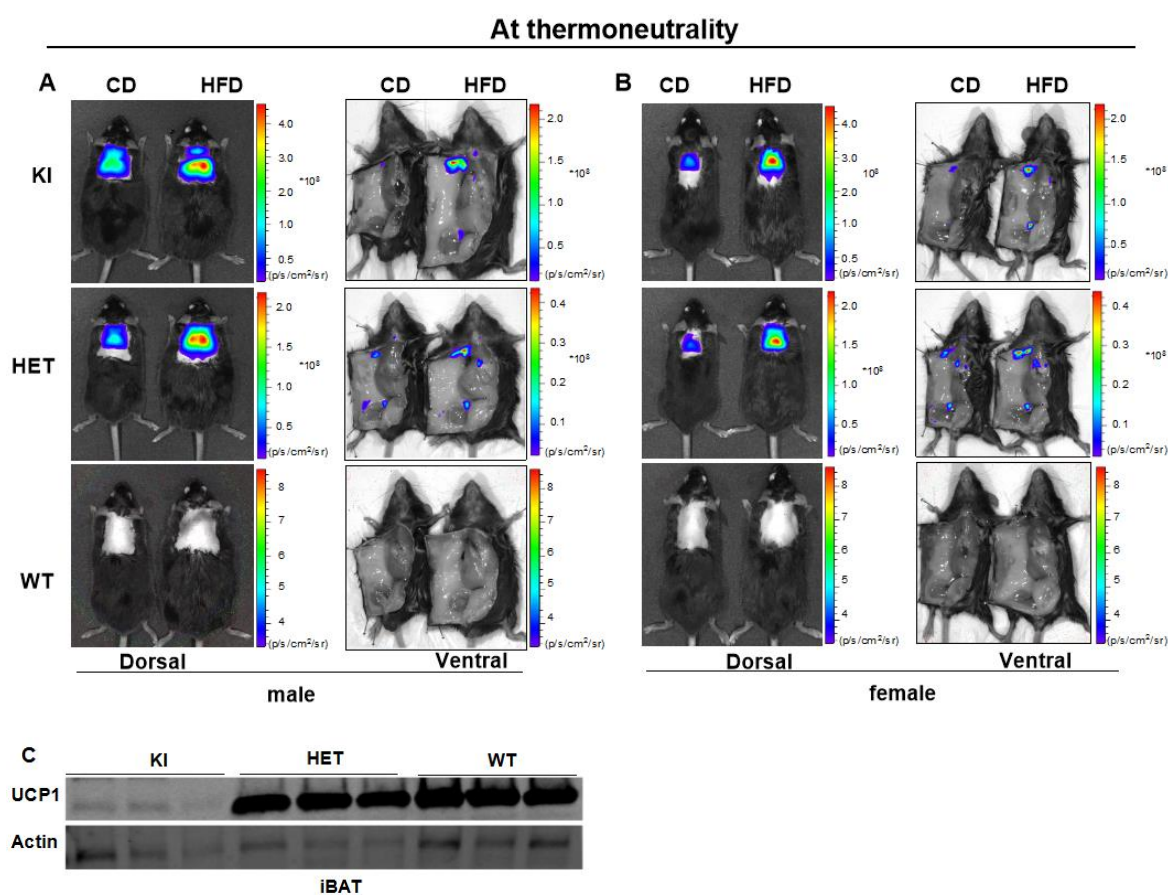
Figure 34: Effects of HFD feeding on mice kept at thermoneutrality.
A-B. Representative *in vivo* and *in situ* bioluminescence imaging of male KI, HET and KI mice consuming either a CD or a HFD for 8 consecutive weeks at thermoneutrality (n=6). **C.** Western blot detection of UCP1 protein expression in iBAT of KI, HET and WT mice after 8 weeks of HFD feeding at thermoneutrality (n=3).

Compared to mice fed with CD, HFD feeding under thermoneutrality increased the body mass, fat mass and lean mass of both male and female mice, with much profound effects in male mice (Fig. 35). However, no significant differences were detected across the three genotypes

under either CD or HFD feeding (Fig. 35). Collectively, these data suggest that UCP1 cannot protect mice from diet-induced obesity at either room temperature or at thermoneutrality.
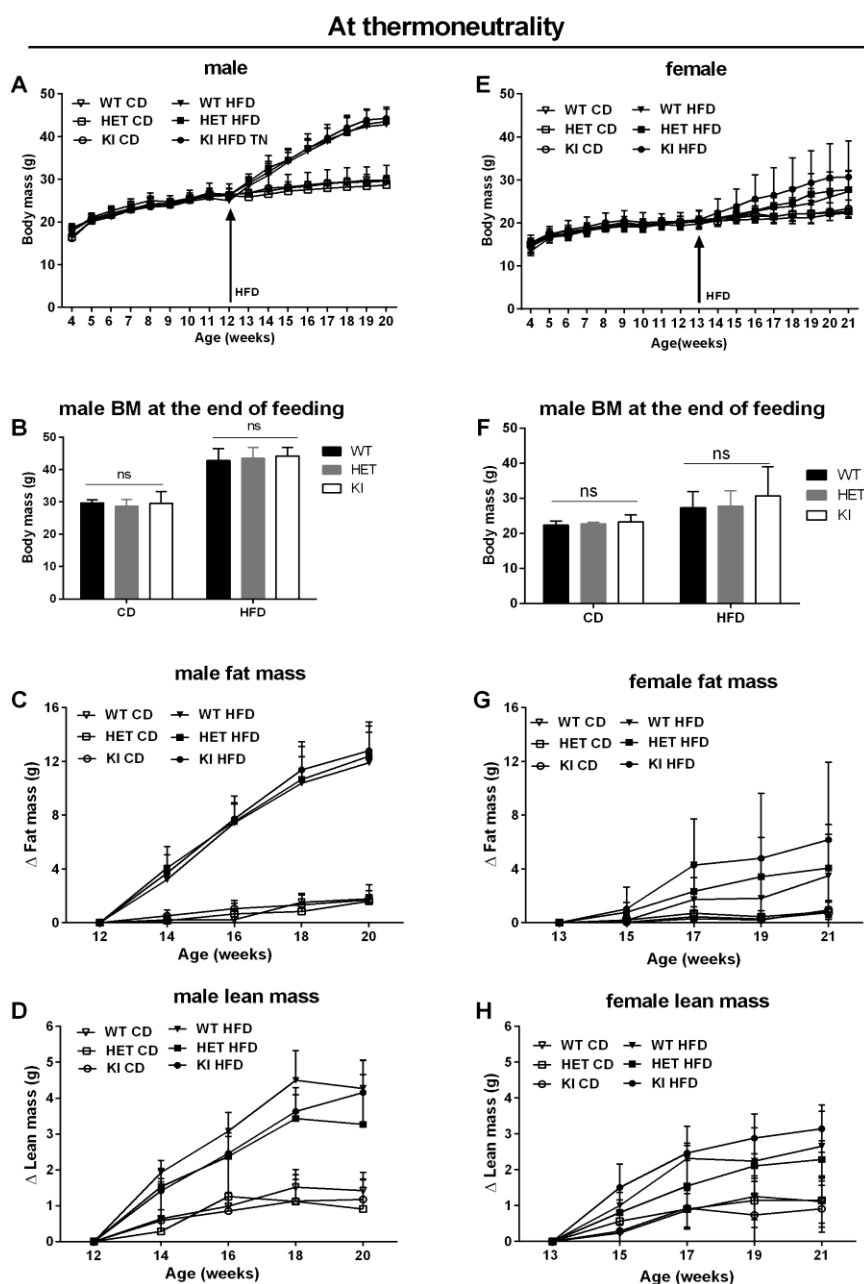
Figure 35: Effects of HFD feeding on body mass and body composition development at thermoneutrality.
A. Body mass development of male WT, HET and KI mice fed with 8 weeks CD or HFD (n=6). **B.** Body mass of male WT, HET and KI mice at the end of the feeding experiment. **C.** Fat mass increases in male WT, HET and KI mice fed with 8 weeks CD or HFD (n=6). **D.** Lean mass increases in male WT, HET and KI mice fed with 8 weeks CD or HFD (n=6). **E.** Body mass development of female WT, HET and KI mice fed with 8 weeks CD or HFD (n=6). **F.** Body mass of female WT, HET and KI mice at the end of the feeding experiment (n=6). **G.** Fat mass increases in WT, HET and KI mice fed with 8 weeks CD or HFD (n=6). **H.** Lean mass increases in female male WT, HET and KI mice fed with 8 weeks CD or HFD (n=6). From **A** to **H**, error bars show mean ± SD, data were analyzed with Two-way ANOVA.

4   DISCUSSION

In this dissertation, a novel *Ucp1-LUC-iRFP713* reporter mouse model was generated in by Taconic Biosciences GmbH, via introducing a foreign DNA coding for firefly luciferase (LUC) and near infrared fluorescence protein (iRFP713) into the endogenous *Ucp1* locus. As expected, both LUC activity and iRFP13 signals reliably report endogenous *Ucp1* expression upon physiological and pharmacological activation. Further detailed phenotypic studies revealed that the reporter mice exhibit a drastic reduction in UCP1 expression, in an allele-dose dependent manner. Therefore, the impairment of UCP1 function in the reporter mice provides a superior model to examine the role of UCP1 in protecting against diet-induced obesity.

4.1   Strengths and limitations of the *Ucp1-LUC-iRFP713* reporter mice

4.1.1   Advantages of LUC as a reporter gene in the *Ucp1-LUC-iRFP713* reporter mice

Firefly luciferase catalyzed bioluminescence in the *Ucp1-LUC-iRFP713* reporter mice works as an effective biomarker to monitor *Ucp1* expression, which permits the qualitative and quantitative detection of *Ucp1* gene expression e*x vivo*, *in vitro* and *in vivo*.

Firstly, *ex vivo* imaging and quantification of mouse organs enables to investigate the global distribution of *Ucp1* expression over a wide dynamic range of detection. Secondly, LUC protein in primary brown adipocyte of the KI mice has a comparable half-life as UCP1 protein ($t_{1/2}$ =10 h). LUC protein and its activity were tightly correlated with UCP1 protein levels in brown and beige adipocytes upon various stimuli, suggesting that both LUC protein and LUC activity work as reliable surrogate maker for *Ucp1* expression *in vitro*. Last but not the least, *in vivo* bioluminescence imaging is capable of monitoring of activation and recruitment of brown and beige adipocytes in living mice under relevant physiological conditions.

Although multiple luciferase-based *Ucp1* gene reporter mouse models have been previously described, the *Ucp1-LUC-iRFP713* reporter mice in this present study have several advantages over the others (Galmozzi et al. 2014; Mao et al. 2017). In the *Ucp1-LUC-iRFP713* reporter mice, the transgene cassette was inserted into the endogenous *Ucp1* locus. Thereby, the regulatory of both reporter genes are dependent on the transcriptional elements of the endogenous *Ucp1* gene *in situ*. The ThermoMouse (MGI:5619504, Addgene 32904) was constructed with a 98 kb bacterial artificial chromosome (BAC) transgene, encoding *luciferase2-T2A-tdTomato* followed by a bovine growth hormone (bGH)-derived polyadenylation signal (polyA) in the first exon of *Ucp1* (Galmozzi et al. 2014). However, the

DISCUSSION

98 kb BAC construction was randomly inserted into Y-chromosome, which excludes the ability to image female mice *in vivo* and thus prevents the identification of sex-associated differences (Galmozzi et al. 2014). It has been known that *Ucp1* expression is tightly regulated by transcriptional cis-elements in its 5'-UTR region (Cannon & Nedergaard 2004), while the BAC recombineering strategy used for the ThermoMouse may hinder the detection of functional distant cis-elements. During the characterization of our reporter mouse, another knock-in *Ucp1* reporter mouse model was established as *Ucp1-2A-Luciferase* mice, whose cDNA sequences coding for 2A peptides and luciferase were also introduced into the endogenous *Ucp1* locus of 129 mice strain, by replacing the stop codon in *Ucp1* exon 6 (Mao et al. 2016). Their *Ucp1-2A-LUC* mouse also acts as a *bona fide* reporter of endogenous *Ucp1* gene expression (Mao et al. 2017).

4.1.2   Advantages of iRFP713 as a reporter gene in the *Ucp1-LUC-iRFP713* mice

The second reporter molecule iRFP713 is also ideally suitable to track endogenous *Ucp1* expression in *ex vivo* and in *in vivo* settings, owing to its effective brightness, high intracellular photostability, deep tissue emission penetrance, low background signals and no requirement of exogenous substrate (Filonov et al. 2011; Shcherbakova et al. 2014). Unlike the detection of previously developed infrared fluorescent proteins (e.g. IRF1.4), which requires frequent injection of the exogenous Biliverdin for *in vivo* imaging, the Biliverdin derived from the breakdown of hemoglobin in mammalian cells are adequate to mediate iRFP713 fluorescence (Filonov et al. 2011). As a result, the iRFP713 fluorescence was directly detected in freshly excised iBAT and iWAT of HET and KI reporter mice, without the supply of extraneous Biliverdin. An unspecific signal identified in liver samples of all the three genotypes is likely due to the auto-fluorescence of hepatic bilirubin-albumin complexes (Croce et al. 2013). Additionally, iRFP713 protein can be observed in brown fat of living HET and KI mice after 4 weeks of chronic cold acclimation, without any exogenous substrate. Previously, several transgenic mouse models employing traditional green and red fluorescent proteins (GFP and RFP) have been established to study the recruitment and activation of brown and beige fat *in vivo*. ThermoMouse expressing tdTomato (Galmozzi et al. 2014) as well as UCP1-GFP and UCP1-CreER:ROSA-tdRFP mice (Rosenwald et al. 2013) were constructed using BAC strategy for the transient or permanent genetic labeling of *Ucp1*-positive adipocytes *in vivo,* but their corresponding fluorescence can only be detected in *ex vivo* tissues. Recently, a *Ucp1-2A-GFP* reporter mouse model was generated with a CRISPR-

DISCUSSION

Cas9 approach, in which GFP intensity serves as a readout of the endogenous UCP1 protein expression *in vitro*, but the GFP signal was not sufficient enough for *in vivo* imaging (Qiu et al. 2018). Taken together, the application of iRFP713 in the *Ucp1*-LUC-iRFP713 reporter mouse model offers an opportunity to monitor *Ucp1* expression in brown fat of living mice in a non-invasive manner.

4.1.3 Technical challenges during imaging

Although both reporter genes fulfill the requirement to monitor *Ucp1* gene expression, there are some technical limitations in imaging *Ucp1*-LUC-iRFP713 reporter mice. Firstly, the random pigmentation in the reporter mice (C57Bl/6N background) quenched the accurate quantification of *in vivo* bioluminescence, varying in size and location (Fig. 12A). It has been described that depilation-induced pigmentation generally found in the skin of transgenic C57Bl/6 mice (Curtis et al. 2011), which makes the repeated measurements on the same mice impossible. Therefore, breeding the reporter mice into a nude mouse model is of the highest interesting to improve *in vivo* imaging. Secondly, it was technically challenging to detect iRFP713 in mice kept at RT or in brown adipocytes *in vitro*, mainly due to the limited sensitivity of available optical detection systems, thereby high-quality emission filters are required in future studies.

4.2 LUC activity facilitates imaging and quantifying of *Ucp1*-expressing tissues

4.2.1 A previously unknown fBAT in mice

In rodents, the principal brown fat depots are located in discrete sites representing interscapular, subscapular, axillary and cervical BAT (Cinti 2001). Recent identification of new brown adipose depots underneath the ears (uBAT) by using a *Ucp1-2A-Luciferase* mouse model (Mao et al. 2017) and in the supraclavicular BAT (scBAT) (Mo et al. 2016) suggests that precise anatomical locations of brown and beige depots in mammals are not yet completely documented.

Using *in situ* bioluminescent imaging, very strong signals were visualized in iBAT, aBAT, cBAT and iWAT depots of the *Ucp1-LUC-iRFP713* reporter mice, indicating a higher *Ucp1* gene expression in these tissues. Notably, an unknown adipose tissue embedded in the cleft of femoris muscle emitted bright bioluminescence (Fig.17) (Wang et al. 2019). The molecular and histological analyses provided evidence that this depot shares prosperities of both brown and beige fat depots. This depot was therefore named as femoral brown adipose tissue (fBAT).

DISCUSSION

Given that the majority of BATs are scattered in the anterior part of the rodent body, it is therefore appealing to hypothesize that fBAT might serve as a site for heat generation to warm the surrounding areas. Due to its small tissue mass (~10 mg) and its anatomical proximity to the apex of subcutaneous iWAT, fBAT was not detected in the recent study using PET-tracers to map an adipose tissue atlas in mice (Zhang et al. 2018). The recently described uBAT depot in *Ucp1-2A-Luciferase* reporter mice (129 background) (Mao et al. 2016) was neither confirmed in the *Ucp1-LUC-iRFP713* reporter mice (C57BL/6N background) (Fig. 16), nor in the adipose tissue atlas study (C57BL/6 background) (Zhang et al. 2018). Probably, this discrepancy is due to the differences in genetic backgrounds of the mouse strains.

4.2.2   Peri-ovarian WAT has higher browning capacity than epididymal WAT

Previous studies proposed that female rats possess higher UCP1 protein content in BAT than males under standard housing conditions (Palou et al. 1998; Quevedo et al. 1998; Rodríguez et al. 2001) suggesting a potential sex-related differences between male and female animals. In this study, however, male and female KI mice showed a similar *ex vivo* bioluminescence in iBAT or iWAT, and a comparable UCP1 protein expression was found in iBAT between the two sexes, as the previously reported (Grefhorst et al. 2015; Kim et al. 2016). Unexpectedly, firefly luciferase activity, brown adipocytes marker genes expression, and the appearance of mutilocular fat cells were significant higher in female poWAT than male eWAT (Fig. 18). These data provide the straightforward evidence that poWAT has a higher browning capacity than eWAT without β_3-AR stimulation. It is probable that the higher *Ucp1* expression in poWAT plays a direct role in thermogenesis during reproduction. However, it is worthwhile to emphasize that the anatomical differences should be taken into consideration, since eWAT can only be found around the testis of male rodents, while poWAT only present in the sites around female ovaries.

4.2.3   *Ucp1* expression in non-adipose tissues

Previous studies provide evidence that UCP1 is exclusively expressed in the inner mitochondrial membrane of brown and beige adipocytes. Considerable evidence have shown the presence of *Ucp1* mRNA in liver (Shinohara et al. 1991), slow-twitch muscle fibers (Yoshida et al. 1998), and in mouse brain as well (Lengacher et al. 2004). UCP1 protein was also found in thymus (Carroll et al. 2004; Clarke et al. 2012), neurons of torpid squirrel brain (Laursen et al. 2015) and in longitudinal smooth muscle layer of ovary uterus, epididymis,

small intestine and stomach (Nibbelink et al. 2001). A follow-up study proposed that UCP1 intestine smooth muscle exerts a role in smooth muscle relaxation instead of thermogenesis (Shabalina et al. 2002). However, contradictory results were described by others, where UCP1 protein cannot be detected in the female uterus with specific antibodies (Rousset et al. 2003). Therefore, systematic profiling is required for better characterization of *Ucp1*'s distribution in mice.

As mentioned earlier, firefly luciferase reporter in *Ucp1-LUC-iRFP713* mice is a reliable readout of *Ucp1* expression. *Ex vivo* LUC bioluminescent quantification uncovered unexpected signals in thymus, brain, epididymis and soleus muscle, but not in uterus, bladder, stomach, small intestine, liver or gastrocnemius muscle (Fig. 19). Previous studies identified UCP1 protein in thymus, but it still remains unclear if UCP1 is expressed specifically in thymocytes or that the UCP1 signal is due to brown adipocytes adjacent to the thymus (Clarke et al. 2012; Frontini et al. 2009). Hence, more specific immunochemistry with proper antibodies for UCP1 or LUC are required to confirm these discoveries in brain, epididmis and soleus muscle and more studies are required to elucidate the physiological roles of the atypical *Ucp1 e*xpression.

4.2.4   Cell-based bioluminescence enables to identify a new Ucp1 modulator

The firefly luciferase activity in the reporter cells act as a *bona fide* surrogate for *Ucp1* gene in cultured brown and beige adipocytes, which can be used as an effective cell-based platform to perform high-throughput screening of new drugs and molecules. It has been known that salt inducible kinases (SIKs) play inhibitory roles on cAMP signaling pathway, mostly by promoting phosphorylation CRTCs and stopping the CRTCs translocation into nucleus (Kim et al. 2015; Paulo et al. 2018). In a proof-of-concept study, the pan-SIKs inhibitor HG-9-91-01 was identified as a powerful stimulant that positively regulates *Ucp1* gene expression and brown adipocyte thermogenic capacity (Fig. 20).

4.3   A new model to study the role of UCP1 in cold-induced thermogenesis

4.3.1   Insertion of the reporter gene cassette impairs endogenous UCP1 expression

To simultaneously express three separate proteins of LUC, iRFP713 and UCP1, Thosea asigna virus 2A (T2A) peptides were added to the C-terminus of LUC and iRFP713, respectively. The T2A sequence, composed of 21 amino acids encoding a highly conserved consensus motif at its C-terminus (conserved motif: Asp-Val/Ile-Glu-X-Asn-Pro-Gly-Pro)

73

DISCUSSION

(Donnelly et al. 2001; Szymczak et al. 2004; Doronina et al. 2008) enables multiple independent genes to be transcribed as a single mRNA, yet translated as distinct proteins. During translation, ribosomes skip the formation of Gly-Pro peptide bond at the C-terminus of the T2A peptide, leading to the cleavage between a T2A peptide and the elongating peptide (Szymczak et al. 2004; Kim et al. 2011). Consequentially, the ribosome skip mechanism results in the attachment of 20 amino acids to the C-terminus of the upstream protein, and the addition of a single Proline to the N-terminus of the downstream protein. However, it remains largely unknown whether the attachments have any impact on targeted protein expression or function.

Further phenotypic studies in the *Ucp1-LUC-iRFP713* reporter mice revealed that *Ucp1* mRNA transcriptional levels were severely impaired in iBAT of KI allele (Fig. 24). Moreover, UCP1 protein abundance in both iBAT and iWAT of KI mice was severely reduced, which may ascribe to the attachment of the Proline on UCP1 protein, resulting from the T2A self-cleavage. Although the basic mechanisms for the reduced transcription remain indefinable, it is possible that insertion of the reporter gene cassettes into the endogenous *Ucp1* locus declines the mRNA stability, intracellular localization, or efficiency of protein translation of the KI allele.

4.3.2   Reduced UCP1 expression in KI mice leads to cold intolerance

As the hallmarker of BAT function, UCP1 protein is the key element for BAT mediated NST thermogenesis. In mice, NE-stimulated NST quantitatively represents the BAT thermogenic capacity (Cannon & Nedergaard 2004). In the present study, although WT, HET and KI mice have a comparable BMR at thermoneutral condition, reporter mice with decreased UCP1 expression showed blunted responses to NE stimulation, in an allele-dosage dependent manner (Fig. 27).

During the cold-tolerance test, the decreasing ambient temperature induced massive heat production in all three genotypes. However, when the ambient temperature was lower than 5°C, KI mice generated less heat than WT controls, and this discrepancy was progressively larger when the ambient temperature falls to 0°C (Fig. 27). In this regard, the thermogenic behavior of the reporter mice resemble the UCP1-KO mice, which are sensitive to acute cold exposure (Enerback et al. 1997; Golozoubova et al. 2001; Meyer et al. 2010). These results demonstrates that the reduced UCP1 protein in HET and KI mice led to decreases in NST

capacity and HPmax, indicating that UCP1 protein plays a essential role in BAT-based thermogenesis.

Furthermore, the decreased UCP1 protein levels in KI mice elicited profound induction of browning effects in iWAT, evidenced by the higher browning maker genes expression and larger amount of small adipocytes recruited in iWAT of KI mice. These findings are in great line with what has been observed in iWAT remodeling of UCP1-KO mice, suggesting the compensatory recruitment of UCP1-independent thermogenesis (Ukropec et al. 2006; Meyer et al. 2010; Granneman et al. 2003; Kazak et al. 2015; Ikeda et al. 2018).

4.4 A new model to study the role of UCP1 in diet-induced obesity

4.4.1 HFD regulates UCP1 expression in a tissue-specific manner

Pertaining to diet-induced thermogenesis, whether and how dietary components influence *Ucp1* expression has not been completely resolved. Previous studies aimed to address these questions, coming up with conflicting data (Ghorbani et al. 1997; Margareto et al. 2001; Rong et al. 2007; Kim & Park 2010).

In the present study, high-fat diet (HFD) feeding at room temperature significantly enhanced the *in vivo* bioluminescence in iBAT of reporter mice when compared to control diet (CD). These results were further confirmed by increased *Ucp1* mRNA and UCP1 protein levels in iBAT of KI mice that were fed a HFD (Fig. 32). In clear contrast, the bioluminescence and *Ucp1* gene expression were reduced in iWAT of mice after HFD feeding.

Similarly, stronger bioluminescent signals were also visualized in iBAT of the reporter mice fed a HFD at thermoneutrality, when compared to the control mice maintained on CD. However, under the thermoneutral housing condition, bioluminescence above iWAT of both KI and HET mice was barely detectable in both CD and HFD, with even lower signals in HFD groups. These observations are consistent with previous studies showing that HFD feeding upregulates *Ucp1* expression in iBAT, but downregulates *Ucp1* in iWAT (Fromme & Klingenspor 2011).

Previous publications proposed that alternative activation of macrophage (M2), also known as an anti-inflammatory macrophage, plays an important role in regulating *Ucp1* expression by secreting catecholamine in white adipose tissue depots in mice (Nguyen et al. 2011; Brestoff et al. 2016; Kumari et al. 2016). Consistently, the expression a marker gene for M2 macrophage polarization state (*CD301*), was largely increased in iBAT and severely deceased

DISCUSSION

in iWAT by HFD feeding, a expressing patter in line with *Ucp1* expression in both tissues upon HFD feeding. In conclusion, these data indicate the potential involvement of M2 macrophage in regulation of UCP1 expression upon HFD feeding; thereby further studies are necessary to confirm a link between M2 macrophage and UCP1 regulation.

4.4.2   UCP1 expression doe not protect mice from diet-induced obesity

Apart from thermoregulation, BAT is highly associated with enhanced energy expenditure according to the implement of diet-induced thermogenesis. Similar to cold-induced thermogenesis, palatable cafeteria diet remarkably increased blood flow and sympathetic activity in BAT, strongly implying the involvement of BAT in diet-induced thermogenesis (Rothwell & Stock 1979; Rothwell & Stock 1980; Landsberg et al. 1984). Although the data in section 4.2.1 demonstrates that HFD significantly increased UCP1 protein levels in iBAT, its abundance in KI mice still remained lower relative to those in HET and WT mice after HFD feeding. Based on the physiological significance of diet-induced thermogenesis, the initial expectation was that the lower UCP1 expression in KI mice would lead to the highest body mass increases, due to the impairments in diet-induced thermogenesis.

In males, HFD feeding elicited robust increases in body mass in each genotype at room temperature, but KI mice with the impaired BAT function did not gain more body mass than their HET and WT littermates (Fig. 33). The possible explanation are: 1) RT housing condition in fact represents a chronic mild cold exposure for mice, which results in profound alternative thermogenesis in KI mice (Feldmann et al. 2009), or 2) the lower UCP1 protein (20% of WT) suffices to exert diet-induced thermogenesis, and thereby protects mice from diet-induced obesity at similar levels to WT mice. To rule out thermal stress at RT, mice were born and kept at thermoneutrality. After 8 week HFD feeding, UCP1 protein in iBAT of KI mice was only weakly detectable at thermoneutrality, being only 1% of corresponding concentration in HET and KI mice. Furthermore, the extremely low UCP1 protein in KI at thermoneutrality limited the functional diet-induced thermogenesis. However, again, there were no significant differences in body mass, fat mass gain and lean mass gain among the three genotypes of the male mice consuming either a CD or a HFD (Fig. 35).

Under HFD feeding, female mice also gained more weights than the mice on a CD. At room temperature, HET mice fed with HFD gained significantly more body mass and fat mass than WT and KI mice, whereas there were no difference between WT and KI mice at the same

housing condition. Furthermore, no significant differences were found across the three genotypes when they were fed with HFD at thermoneutrality. Therefore, it is impossible that the high body weight in HET mice maintained at room temperature are due to the higher individual variabilities in female animals. In addition, a profound sex-related phenotype was observed after the switch to a HFD (Fig. 33 and 35). Compare to the progressive increases in male body mass, female mice increased their body weight in a less degree, indicating the higher susceptibility of male mice to diet-induced obesity. This is quite interesting, because several studies have proposed that male have similar energy intake to female mice under prolonged HFD (Hwang et al. 2009; Choi et al. 2015).

Taken together, contrary to the expectation, expression of UCP1 fails to protect mice from diet-induced obesity. Since UCP1 activity largely depends on the stimulation of β-ARs and the innervation of sympathetic nervous system (Bachman et al. 2002; Landsberg et al. 1984), it is highly likely that prolonged administration of rich nutrients might attenuate or impair β-ARs signaling pathway or sympathetic innervation to brown adipose tissue. However, a growing body of evidence demonstrates that β_3-adrenergic stimulation (CL316,243) potentially reverses the diet-induced obesity in rodents (Ghorbani & Himms-Hagen 1997; Guerra et al. 1998; Wang et al. 2016), indicting the intact and functional β_3-AR signaling cascade in brown adipose tissue of obese animals. More importantly, recent studies conducted a chronic cafeteria diets on WT and UCP1-KO mice revealed similar increases in body mass of both mice, while the daily CL316,243 injection to the diet-induced obese mice results in remarkably reduced body mass in WT mice, but not in KO mice. These results highly suggested the indispensable role of UCP1 for anti-obesity effects of CL316,243 administration (Inokuma et al. 2006; Olsen et al. 2016). Thereby, probably, UCP1 protein induced by HFD feeding is not sufficiently activated in mice. Finally, the hypothesis rises that KI mice which has the lowest UCP1 protein would have the less body mass decreases upon CL316,243 stimulation, while the HET and WT mice with enriched UCP1 protein could dramatically decrease their body mass in an UCP1 dose-dependent manner. To clarify this hypothesize, future studies are required to elucidate this issue.

DISCUSSION

4.5   Conclusions and outlooks

In summary, in the present study, a new *Ucp1*-LUC-iRFP713 reporter mouse line was established, wherein both genes work as reliable surrogate to monitor *Ucp1* expression *ex vivo*, *in vitro* and *in vivo*.

1. The bioluminescent visualization and quantification in the reporter mice enables unprecedented access to systemically profile *Ucp1*-expressing cells in adipose and non-adipose tissues and organs. First of all, the reporter gene strategy offers an opportunity to directly distinguish the *Ucp1*-postitive tissues from the *Ucp1*-negtive organs by *in situ* imaging, facilitating the identification of unknown *Ucp1*-expressing femoral brown adipose tissue in the reporter mice. The *ex vivo* bioluminescent quantification expands the knowledge on the overall *Ucp1* distribution, manifested the detection of atypical *Ucp1* expression in thymus, brain, epididymis and soleus muscle, and also disclosed a sex-associated divergence in browning propensity between male eWAT and female gWAT. Secondly, the *in vitro* luciferase imaging assay acts as an accurate and easy-to-use system to track *Ucp1* expression *in vitro*, which is potentially suitable for high-throughput-screening of new drug molecules to promote *Ucp1* expression in the future study. In a proof-of-concept study, the pan-SIKs inhibitor HG-9-91-01 was identified as a powerful *Ucp1* activator, which positively regulates *Ucp1* gene expression and brown adipocyte thermogenic functionality. Finally, LUC and iRFP713 signals suffice the *in vivo* imaging in the relevance context of physiological process, which would be highly beneficial in the efforts to identify and test the physiological and pharmacological modulators on *Ucp1* expression in a more physiologically relevant manner.

2. Interestingly, the phenotypic analysis of WT, HET and KI mice revealed the reduced UCP1 protein expression in iBAT and iWAT of reporter mice, in an allele-dose dependent fashion. The reduced UCP1 expression can be put forward to investigate the physiological essence of UCP1 protein in BAT-mediated NST and in the protection of diet-induced obesity. Interestingly, the allele-dose dependent decrease in UCP1 protein expression resulted in the phenotypic consequences of reduced capacity for NST, making KI mice more cold sensitive. Although HFD feeding significantly increased UCP1 expression in iBAT, the UCP1 content remained lower in KI mice than HET and WT mice. Conversely, the different amounts of UCP1 protein among the three genotypes did not resulted in body mass differences, even though they were subjected to prolonged HFD feeding at either room temperature or thermoneutrality. Although these data show that UCP1 cannot protect mice from diet-induced obesity, it is highly likely that HFD-feeding induced UCP1 protein is not activated. To clarify

DISCUSSION

this hypothesis, CL316,243 injection is required to activate UCP1-mediated thermogenesis and the reduced effects on body mass.

REFERENCE

Abreu-vieira, G. et al., 2015. Adrenergically stimulated blood flow in brown adipose tissue is not dependent on thermogenesis. *Am J Physiol Endocrinol Metab*, (308), pp.822–829.

Ahmadian, M. et al., 2011. Desnutrin/ATGL is regulated by AMPK and is required for a brown adipose phenotype. *Cell Metabolism*, 13(6), pp.739–748. Available at: http://dx.doi.org/10.1016/j.cmet.2011.05.002.

Alvarez, R. et al., 2000. Both retinoic-acid-receptor- and retinoid-X-receptor-dependent signalling pathways mediate the induction of the brown-adipose-tissue-uncoupling-protein-1 gene by retinoids. *Biochemical Journal*, 345(1), pp.91-96. Available at: http://www.biochemj.org/bj/345/bj3450091.htm.

Anunciado-Koza, R. et al., 2008. Inactivation of UCP1 and the glycerol phosphate cycle synergistically increases energy expenditure to resist diet-induced obesity. *Journal of Biological Chemistry*, 283(41), pp.27688–27697.

Atgié, C., Allaire, F.D. & Bukowiecki, L.J., 1997. Role of β_1-and β_3-adrenoceptors in the regulation of lipolysis and thermogenesis in rat brown adipocytes. *Am J Physiol Cell Physiol*, 273, pp.1136–1142.

Bachman, E.S. et al., 2002. βAR signaling required for diet-induced thermogenesis and obesity resistance. *Science*, 297(5582), pp.843–845.

Bamshad, M., Song, C.K. & Bartness, T.J., 1999. CNS origins of the sympathetic nervous system outflow to brown adipose tissue. *The American journal of physiology*, 276(6), pp.1569-78. Available at: http://www.ncbi.nlm.nih.gov/pubmed/10362733.

Baron, D.M. et al., 2012. In vivo noninvasive characterization of brown adipose tissue blood flow by contrast ultrasound in mice. *Circ Cardiovasc Imaging*, 5(5), pp.652–659.

Bartness, T., Vaughan, C. & Song, C., 2010. Sympathetic and sensory innervation of brown adipose tissue. *International Journal of Obesity*, 34(01), pp.S36–S42.

BIO-Rad, 2014. Bio-rad Droplet Digital PCR protocol, pp.1–111. Available at: papers3://publication/uuid/8D70BC7D-3BBF-487A-B9F2-308F4F522F88.

Branca, R.T. et al., 2014. Detection of brown adipose tissue and thermogenic activity in mice by hyperpolarized xenon MRI. *Proceedings of the National Academy of Sciences*, 111(50), pp.18001–18006. Available at: http://www.pnas.org/lookup/doi/10.1073/pnas.1403697111.

Brestoff, J.R. et al., 2016. Group 2 innate lymphoid cells promote beiging of adipose and limit obesity. *Nature*, 519(7542), pp.242–246.

Brestoff, J.R. et al., 2014. Group 2 innate lymphoid cells promote beiging of white adipose tissue and limit obesity. *Nature*, 519(7542), pp.242–6. Available at: http://dx.doi.org/10.1038/nature14115.

Cannon, B., Hedin, A. & Nedergaard, J., 1982. Exclusive occurrence of thermogenin brown adipose tissue antigen in brown adipose tissue. *FEBS Letters*, 150(1), pp.129–132.

Cannon, B. & Nedergaard, J., 2004. Brown adipose tissue: function and physiological significance. *Physiological reviews*, 84(1), pp.277–359.

Carroll, A.M. et al., 2004. Immunodetection of UCP1 in rat thymocytes. *Biochemical Society Transactions*, 32, pp.1066–1067.

Cassard-Doulcier, A.-M. et al., 1998. A 211-bp enhancer of the rat uncoupling protein-1 (UCP-1) gene controls specific and regulated expression in brown adipose tissue. *Biochem. J.*, 246, pp.243–246.

Cassard-Doulcier, A.-M. et al., 1993. Tissue-specific and β-adrenergic regulation of the mitochondrial uncoupling protein gene : Control by c & -Acting Elements in the 5 '

REFERENCE

Flanking Region. *Molecular endocinology*, 7(4), pp.497–506.

Choi, M. et al., 2015. High-fat diet decreases energy expenditure and expression of genes controlling lipid metabolism , mitochondrial function and skeletal system development in the adipose tissue , along with increased expression of extracellular matrix remodelling- and inflammation-related genes. *British Journal of Nutrition*, pp.867–877.

Cinti, S., 2001. The adipose organ: Morphological perspectives of adipose tissues. *Proceedings of the Nutrition Society*, (60), pp.319–328.

Clarke, K.J. et al., 2012. A role for ubiquitinylation and the cytosolic proteasome in turnover of mitochondrial uncoupling protein 1 (UCP1). *Biochimica et Biophysica Acta - Bioenergetics*, 1817(10), pp.1759–1767. Available at: http://dx.doi.org/10.1016/j.bbabio.2012.03.035.

Cohen, P. et al., 2014. Ablation of PRDM16 and beige adipose causes metabolic dysfunction and a subcutaneous to visceral fat switch. *Cell*, 156(1–2), pp.304–316. Available at: http://linkinghub.elsevier.com/retrieve/pii/S0092867413015900.

Collins, S. et al., 1997. Strain-specific response to beta 3-adrenergic receptor agonist treatment of diet-Induced obesity in mice. *Society*, 138(1), pp.405–413.

Cousin, B. et al., 1992. Occurrence of brown adipocytes in rat white adipose tissue : molecular and morphological characterization. *Journal of Cell Science*, 103, pp.931–942.

Croce, A.C. et al., 2013. Bilirubin: An autofluorescence bile biomarker for liver functionality monitoring. *Journal of Biophotonics*, 7(10), pp.810–817.

Cui, X. et al., 2016. Thermoneutrality decreases thermogenic program and promotes adiposity in high-fat diet-fed mice. *Physiological Reports*, 4(10), pp.1–14.

Curtis, A. et al., 2011. Temporal variations of skin pigmentation in C57Bl/6 mice affect optical bioluminescence quantitation. *Molecular Imaging and Biology*, 13(6), pp.1114–1123.

Cypess, A.M. et al., 2015. Activation of human brown adipose tissue by a β3-adrenergic receptor agonist. *Cell Metabolism*, 21(1), pp.33–38.

Cypess, A.M. et al., 2009. Identification and importance of brown adipose tissue in adult humans. *New England Journal of Medicine*, 360(15), pp.1509–1517. Available at: http://www.nejm.org/doi/abs/10.1056/NEJMoa0810780.

Cypess, A.M. & Kahn, C.R., 2013. Brown fat as a therapy for obesity and diabetes Aaron. *Curr Opin Endocrinol Diabetes Obes*, 17(2), pp.1–14.

Din, M. u et al., 2016. Human brown adipose tissue [^{15}O]O$_2$ PET imaging in the presence and absence of cold stimulus. *European Journal of Nuclear Medicine and Molecular Imaging*, 43(10), pp.1878–1886. Available at: http://dx.doi.org/10.1007/s00259-016-3364-y.

Din, M.U. et al., 2018. Clinical and translational report postprandial oxidative metabolism of Human Brown Fat Indicates Thermogenesis, *Cell Metabolism*, pp.1–10. Available at: https://doi.org/10.1016/j.cmet.2018.05.020.

Donnelly, M.L.L. et al., 2001. The "cleavage" activities of foot-and-mouth disease virus 2A site-directed mutants and naturally occurring "2A-like" sequences. *Journal of General Virology*, 82(5), pp.1027–1041.

Doronina, V.A. et al., 2008. Site-specific release of nascent chains from ribosomes at a sense codon. *Molecular and cellular biology*, 28(13), pp.4227–4239. Available at: /Users/yurikoharigaya/Documents/ReadCube Media/dronina2008.pdf%5Cnhttp://dx.doi.org/10.1128/MCB.00421-08.

Encinos, W.E. et al., 2006. Healthcare utilization and outcomes after bariatric surgery. *Medical care*, 44(8), pp.706–712. Available at: http://www.embase.com/search/results?subaction=viewrecord&from=export&id=L4428

REFERENCE

        1710%5Cnhttp://sfx.library.uu.nl/utrecht?sid=EMBASE&issn=00257079&id=doi:&atitl e=Healthcare+utilization+and+outcomes+after+bariatric+surgery.&stitle=Med+Care&tit le=Medical+care&vol.

Enerback, S. et al., 1997. Mice lacking mitochondrial uncoupling protein are cold sensitive but not obese.pdf. *Nature*, 387, pp.90–94.

Fedorenko, A., Lishko, P.V. & Kirichok, Y., 2012. Mechanism of fatty-acid-dependent UCP1 uncoupling in brown fat mitochondria. *Cell*, 151(2), pp.400–413. Available at: http://linkinghub.elsevier.com/retrieve/pii/S0092867412011130.

Feldmann, H.M. et al., 2009. UCP1 Ablation induces obesity and abolishes diet-induced thermogenesis in mice exempt from thermal stress by living at thermoneutrality. *Cell Metabolism*, 9(2), pp.203–209. Available at: http://dx.doi.org/10.1016/j.cmet.2008.12.014.

Filonov, G.S. et al., 2011. Bright and stable near-infrared fluorescent protein for in vivo imaging. *Nature Biotechnology*, 29(8), pp.757–761. Available at: http://www.nature.com/doifinder/10.1038/nbt.1918.

Foster, D.O. & Frydman, M.L., 1978. Measurements of blood flow with microspheres point to brown adipose tissue as the dominant site of the calorigenesis induced by noradrenaline. *Canadian Journal of Physiology and Pharmacology*, 56(1), pp.110–122. Available at: https://doi.org/10.1139/y78-015.

Foster, D.O. & Frydman, M.L., 1979. Tissue distribution of cold-induced thermogenesis in conscious warm- or cold-acclimated rats reevaluated from changes in tissue blood flow: The dominant role of brown adipose tissue in the replacement of shivering by nonshivering thermogenesis. *Canadian Journal of Physiology and Pharmacology*, 57(3), pp.257–270.

Fromme, T. & Klingenspor, M., 2011. Uncoupling protein 1 expression and high-fat diets. *Am J Physiol Regul Integr Comp Physiol*, 300, pp.R1–R8.

Frontini, A. et al., 2009. Thymus uncoupling protein 1 is exclusive to typical brown adipocytes and is not found in thymocytes. *Journal of Histochemistry and Cytochemistry*, 55(2), pp.183–189.

Gaidhu, M.P. et al., 2010. Dysregulation of lipolysis and lipid metabolism in visceral and subcutaneous adipocytes by high-fat diet: role of ATGL, HSL, and AMPK. *AJP: Cell Physiology*, 298(4), pp.C961–C971. Available at: http://ajpcell.physiology.org/cgi/doi/10.1152/ajpcell.00547.2009.

Galmozzi, A. et al., 2014. ThermoMouse: an in vivo model to identify modulators of UCP1 expression in brown adipose tissue. *Cell Reports*, 9(5), pp.1584–1593. Available at: http://www.sciencedirect.com/science/article/pii/S2211124714009358.

Gerngroß, C. et al., 2017. Active brown fat during ^{18}F-FDG PET/CT imaging defines a patient group with characteristic traits and an increased probability of brown fat redetection. *Journal of Nuclear Medicine*, 58(7), pp.1104–1110. Available at: http://jnm.snmjournals.org/lookup/doi/10.2967/jnumed.116.183988.

Gesta, S., Tseng, Y.H. & Kahn, C.R., 2007. Developmental origin of fat: tracking obesity to its source. *Cell*, 131(2), pp.242–256.

Ghorbani, M., Claus, T.H. & Himms-hagenl, J., 1997. Hypertrophy of brown adipocytes in brown and white adipose tissues and reversal of obesity in rats treated with a agonist. *Biochemical phamocology*, 54, pp.121–131.

Ghorbani, M. & Himms-Hagen, J., 1997. Appearance of brown adipocytes in white adipose tissue during CL 316,243-induced reversal of obesity and diabetes in Zucker fa/fa rats. *International Journal of Obesity*, 21(6), pp.465–475.

Glick, Z., Teague, R.J. & Bray, G.A., 1981. Brown adipose tissue : thermic response

REFERENCE

increased by a single low protein, high carbohydrate meal. *Science*, 213, pp.1125–1128.

Golozoubova, V. et al., 2001. Only UCP1 can mediate adaptive nonshivering thermogenesis in the cold. *Faseb J*, 15(9), pp.1601–1603. Available at: http://www.ncbi.nlm.nih.gov/pubmed/11427499%5Cnhttp://www.fasebj.org/content/early/2001/07/02/fj.00-0841fje.full.pdf.

Gordon, C.J., 2012. Thermal physiology of laboratory mice: Defining thermoneutrality. *Journal of Thermal Biology*, 37(8), pp.654–685. Available at: http://dx.doi.org/10.1016/j.jtherbio.2012.08.004.

Granneman, J.G. et al., 2003. White adipose tissue contributes to UCP1-independent thermogenesis. *American Journal of Physiology-Endocrinology and Metabolism*, 285(6), pp.E1230-6. Available at: http://www.ncbi.nlm.nih.gov/pubmed/12954594.

Grefhorst, A. et al., 2015. Estrogens increase expression of bone morphogenetic protein 8b in brown adipose tissue of mice. *Biology of Sex Differences*, 6(1), pp.1–13.

Guerra, C. et al., 1998. Emergence of brown adipocytes in white fat in mice is under genetic control effects on body weight and adiposity. *The American Society for Clinical Investigation*, 102(2), pp.412–420.

Haman, F. & Blondin, D.P., 2017. Shivering thermogenesis in humans : Origin , contribution and metabolic requirement. *Temperature (Austin)*, 2017(4). pp.9-12. Available at: https://doi.org/10.1080/23328940.2017.1328999.

Harms, M.J. et al., 2014. Prdm16 is required for the maintenance of brown adipocyte identity and function in adult mice. *Cell Metabolism*, 19(4), pp.593–604. Available at: http://dx.doi.org/10.1016/j.cmet.2014.03.007.

Hart, J.S., Heroux, O. & Depocas, F., 1956. Cold acclimation and the electromyogram of unanesthetized rates. Journal of Applied Physiology, 9(3), pp404-408.

Heldmaier, G., 1975. Metabolic and thermoregulatory responses to heat and cold in the Djungarian Hamster , Phodopus sungorus. *J. comp. Physiol.*, 122, pp.115–122.

Heldmaier, G. & Buchberger, A., 1985. Sources of heat during nonshivering thermogenesis in Djungarian hamsters : a dominant role of brown adipose tissue during cold adaptation. *J Comp Physiol B*, 156, pp.237–245.

Himms-Hagen, J. et al., 2000. Multilocular fat cells in WAT of CL-316243-treated rats derive directly from white adipocytes. *American Journal of Physiology-Cell Physiology*, 279(3), pp.C670–C681. Available at: http://www.physiology.org/doi/10.1152/ajpcell.2000.279.3.C670.

Himms-Hagen, J., 1984. Nonshivering Thermogenesis. *Brain Research Bullet*, 12, pp.151–160.

Hohtola, E., 2002. Facultative and obligatory thermogenesis in young birds: A cautionary note. *Comparative Biochemistry and Physiology-A Molecular and Integrative Physiology*, 131(4), pp.733–739.

Holm, C., 2003. Molecular mechanisms regulating hormone-sensitive lipase and lipolysis. *Biochemical Society Transactions*, 31, pp.1120–1124.

Hwang, L. et al., 2009. Sex differences in high-fat diet-induced obesity, metabolic alterations and learning, and synaptic plasticity deficits in mice. *Obesity*, 18(3), pp.463–469. Available at: http://dx.doi.org/10.1038/oby.2009.273.

Ikeda, K. et al., 2018. UCP1-independent signaling involving SERCA2b-mediated calcium cycling regulates beige fat thermogenesis and systemic glucose homeostasis. , 23(12), pp.1454–1465.

Inokuma, K. et al., 2006. Indispensable role of mitochondrial UCP1 for antiobesity effect of β3-adrenergic stimulation. *Am J Physiol Endocrinol Metab*, 290, pp.1014–1021.

de Jong, J.M. a et al., 2015. A stringent validation of mouse adipose tissue identity markers.

American journal of physiology. Endocrinology and metabolism, p.ajpendo.00023.2015. Available at: http://www.ncbi.nlm.nih.gov/pubmed/25898951.

Jubrias, S.A. et al., 2008. Contraction coupling efficiency of human first dorsal interosseous muscle. *Journal of Physiology*, 586(7), pp.1993–2002.

Kajimura, S. et al., 2009. Initiation of myoblast to brown fat switch by a PRDM16–C/EBP-β transcriptional complex. *Nature*, 460(7259), pp.1154–1158. Available at: http://www.nature.com/doifinder/10.1038/nature08262.

Kajimura, S. & Saito, M., 2014. A new era in brown adipose tissue biology: molecular control of brown fat development and energy homeostasis. *Annual review of physiology*, 76(October 2013), pp.225–49.

Katoh, Y. et al., 2006. Silencing the constitutive active transcription factor CREB by the LKB1-SIK signaling cascade. *FEBS Journal*, 273(12), pp.2730–2748.

Kazak, L. et al., 2015. A creatine-driven substrate cycle enhances energy expenditure and thermogenesis in beige fat. *Cell*, 163(3), pp.643–655. Available at: http://dx.doi.org/10.1016/j.cell.2015.09.035.

Kim, A. & Park, T., 2010. Diet-induced obesity regulates the galanin-mediated signaling cascade in the adipose tissue of mice. *Molecular Nutrition & Food Research*, 54(9), pp.1361–1370.

Kim, J.H. et al., 2011. High cleavage efficiency of a 2A peptide derived from porcine teschovirus-1 in human cell lines, zebrafish and mice. *PLoS ONE*, 6(4), pp.1–8.

Kim, M.-J. et al., 2015. Salt inducible kinase 1 terminates cAMP signaling by an evolutionarily conserved negative feedback loop in beta cells. *Diabetes,* 64(9), pp.3189-202. Available at:10.2337/db14-1240

Kim, S.-N. et al., 2016. Sex differences in sympathetic innervation and browning of white adipose tissue of mice. *Biology of sex differences*, 7, p.67. Available at: http://www.ncbi.nlm.nih.gov/pubmed/27990249.

Kingma, B., 2012. The thermoneutral zone implications for metabolic studies. *Frontiers in Bioscience*, E4(5), p.518. Available at: https://www.bioscience.org/2012/v4e/af/518/list.htm.

Klein, J. et al., 2002. Novel adipocyte lines from brown fat: A model system for the study of differentiation, energy metabolism, and insulin action. *BioEssays*, 24(4), pp.382–388.

Klingenberg, M. & Winkler, E., 1985. The reconstituted isolated uncoupling protein is a membrane potential driven H+ translocator. *The EMBO Journal*, 4(12), pp.3087–3092.

Klingenspor, M. et al., 2017. Brown Adipose Tissue. In *Adipose Tissue Biology*. Springer, Cham, pp. 91–147.

Koh, Y.J. et al., 2009. Activation of PPAR γ induces profound multilocularization of adipocytes in adult mouse white adipose tissues. *Expeimental and Molecular Medicine*, 41(12), pp.880–895.

Kontani, Y. et al., 2005. UCP1 deficiency increases susceptibility to diet-induced obesity with age. *Aging Cell*, 4(3), pp.147–155.

Kozak, U.C. et al., 1994. An upstream enhancer regulating brown-fat-specific expression of the mitochondrial uncoupling protein gene. *Molecular and cellular biology*, 14(1), pp.59–67.

Kumari, M. et al., 2016. IRF3 promotes adipose inflammation and insulin resistance and represses browning. *Journal of Clinical Investigation*, 126(8), pp.2839–2854.

Lafontan, M. & Berlan, M., 1993. Fat cell adrenergic receptors and the control of white and brown fat cell function. *Journal of Lipid Research*, 34(7), pp.1057-91.

Landsberg, L., Saville, M.E. & Young, J.B., 1984. Sympathoadrenal system and regulation of thermogenesis. *American Journal of Physiology-Endocrinology and Metabolism*, 247(2),

REFERENCE

pp.E181–E189. Available at:
http://www.physiology.org/doi/10.1152/ajpendo.1984.247.2.E181.

Lans, A.A.J.J. Van Der et al., 2013. Cold acclimation recruits human brown fat and increases nonshivering thermogenesis. *The Journal of Clinical Investigation*, 123, pp.3395–3403.

Larose, M. et al., 1996. Essential cis-acting elements in rat uncoupling protein gene are in an enhancer containing a complex retinoic acid response domain. *Journal of Biological Chemistry*, 271(49), pp.31533–31542.

Lasar, D. et al., 2013. Browning attenuates murine white adipose tissue expansion during postnatal development. *Biochimica et biophysica acta*, 1831(5), pp.960–968. Available at: http://www.ncbi.nlm.nih.gov/pubmed/23376694.

Laursen, W.J. et al., 2015. Neuronal UCP1 expression suggests a mechanism for local thermogenesis during hibernation. *Proceedings of the National Academy of Sciences*, 112(5), pp.1607–1612. Available at: http://www.pnas.org/lookup/doi/10.1073/pnas.1421419112.

Lengacher, S., Magistretti, P.J. & Pellerin, L., 2004. Quantitative RT-PCR analysis of uncoupling protein isoforms in mouse brain cortex : methodological optimization and comparison of expression with Brown Adipose Tissue and skeletal muscle. *Journal of Cerebral Blood Flow & Metabolism*, 24, pp.780–788.

Li, Y. et al., 2018. Secretin-activated brown fat mediates prandial thermogenesis to induce satiation. *Cell*, 175(6), pp.1561-1574.

Li, Y., Fromme, T. & Klingenspor, M., 2017. Meaningful respirometric measurements of UCP1-mediated thermogenesis. *Biochimie*, 134, pp.56–61. Available at: http://dx.doi.org/10.1016/j.biochi.2016.12.005.

Liu, X. et al., 2003. Paradoxical resistance to diet-induced obesity in UCP1-deficient mice.[Erratum appears in J Clin Invest. 2003 Mar;111(5):759]. *Journal of Clinical Investigation*, 111(3), pp.399–407. Available at: http://ovidsp.ovid.com/ovidweb.cgi?T=JS&CSC=Y&NEWS=N&PAGE=fulltext&D=med4&AN=12569166%5Cnhttp://imp-primo.hosted.exlibrisgroup.com/openurl/44IMP/44IMP_services_page?sid=OVID&isbn=&issn=0021-9738&volume=111&issue=3&date=2003&title=Journal+of+Clinical+Inves.

Lowell, B.B. et al., 1993. Development of obesity in transgenic mice after genetic ablation of brown adipose tissue. *Nature*, 366(6457), pp.740–742.

Lowell, B.B. & Spiegelman, B.M., 2000. Towards a molecular understanding of adaptive thermogenesis. *Nature*, 404(6778), pp.652–660.

Manthorpe, M. et al., 1993. Gene therapy by intramuscular injection of plasmind DNA : Studies on Firefly Luciferase gene expression in mice. *Human Gene Therapy*, 4, pp.419–431.

Mao, L. et al., 2017. Visualization and quantification of browning using a Ucp1-2A-luciferase knock-in mouse model. *Diabetes*, 66(2), pp.407–417.

Margareto, J. et al., 2001. Up-regulation of a thermogenesis-related gene (UCP1) and down-regulation of PPARg and aP2 genes in adipose tissue : possible features of the antiobesity effects of a β3-adrenergic agonist. Biochem Pharmacol. , 61, pp.1471–1478.

van Marken Lichtenbelt, W. et al., 2009. Cold-Activated Brown Adipose Tissue in Healthy Men. *The New England Journal of Medicine*, 360(15), pp.1500–1508. Available at: http://www.ncbi.nlm.nih.gov/pubmed/19357405.

Marken Lichtenbelt, W.D. et al., 2009. Cold-activated brown adipose tissue in healthy men 674. *N.Engl.J Med.*, 360(1533–4406 (Electronic)), pp.1500–1508.

Meyer, C.W. et al., 2010. Adaptive thermogenesis and thermal conductance in wild-type and

REFERENCE

UCP1-KO mice. *AJP: Regulatory, Integrative and Comparative Physiology*, 299(5), pp.R1396–R1406. Available at: http://ajpregu.physiology.org/cgi/doi/10.1152/ajpregu.00021.2009.

Mitchell, P., 1961. Coupling of phosphorylation to electron and hydrogen transfer by a chemi-osmotic type of mechanism. *Nature*, 191(4784), pp.144–148.

Mo, Q. et al., 2017. Identification and characterization of a supraclavicular brown adipose tissue in mice. *JCI insight*, 2(11), pp.1–14.

Nakamura, K., 2014. Central circuitries for body temperature regulation and fever. American journal of physiology, Regulatory, integrative and comparative physiolo 301(5), ppR1207-28.

Nakayama, A. et al., 2003. Quantification of brown adipose tissue perfusion in transgenic mice using near-infrared fluorescence imaging. *Molecular Imaging*, 2(1), pp.37–49.

Nedergaard, J., Bengtsson, T. & Cannon, B., 2007. Unexpected evidence for active brown adipose tissue in adult humans. *American Journal of Physiology Endocrinology Metabolism*, 293, pp.444–452.

Nguyen, K.D. et al., 2011. Alternatively activated macrophages produce catecholamines to sustain adaptive thermogenesis. *Nature*, 480(7375), pp.104–108. Available at: http://dx.doi.org/10.1038/nature10653.

Nibbelink, M. et al., 2001. Brown fat UCP1 is specifically expressed in Uterine longitudinal smooth muscle cells. *The Jornal of Biological Chemistry*, 276(50), pp.47291–47295.

Nicholls, G. & Locke, R.M., 1984. Thermogenic mechanisms in brown fat. *Physiological reviews*, 64(1), pp.1–55.

Nishikawa, S. et al., 2007. Involvement of Sex, Strain and Age Factors in High Fat Diet-Induced Obesity in C57BL/6J and BALB/cA Mice. *Experimental Animals*, 56(4), pp.263–272.

Ohyama, K. et al., 2016. A Synergistic Antiobesity Effect by a Combination of Capsinoids and Cold Temperature Through Promoting Beige Adipocyte Biogenesis. *Diabetes*, 65(May), pp.1410–1423.

Olsen, J.M. et al., 2017. β3-Adrenergically induced glucose uptake in brown adipose tissue is independent of UCP1 presence or activity: Mediation through the mTOR pathway. *Molecular Metabolism*, 6(6), pp.611–619.

Osuna-prieto, F.J. et al., 2019. Activation of human brown adipose tissue by capsinoids, catechins, ephedrine, and other dietary components : a systematic eeview. *Advances in Nutrition*, pp.1–12.

Palou, A. et al., 1998. Molecules in focus the uncoupling protein, thermogenin. *International Journal of Biochemistry and Cell Biology*, 30(1), pp.7–11.

Patel, K. et al., 2014. The LKB1-salt-inducible kinase pathway functions as a key gluconeogenic suppressor in the liver. *Nature communications*, 5, p.4535.

Paulo, E. et al., 2018. Sympathetic inputs regulate adaptive thermogenesis in brown adipose tissue through cAMP-Salt inducible kinase axis. *Scientific Reports*, 8(1), pp.1–14. Available at: http://dx.doi.org/10.1038/s41598-018-29333-6.

Petrovic, N. et al., 2010. Chronic peroxisome proliferator-activated receptor gamma (PPARg) activation of epididymally derived white adipocyte cultures reveals a population of thermogenically competent, UCP1-containing adipocytes molecularly distinct from classic brown adipocytes. *Journal of Biological Chemistry*, 285(10), pp.7153–7164.

Puchalski, W., Bockler, H. & Langefeld, M., 1987. Organ blood flow and brown adipose tissue oxygen consumption during noradrenaline-induced nonshivering thermogenesis in the Djungarian Hamster. *The Journal of Experimental Zoology*, 242, pp.263–271.

Puigserver, P. et al., 1998. A cold-inducible coactivator of nuclear receptors linked to adaptive

thermogenesis. *Cell*, 92(6), pp.829–39. Available at: http://www.ncbi.nlm.nih.gov/pubmed/9529258.

Qiu, Y. et al., 2018. Screening of FDA-approved drugs identifies sutent as a modulator of UCP1 expression in brown adipose tissue. *EBioMedicine*, 37, pp.344–355. Available at: https://doi.org/10.1016/j.ebiom.2018.10.019.

Quevedo, S. et al., 1998. Sex-associated differences in cold-induced UCP1 synthesis in rodent brown adipose tissue. *Eur J Physiol*, 436, pp.689–695.

Reber, J. et al., 2018. Non-invasive Measurement of Brown Fat Metabolism Based on Optoacoustic Imaging of Hemoglobin Gradients. *Cell Metabolism*, 27(3), p.689–701.e4.

Reusch, J.E.B., Colton, L.A. & Klemm, D.J., 2000. CREB Activation Induces Adipogenesis in 3T3-L1 Cells. *Molecuar and cellular biology*, 20(3), pp.1008–1020.

Rial, E. et al., 1999. Retinoids activate proton transport by the uncoupling proteins UCP1 and UCP2. *EMBO Journal*, 18(21), pp.5827–5833.

Richie, C.T. et al., 2018. Near-infrared fluorescent protein iRFP713 as a reporter protein for optogenetic vectors, a transgenic Cre-reporter rat, and other neuronal studies. *Journal of Neuroscience Methods*, 284, pp.1–14.

Rim, J.S. & Kozak, L.P., 2002. Regulatory motifs for CREB-binding protein and Nfe2l2 transcription factors in the upstream enhancer of the mitochondrial uncoupling protein 1 gene. *The Journal of Biological Chemistry*, 277(37), pp.34589–34600.

Rodríguez, E. et al., 2001. Sexual dimorphism in the adrenergic control of rat brown adipose tissue response to overfeeding. *Eur J Physiol*, 442, pp.396–403.

Rong, J.X. et al., 2007. Adipose mitochondrial biogenesis is suppressed in db/db and high-fat diet-fed mice and improved by rosiglitazone. *Diabetes*, 56(7), pp.1751–1760.

Rosenwald, M. et al., 2013. Bi-directional interconversion of brite and white adipocytes. *Nature Cell Biology*, 15(6), pp.659–667.

Rothwell, N.J. & Stock, M.J., 1979. A role for brown adipose tissue in diet-induced thermogenesis. *Obesity Research*, 281, pp.31–35.

Rothwell, N.J. & Stock, M.J., 1980. Similarities between cold- and diet-induced thermogenesis in the rat. *Canadian Journal of Physiology and Pharmacology*, 58, pp.842–848.

Rousset, S. et al., 2003. Uncoupling protein 2, but not uncoupling protein 1, is expressed in the female mouse reproductive tract. *Journal of Biological Chemistry*, 278(46), pp.45843–45847. Available at: http://www.jbc.org/lookup/doi/10.1074/jbc.M306980200.

Saito, M. & Yoneshiro, T., 2013. Capsinoids and related food ingredients activating brown fat thermogenesis and reducing body fat in humans. *Nutrition and metabolism*, 24(1), pp.71–77.

Sarantopoulos, A., Themelis, G. & Ntziachristos, V., 2011. Imaging the bio-distribution of fluorescent probes using multispectral epi-illumination cryoslicing imaging. *Molecular Imaging and Biology*, 13(5), pp.874–885.

Sbarbati, A. et al., 1997. Chemical shift imaging at 4.7 tesla of brown adipose tissue. *The Journal of Lipid Research*, 38, pp.343–347.

Sbarbati, A. et al., 1991. In vivo morphometry and functional morphology of brown adipose tissue by magnetic resonance imaging. *Anatomical record*, 231(3), pp 293-297.

Schlüter, A. et al., 2002. Phytanic acid, a novel activator of uncoupling protein-1 gene transcription and brown adipocyte differentiation. *The Biochemical journal*, 362(1), pp.61–9.

Seale, P. et al., 2008. PRDM16 controls a brown fat/skeletal muscle switch. *Nature*, 454(7207), pp.961–967. Available at: http://www.nature.com/doifinder/10.1038/nature07182.

REFERENCE

Seale, P. et al., 2011. Prdm16 determines the thermogenic program of subcutaneous white adipose tissue in mice. *The Journal of clinical investigation*, 121(1), pp.96–105.

Seale, P. et al., 2007. Transcriptional control of brown fat determination by PRDM16. *Cell Metabolism*, 6(1), pp.38–54. Available at: http://linkinghub.elsevier.com/retrieve/pii/S155041310700157X.

Sears, I.B. et al., 1996. Differentiation-dependent expression of the brown adipocyte uncoupling protein gene: Regulation by PPARg. *Molecular and Cellular Biology*, 16(7), pp.3410–3419.

Shabalina, I. et al., 2013. UCP1 in brite/beige adipose tissue mitochondria is functionally thermogenic. *Cell Reports*, 5(5), pp.1196–1203. Available at: http://dx.doi.org/10.1016/j.celrep.2013.10.044.

Shabalina, I. et al., 2002. Uncoupling protein-1 : involvement in a novel pathway for β-adrenergic, cAMP-mediated intestinal relaxation. *Am J Physiol Gastrointest Liver Physiol*, 283, pp.1107–1116.

Shcherbakova, D.M., Verkhusha, V. V & Biology, S., 2014. Near-infrared fluorescent proteins for multicolor in vivo imaging. *Nat Methods.*, 10(8), pp.751–754.

Shinohara, Y. et al., 1991. Uncoupling protein is expressed in liver mitochondria and newborn rats. *FEBS Letters*, 293, pp.173–174.

Shore, a. et al., 2010. Role of Ucp1 enhancer methylation and chromatin remodelling in the control of Ucp1 expression in murine adipose tissue. *Diabetologia*, 53, pp.1164–1173.

Smith, E., Roberts, C. & Robert, E., 1963. Thermogenesis of brown adipose tissue in cold-acclimated rats. *American Journal of Physiology*, 206, pp.143–148. Available at: http://ajplegacy.physiology.org/content/206/1/143.short.

Smith, R.E. & Hock, R.J., 1963. Brown fat: Thermogenic effector of arousal in hibernators. *Science*, 140(3563), pp.199–200.

Strosberg, D. & Pietri-Reuxel, F., 1996. Function and regulation of the β3-adrenoceptor Pharmacological properties. *Trends in Pharmacological Sciences,* 17(10), pp.373-381, Available at: https://ac.els-cdn.com/S0165614796800113/1-s2.0-S0165614796800113-main.pdf?_tid=555849ba-1a67-4d62-9814-1666d516ab71&acdnat=1527882392_58a1da09d4c0beee1a20c66a86904ce9.

Susulic, V.S. et al., 1995. Targeted Disruption of the beta 3 -Adrenergic Receptor Gene. *The Jornal of Biological Chemistry*, 270(49), pp.29483–29492.

Symvoulidis, P. et al., 2014. Serial sectioning and multispectral imaging system for versatile biomedical applications, in 2014 IEEE 11th International Symposium on Biomedical Imaging (ISBI). In pp. 890–893.

Szymczak, A.L. et al., 2004. Correction of multi-gene deficiency in vivo using a single 'self-cleaving' 2A peptide–based retroviral vecto. *Nature Biotechnology*, 22(5), pp.589–595.

Teruel, T. et al., 2003. Rosiglitazone and retinoic acid induce uncoupling protein-1 (UCP-1) in a p38 mitogen-activated protein kinase-dependent manner in fetal primary brown adipocytes. *Journal of Biological Chemistry*, 278(1), pp.263–269.

Townsend, K. & Tseng, Y.-H., 2012. Brown adipose tissue: Recent insights into development, metabolic function and therapeutic potential. *Adipocyte*, 1(1), pp.13–24.

Tseng, Y.H., Cypess, A.M. & Kahn, C.R., 2010. Cellular bioenergetics as a target for obesity therapy. *Nature Reviews*, 9, pp.465–481.

Ukropec, J. et al., 2006. UCP1-independent thermogenesis in white adipose tissue of cold-acclimated Ucp1$^{-/-}$ mice. *Journal of Biological Chemistry*, 281(42), pp.31894–31908.

Uldry, M. et al., 2006. Complementary action of the PGC-1 coactivators in mitochondrial biogenesis and brown fat differentiation. *Cell Metabolism*, 3(5), pp.333–341.

Virtanen, K.A. et al., 2009. Functional brown adipose tissue in healthy adults. *The new

england journal of medicine brief, 360(15), pp.1518–1525.

Virtue, S. & Vidal-Puig, A., 2013. Assessment of brown adipose tissue function. *Frontiers in Physiology*, 4, pp.1–18.

Vosselman, M.J. et al., 2013. Brown adipose tissue activity after a high-calorie meal in humans 1 – 3. *Am J Clin Nutr*, 98(7), pp.57–64.

w. T. Noonan & Banks, R.O., 2000. Renal function and glucose transport in male and female mice with diet-induced type II diabetes mellitus (44568). *Proceedings of the Society for Experimental Biology and Medicine*, (44568), pp.221–230.

Wang, H. et al., 2019. A dual Ucp1 reporter mouse model for imaging and quantitation of brown and brite fat recruitment. *Molecular Metabolism*, 20, pp.14-27.

Wang, H. et al., 2016. Browning of White Adipose Tissue with Roscovitine Induces a Distinct Population of UCP1^{+} Adipocytes. *Cell Metabolism*, 24(6), pp.835–847. Available at: http://dx.doi.org/10.1016/j.cmet.2016.10.005.

Wu, J. et al., 2012. Beige Adipocytes Are a Distinct Type of Thermogenic Fat Cell in Mouse and Human. *Cell*, 150(2), pp.366–376. Available at: http://linkinghub.elsevier.com/retrieve/pii/S0092867412005958.

Xue, B. et al., 2007. Genetic variability affects the development of brown adipocytes in white fat but not in interscapular brown fat. *Journal of Lipid Research*, 48(1), pp.41–51. Available at: http://www.ncbi.nlm.nih.gov/pubmed/17041251.

Yoneshiro, T. et al., 2012. Nonpungent capsaicin analogs (capsinoids) increase energy expenditure through the activation of brown adipose tissue in humans. *The American Journal of Clinical Nutrition*, (95), pp.845–850.

Yoneshiro, T. et al., 2013. Recruited brown adipose tissue as an antiobesity agent in humans. *The Journal of clinical investigation*, 123(8), pp.3404–3408.

Yoshida, T. et al., 1998. β3 -Adrenergic agonist induces a functionally active uncoupling protein in fat and slow-twitch muscle fibers. *American Journal of Physiology*, 274, pp.469–475.

Young, P., Arch, J.R.S. & Ashwell, M., 1984. Brown adipose tissue in the parametrial fat pad of the mouse. *FEBS Letters*, 167(1), pp.10–14.

Zancanaro, C. et al., 1994. Magnetic resonance spectroscopy investigations of brown adipose tissue and isolated brown adipocytes. *Journal of lipid research*, 35, pp.2191–2199.

Zhang, F. et al., 2018. An adipose tissue atlas : an image-guided identification of human-like BAT and beige depots in rodents. *Cell Metabolism*, (27), pp.252–262.

Zingaretti, M.C. et al., 2009. The presence of UCP1 demonstrates that metabolically active adipose tissue in the neck of adult humans truly represents brown adipose tissue. *The FASEB Journal*, 23(9), pp.3113–3120.

APPENDIX

Appendix 1: The gDNA sequences alignment using CLUSTAL W (1.81) between *Ucp1*-WT allele and *Ucp1*-KI allele

```
Ucp1-WT-allele    catcaggcaacagtgccactgttgtcttcagggctgagtccttttgttcttgcactcacg    5700
Ucp1-KI-allele    catcaggcaacagtgccactgttgtcttcagggctgagtccttttgttcttgcactcacg    5700
                  ************************************************************

Ucp1-WT-allele    cctctctgccctccaagc------------------------------------------    5718
Ucp1-KI-allele    cctctctgccctccaagccaggatggaagacgccaaaaacataaagaaaggcccggcgcc    5760
                  ******************

Ucp1-WT-allele    ------------------------------------------------------------
Ucp1-KI-allele    attctatccgctggaagatggaaccgctggagagcaactgcataaggctatgaagagata    5820

Ucp1-WT-allele    ------------------------------------------------------------
Ucp1-KI-allele    cgccctggttcctggaacaattgcttttacagatgcacatatcgaggtggacatcactta    5880

Ucp1-WT-allele    ------------------------------------------------------------
Ucp1-KI-allele    cgctgagtacttcgaaatgtccgttcggttggcagaagctatgaaacgatatgggctgaa    5940

Ucp1-WT-allele    ------------------------------------------------------------
Ucp1-KI-allele    tacaaatcacagaatcgtcgtatgcagtgaaaactctcttcaattctttatgccggtgtt    6000

Ucp1-WT-allele    ------------------------------------------------------------
Ucp1-KI-allele    gggcgcgttatttatcggagttgcagttgcgcccgcgaacgacatttataatgaacgtga    6060

Ucp1-WT-allele    ------------------------------------------------------------
Ucp1-KI-allele    attgctcaacagtatgggcatttcgcagcctaccgtggtgttcgtttccaaaaaggggtt    6120

Ucp1-WT-allele    ------------------------------------------------------------
Ucp1-KI-allele    gcaaaaaattttgaacgtgcaaaaaaagctcccaatcatccaaaaaattattatcatgga    6180

Ucp1-WT-allele    ------------------------------------------------------------
Ucp1-KI-allele    ttctaaaacggattaccagggatttcagtcgatgtacacgttcgtcacatctcatctacc    6240

Ucp1-WT-allele    ------------------------------------------------------------
Ucp1-KI-allele    tcccggttttaatgaatacgattttgtgccagagtccttcgatagggacaagacaattgc    6300

Ucp1-WT-allele    ------------------------------------------------------------
Ucp1-KI-allele    actgatcatgaactcctctggatctactggtctgcctaaaggtgtcgctctgcctcatag    6360

Ucp1-WT-allele    ------------------------------------------------------------
Ucp1-KI-allele    aactgcctgcgtgagattctcgcatgccagagatcctattttttggcaatcaaatcattcc    6420

Ucp1-WT-allele    ------------------------------------------------------------
Ucp1-KI-allele    ggatactgcgattttaagtgttgttccattccatcacggttttggaatgtttactacact    6480

Ucp1-WT-allele    ------------------------------------------------------------
Ucp1-KI-allele    cggatatttgatatgtggatttcgagtcgtcttaatgtatagatttgaagaagagctgtt    6540

Ucp1-WT-allele    ------------------------------------------------------------
Ucp1-KI-allele    tctgaggagccttcaggattacaagattcaaagtgcgctgctggtgccaaccctattctc    6600

Ucp1-WT-allele    ------------------------------------------------------------
Ucp1-KI-allele    cttcttcgccaaaagcactctgattgacaaatacgatttatctaatttacacgaaattgc    6660
```

Ucp1-WT-allele	---	
Ucp1-KI-allele	ttctggtggcgctcccctctctaaggaagtcggggaagcggttgccaagaggttccatct	6720
Ucp1-WT-allele	---	
Ucp1-KI-allele	gccaggtatcaggcaaggatatgggctcactgagactacatcagctattctgattacacc	6780
Ucp1-WT-allele	---	
Ucp1-KI-allele	cgagggggatgataaaccgggcgcggtcggtaaagttgttccattttttgaagcgaaggt	6840
Ucp1-WT-allele	---	
Ucp1-KI-allele	tgtggatctggataccgggaaaacgctgggcgttaatcaaagaggcgaactgtgtgtgag	6900
Ucp1-WT-allele	---	
Ucp1-KI-allele	aggtcctatgattatgtccggttatgtaaacaatccggaagcgaccaacgccttgattga	6960
Ucp1-WT-allele	---	
Ucp1-KI-allele	caaggatggatggctacattctggagacatagcttactgggacgaagacgaacacttctt	7020
Ucp1-WT-allele	---	
Ucp1-KI-allele	catcgttgaccgcctgaagtctctgattaagtacaaaggctatcaggtggctcccgctga	7080
Ucp1-WT-allele	---	
Ucp1-KI-allele	attggaatccatcttgctccaacaccccaacatcttcgacgcaggtgtcgcaggtcttcc	7140
Ucp1-WT-allele	---	
Ucp1-KI-allele	cgacgatgacgccggtgaacttcccgccgccgttgttgttttggagcacggaaagacgat	7200
Ucp1-WT-allele	---	
Ucp1-KI-allele	gacggaaaaagagatcgtggattacgtcgccagtcaagtaacaaccgcgaaaaagttgcg	7260
Ucp1-WT-allele	---	
Ucp1-KI-allele	cggaggagttgtgtttgtggacgaagtaccgaaaggtcttaccggaaaactcgacgcaag	7320
Ucp1-WT-allele	---	
Ucp1-KI-allele	aaaaatcagagagatcctcataaaggccaagaagggcggaaagatcgccgtggagggcag	7380
Ucp1-WT-allele	---	
Ucp1-KI-allele	aggaagtcttctaacatgcggtgacgtggaggagaatcccggccctatggctgaaggatc	7440
Ucp1-WT-allele	---	
Ucp1-KI-allele	cgtcgccaggcagcctgacctcttgacctgcgacgatgagccgatccatatccccggtgc	7500
Ucp1-WT-allele	---	
Ucp1-KI-allele	catccaaccgcatggactgctgctcgccctcgccgccgacatgacgatcgttgccggcag	7560
Ucp1-WT-allele	---	
Ucp1-KI-allele	cgacaaccttcccgaactcaccggactggcgatcggcgccctgatcggccgctctgcggc	7620
Ucp1-WT-allele	---	
Ucp1-KI-allele	cgatgtcttcgactcggagacgcacaaccgtctgacgatcgccttggccgagcccggggc	7680
Ucp1-WT-allele	---	
Ucp1-KI-allele	ggccgtcggagcaccgatcactgtcggcttcacgatgcgaaaggacgcaggcttcatcgg	7740
Ucp1-WT-allele	---	
Ucp1-KI-allele	ctcctggcatcgccatgatcagctcatcttcctcgagctcgagcctccccagcgggacgt	7800

```
Ucp1-WT-allele    -----------------------------------------------------------------------
Ucp1-KI-allele    cgccgagccgcaggcgttcttccgccgcaccaacagcgccatccgccgcctgcaggccgc      7860


Ucp1-WT-allele    -----------------------------------------------------------------------
Ucp1-KI-allele    cgaaaccttggaaagcgcctgcgccgccgcggcgcaagaggtgcggaagattaccggctt      7920

Ucp1-WT-allele    -----------------------------------------------------------------------
Ucp1-KI-allele    cgatcgggtgatgatctatcgcttcgcctccgacttcagcggcgaagtgatcgcagagga      7980

Ucp1-WT-allele    -----------------------------------------------------------------------
Ucp1-KI-allele    tcggtgcgccgaggtcgagtcaaaactaggcctgcactatcctgcctcaaccgtgccggc      8040

Ucp1-WT-allele    -----------------------------------------------------------------------
Ucp1-KI-allele    gcaggcccgtcggctctataccatcaacccggtacggatcattcccgatatcaattatcg      8100

Ucp1-WT-allele    -----------------------------------------------------------------------
Ucp1-KI-allele    gccggtgccggtcaccccagacctcaatccggtcaccgggcggccgattgatcttagctt      8160

Ucp1-WT-allele    -----------------------------------------------------------------------
Ucp1-KI-allele    cgccatcctgcgcagcgtctcgcccgtccatctggaattcatgcgcaacataggcatgca      8220


Ucp1-WT-allele    -----------------------------------------------------------------------
Ucp1-KI-allele    cggcacgatgtcgatctcgattttgcgcggcgagcgactgtggggattgatcgtttgcca      8280

Ucp1-WT-allele    -----------------------------------------------------------------------
Ucp1-KI-allele    tcaccgaacgccgtactacgtcgatctcgatggccgccaagcctgcgagctagtcgccca      8340

Ucp1-WT-allele    -----------------------------------------------------------------------
Ucp1-KI-allele    ggttctggcctggcagatcggcgtgatggaagaggagggcagaggaagtcttctaacatg      8400

Ucp1-WT-allele    ------------------------------ caggatggtgaacccgacaacttccgaagtgcaacc   5754
Ucp1-KI-allele    cggtgacgtggaggagaatcccggccctatggtgaacccgacaacttccgaagtgcaacc   8460
                              *      ****************************

Ucp1-WT-allele    caccatgggggtcaagatcttctcagccggagtttcagcttgcctggcagatatcatcac   5814
Ucp1-KI-allele    caccatgggggtcaagatcttctcagccggagtttcagcttgcctggcagatatcatcac   8520
                  ************************************************************

Ucp1-WT-allele    cttcccgctggacactgccaaagtccgccttcaggtagagttagtgacattgatgaggct   5874
Ucp1-KI-allele    cttcccgctggacactgccaaagtccgccttcaggtagagttagtgacattgatgaggct   8580
                  ************************************************************

Ucp1-WT-allele    tctccaagcaggactgctgtgggcatccctgtgatgtgtgctacggtttaaccactcttc   5934
Ucp1-KI-allele    tctccaagcaggactgctgtgggcatccctgtgatgtgtgctacggtttaaccactcttc   8640
                  ************************************************************

Ucp1-WT-allele    ctcagggtggctctgtcttgggaatgggtgctattaggaaggaaatggggcccttggatt   5994
Ucp1-KI-allele    ctcagggtggctctgtcttgggaatgggtgctattaggaaggaaatggggcccttggatt   8700
                  ************************************************************

Ucp1-WT-allele    ggctgaagaaccgctgttgatgggttaaaaatggcctctgccaaatccttcataaggcaa   6054
Ucp1-KI-allele    ggctgaagaaccgctgttgatgggttaaaaatggcctctgccaaatccttcataaggcaa   8760
                  ************************************************************

Ucp1-WT-allele    tggtgtcctgagcatgtggggtctaaataataataataattcaaatccctcagagtttac   6114
Ucp1-KI-allele    tggtgtcctgagcatgtggggtctaaataataataataattcaaatccctcagagtttac   8820
                  ************************************************************

Ucp1-WT-allele    aggcctggcgcttttacctttctttgatttggggcacggggtggtgtactatcccatcct   6164
Ucp1-KI-allele    aggcctggcgcttttacctttctttgatttggggcacggggtggtgtactatcccatcct   8880
                  ************************************************************
```

Appendix 2: Crude nutrient composition of experimental diets.

Nutrients	Commpositions	High fat diet	Control diet
Crude nutrients			
Protein	Casein	24.0	24.0
Carbohydrate	Corn starch	27.8	47.8
	Maltodextrin	5.6	5.6
	Sucrose	5.0	5.0
Fiber	Cellulose	5.0	5.0
Additives	Vitamins	1.2	1.2
	Minerals	6.0	6.0
	L-Cystine	0.2	0.2
	Choline-Cl	0.2	0.2
Fat	Soybean oil	5	5
	Palm oil	20	-
Metabolizable energy [MJ/kg]		19.7	15.5
Protein (%)		18	23
FAT (%)		**48**	**12**
Carbohydrate (%)		34	65

High-fat diet: Sniff article S5745-E712. Control diet: Sniff article S5745-E70

APPENDIX

Appendix 3: Flow chart to measure cellular UCP1 activity

Protocol for *UCP1* activity
1- Calibrate probes
2-Equilibrate 12 min*
3-Loop 3 times
4-(1-2-3) Mix 2min
5- Time Delay of 2 min
6-(1-2-3) Measure 3 min
7-Loop end
8-Inject **Oligomycin**
9-Loop 3 times
10-(4-5-6) Mix 2min
11- Time Delay of 2 min
12-(4-5-6) Measure 3 min
13-Loop end
14-Inject **Isoproterenol**
15-Loop 5 times
16-(7-8-9-10-11) Mix 2min
16- Time Delay of 2 min
18-(7-8-9-10-11) Measure 3 min
19-Loop end
20-Inject **FCCP**
21-Loop 3 times
22-(12-13-14) Mix 2min
23- Time Delay of 2 min
24-(12-13-14) Measure 3 min
25-Loop end
26-Inject **Antimycin A**
27-Loop 3 times
28-(15-16-16) Mix 2min
29- Time Delay of 2 min
30-(15-16-16) Measure 3 min
31-Loop end
32-Program end

Appendix 4: Primers lists for gene expression in RT-qPCR and ddPCR

Primers	Forward primer 5'-3'	Reverse primer 5'-3'
AdipoQ	GCACTGGCAAGTTCTACTGCAA	GTAGGTGAAGAGAACGGCCTTGT
Adrb3	TGAAGATCCAGCAAGGAAGC	TTCTGGAGCGTTGGAGAGTT
Acc	TTTTCGATGTCCTCCCAAAC	ACATTCTGTTTAGCGTGGGG
Atgl	GGAAATTGGGTGACCATCTG	AAGGCCACATTGGTGCAG
Cidea	TGCTCTTCTGTA TCG CCC AGT	GCCGTGTTAAGGAATCTGCTG
CD301	CTCTGGAGAGCACAGTGGAG	ACTTCCGAGCCGTTGTTCT
Cox7a1	CCGACAATGACCTCCCAGTA	TGTTTGTCCAAGTCCTCCAA
Dio2	TGTCTGGAACAGCTTCCTCC	TGAACCAAAGTTGACCACCA
Elovl3	TCC GCG TTC TCA TGT AGG TCT	GGA CCT GAT GCA ACC CTA TGA
ERRa	GGAGGACGGCAGAAGTACAAA	GCGACACCAGAGCGTTCAC
Fabp4	GATGGTGACAAGCTGGTGGT	TTTATTTAATCAACATAACCATATCCA
Fasn	GCATTCAGAATCGTGGCATA	TTGCTGGCACTACAGAATGC
Flirefly luciferase	GCATTCAGAATCGTGGCATA	AGGAACCAGGGCGTATCTCT
Hsl	GCTTGGTTCAACTGGAGAGC	GCCTAGTGCCTTCTGGTCTG
human Vegf	GAGATGAGCT TCCTACAGCAC	TCACCGCCTCGGCTTGTCACAT
iRFP713	CGAGTCAAAACTAGGCCTGC	GGCGAAGCTAAGATCAATCG
Nrg4	TGTGGACCATACGACGAGAG	GTGCAAGGTCAACACAGGAA
Pgc1a	GGACGGAAGCAATTTTTCAA	GAGTCTTGGGAAAGGACACG
Prdm16	CAGCACGGTGAAGCCATTC	GCGTGCATCCGCTTGTG
Pparg	TCAGCTCTGTGGACCTCTCC	ACCCTTGCATCCTTCACAAG
Slc25a1	GCTGTCAGGTTTGGGATGTT	GGAGGAAGTCTGGTCATGGA
TF2B housekeeper	TGGAGATTTGTCCACCATGA	GAATTGCCAAACTCATCAAAACT
Ucp1 (bind to exon 1)	TTTTGTTCTTGCACTCACGC	CTGAAACTCCGGCTGAGAAG
Ucp1 (bind to exon 5)	GTACACCAAGGAAGGACCGA	TTTATTCGTGGTCTCCCAGC
Zic1	AACCTCAAGATCCACAAAAGGA	CCTCGAACTCGCACTTGAA

Appendix 5: Process for sample dehydration and Hematoxylin & eosin staining

	Dehydration		Hematoxylin & eosin staining	
Steps	**Chemicals**	**Incubation**	**Chemicals**	**Incubation**
1	Ethanol (70%)	60 min	Xylol	3 min
2	Ethanol (70%)	60 min	Xylol	3 min
3	Ethanol (80%)	60 min	Ethanol (100%)	2 min
4	Ethanol (96%)	60 min	Ethanol (96%)	2 min
5	Ethanol (96%)	60 min	Ethanol (70%)	1 min
6	Ethanol (100%)	60 min	H_2O	1 min
7	Ethanol (100%)	60 min	Hermalum	4 min
8	Ethanol (100%)	60 min	H_2O	2 min
9	Xylol	60 min	Eosin	2 min
10	Xylol	60 min	Ethanol (70%)	1 min
11	Paraplast	60 min	Ethanol (96%)	1 min
12	Paraplast	60 min	Ethanol (100%)	1 min
13			Ethanol (100%)	1.5 min
14			Xyol and Ethanol (1:1)	1.5 min
15			Xylol	2 min
16			Xylol	2 min

ACKNOWLEDGEMENT

EIDESSTATTLICHE ERKLÄRUNG

Ich erkläre an Eides statt, dass ich die bei der Fakultät Wissenschaftszentrum Weihenstephan für Ernährung, Landnutzung und Umwelt der TUM zur Promotionsprüfung vorgelegte Arbeit mit der Title:

Phenotypic characterization of a novel *Ucp1-LUC-iRFP713* reporter mouse model for visualization and quantification of brown and beige fat recruitment

am Lehrstuhl für Molekulare Ernährungsmedizin unter der Anleitung und Betreuung durch Univ.-Prof. Dr. Martin Klingenspor ohne sonstige Hilfe erstellt und bei der Abfassung nur die gemäß § 6 Abs. 6 und 7 Satz 2 angegebenen Hilfsmittel benutzt habe.

Ich habe keine Organisation eingeschaltet, die gegen Entgelt Betreuerinnen und Betreuer für die Anfertigung von Dissertationen sucht, oder die mir obliegenden Pflichten hinsichtlich der Prüfungsleistungen für mich ganz oder teilweise erledigt.

Ich habe die Dissertation in dieser oder ähnlicher Form in keinem anderen Prüfungsverfahren als Prüfungsleistung vorgelegt.

Die vollständige Dissertation wurde noch nicht veröffentlicht.

Ich habe den angestrebten Doktorgrad **noch nicht** erworben und bin **nicht** in einem früheren Promotionsverfahren für den angestrebten Doktorgrad endgültig gescheitert.

Die öffentlich zugängliche Promotionsordnung der TUM ist mir bekannt, insbesondere habe ich die Bedeutung von § 28 (Nichtigkeit der Promotion) und § 29 (Entzug des Doktorgrades) zur Kenntnis genommen. Ich bin mir der Konsequenzen einer falschen Eidesstattlichen Erklärung bewusst.

Mit der Aufnahme meiner personenbezogenen Daten in die Alumni-Datei bei der TUM bin ich einverstanden

Freising, den_____   _____

CURRICULUM VITAE

Personal information:

Name: **Hui Wang**

Birthday: 19.05.1987

Birth of place: Suqian, Jiangsu, China

Nationality: Chinese

Education

From 09/2013	**Ph.D**: Molecular Nutritional Medicine
	Technical University of Munich, Freising, Germany
09/2010-07/2013	**Master**: Animal Genetics
	Northwest A&F University, Shaanxi, China
09/2006-07/2010	**Bachelor**: Animal Nutrition
	Northwest A&F University, Shaanxi, China

Academic Awards and Honors

2013-2016 China Scholarship Council (CSC)

Publications

1. Hui Wang, Monja Willershäuser, Angelos Karlas, Dimitris Gorpas, Josefine Reber, Vasilis Ntziachristos, Stefanie Maurer, Tobias Fromme, Yongguo Li, Martin Klingenspor. (2019). A dual Ucp1 reporter mouse model for imaging and quantitation of brown and brite fat recruitment. *Molecular Metabolism.*

2. Hui Wang, **Monja Willershäuser**, Yongguo Li, Tobias Fromme, Katharina Schnabl, Andrea Bast-Habersbrunner, Martin Klingenspor. Impaired BAT thermogenesis does not cause excessive body weight gain independent of ambient temperature (In preparation).

3. Wang-Sheng Zhao, Shi-Liang Hu, Kang Yu, **Hui Wang**, Wei Wang, Juan Loor, Jun Luo. (2014). Lipoprotein lipase, tissue expression and effects on genes related to fatty acid synthesis in goat mammary epithelial cells. *International Jthenal of Molecular Sciences*, 15(12), pp.22757–22771.